FACULDADE DE ENGENHARIA DA UNIVERSIDADE DO PORTO

On the relationship between friction and film parameters in EHL contacts

Pedro Daniel Freitas Rebolo

Master's in Mechanical Engineering

Supervisor: Carlos Miguel da Costa Gomes Fernandes

Co-Supervisor: David Emanuel Pimentel Gonçalves

October 28, 2022

On the relationship between friction and film parameters in EHL contacts

Pedro Daniel Freitas Rebolo

Master's in Mechanical Engineering

October 28, 2022

Abstract

The knowledge of film parameters is important to understand the lubrication regime that a certain machine element operates. Various types of film parameters have been proposed to find the regime in which a machine element operates. Of course, with this parameters a relationship with the friction present in the machine element can be established.

In this dissertation, a literature review on Elastohydrodynamic lubrication was first performed. This review included a brief look at the film thickness equations proposed throughout the years, a short look at the different types of surface roughness, a look at the different film parameters as well as how they are calculated. Finally the literature review ends with a brief explanation of the theory behind the friction in EHL contacts, as well as theoretical equations to obtain the friction in a mixed lubrication regime condition.

Experiments to evaluate the film thickness and the friction coefficients were performed using two different types of lubricant oils, with the properties of two lubricants having been analysed. All of these experiments were made by using the PCS Instruments EHD2 Ultra Thin film Measurement System, on a ball-disc contact geometry.

For the film thickness experiments it was used two discs, one made from glass and another made of sapphire. For the friction coefficients experiments the surface roughness of the three steel discs used, as well as the steel balls, was first obtained. Afterwards, a series of experiments between the steel discs and steel balls were performed in order to obtain the friction coefficients. The experimental film thickness were compared with theoretical results using the film thickness equations, to understand if there was a significant difference in results. The same was done in regard to the friction coefficient experiments.

Finally, a value for the boundary film regime using the Larsson film parameter was proposed by analysing the friction coefficients while using the steel disc and steel ball with the roughest surface, it was possible to determine a value for the boundary film regime for the Larsson film parameter, the value that was proposed was of 0.1. Afterwards, three equations for ξ are proposed by modifying the previous ξ equations using a minimum squares method. These obtained equations were then compared with the experimental results.

It was possible to see that the Diab film parameter produce, in general, the worst friction coefficient predictions, the Doleschel and Matsumoto film parameters were clearly superior.

Keywords: Tallian, Doleschel, Larsson, EHL Regime, Friction Coefficients, Film Thicknesses, Dowson, Surface Roughness

Acknowledgements

This work wouldn't be possible without the help of several individuals that shared their knowledge and experience, that were part of my journey and to whom I would like to express my acknowledgements.

First of all, I would like to express my acknowledgement to Faculdade de Engenharia da Universidade do Porto, that has been like a second home for me for the past 5 years, for providing all the resources for my Master's Degree in Mechanical Engineering.

My sincere thanks to Professor Carlos Fernandes and Professor David Gonçalves for sharing their knowledge and expertise about the topic, the constant help, their patience, guidance and permanent support. Without their guidance the fulfilment of this work wouldn't be possible.

A special thanks to the people I met at CETRIB, that welcomed me as one of their own, for providing the means necessary to complete this work and for allowing me to have a little idea of what real life work is.

To my family, for all the unconditional support that they have given me in these last years, the comprehension and the words of encouragement that they gave me.

To all my friends that entered at the same time as me, with a special mention to the RL group, João Madeira and Francisco Lázaro, I would like to express my absolute gratitude for spending these last years with me, for all the classes we spent together, late night study session's we had, all works we had that we helped each other mutually, all the party's we went to. Thank you for these last 5 years where all of you helped me, for all the good times we spent together, for all the support you guys gave me and for shaping me as a person.

Finally, I would like to express my gratitude to the ones that entered a year after me, with a special mention to Afonso Costa, Beatriz Ferreira and specially Maria Ribas, thank you for making my final year in university such a joyful one.

Pedro Rebolo

"Even if no salvation should come,
I want to be worthy of it at every moment"

Franz Kafka

Contents

List of Figures

List of Tables

Nomenclature

Symbol	Description	Units
Δu	Sliding speed	m s^{-1}
A	Contact area	m^2
b	Contact half-width	m
$b_{x/y,a}$	Asperity's width	m
c	Specific heat	J $Kg^{-1}K^{-1}$
E	Young's modulus	Pa
E'	Young's modulus	Pa
E_a	Activation energy	J
F	Friction force	N
G	Dimensionless material parameter	-
G_p	Elastic shear modulus	Pa
h_c	Central film thickness	m
h_m	Minimum film thickness	m
k	Thermal conductivity	W $m^{-1}K^{-1}$
K_D	Diffusion rate	m^2 s^{-1}
K_oil	Thermal conductivity of the oil	W $m^{-1}K^{-1}$
K_S	Thermal conductivity of the solid	W $m^{-1}K^{-1}$
p	Pressure	Pa
R'	Effective radius	m
$R_{x,y}$	Principal radii of curvature	m
SRR	Slide-to-roll ratio	-
T	Temperature	K
u_e	Rolling speed	m s^{-1}
U	Dimensionless speed parameter	-
V_e	Sliding rate	-
W	Dimensionless load parameter	-
W_L	Dimensionless load parameter per unit length	m^{-1}
z_a	Asperity's height	m

Abbreviations	Description
ASTM	American Society for Testing and Materials
BL	Boundary lubrication
COF	Coefficient of Friction
EHL	Elastohydrodynamic lubrication
FF	Full film
ML	Mixed lubrication
PAO	Polyalphaolefin
TOTM	Trioctyl Trimellitate

Greek Symbol	Description	Units
α^*	Piezoviscosity coefficient	Pa^{-1}
β	Thermoviscosity coefficient	K^{-1}
$\dot{\gamma}$	Strain rate	s^{-1}
δ_a	micro-EHL film thickness	m
η	Dynamic viscosity	Pa s
η_p	Low shear rate Newtonian dynamic viscosity	Pa s
Λ	Specific film thickness	-
λ_c	Cut-off length	-
μ	Friction coefficient	-
ν	Kinematic viscosity	cSt
ν^*	Poisson coefficient	-
ξ	Load sharing function	-
ρ	Density	Kg m^{-3}
τ	Shear stress	Pa
τ_c	Eyring stress	Pa
ϕ_T	Thermal correction factor	-

Chapter 1

Introduction

Machine elements like gears or rolling bearings operate in an elastohydrodynamic lubrication in three different types of film regimes: the boundary, the mixed film and the full film. In order to determine the type of lubrication regime a machine element operates, the film thickness of the lubricant and the surface roughness of the machine element needs to be known. By knowing this two parameters it's possible to determine a specific film parameter (Λ) that correlates both of these parameters. It's also possible to correlate this specific film parameter with a load sharing function (ξ) in order to have a prediction for coefficients of friction in a mixed film regime.

In this work, three well known specific film parameters will be used, Diab, Doleschel and Matsumoto film parameters, plus a new film parameter that was proposed recently by Larsson.

Experiments will be conducted with two types of lubricants as well with different types of discs in order to guarantee that the three types of film regimes are analysed.

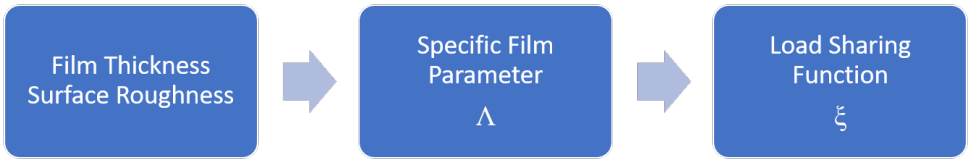

Figure 1.1: Precedure

1.1 Objectives

The main objective was to analyse and compare the existing relationship between the existing film parameters and the friction coefficients with experimental results to observe which film parameter delivered better results in terms of predicting the friction coefficient. Another objective of this dissertation was to analyse the new film parameter proposed by Hansen, Björling and Larsson, in order to get a Λ value for the boundary film regime as well as to propose an equation for the friction coefficients predictions in a mixed film lubrication.

For this, the following aspects were attend to:

- Analyse the film thicknesses equations
- Understand the surface roughness parameters
- Study the known specific film parameters equations and their respective load sharing function (ξ)
- Compare the frictions coefficient predictions for each type of load sharing function (ξ) and compare it to the experimental friction results

1.2 Dissertation Structure

This document has the following structure:

Chapter 2 - State of the Art: A literature review was done on a number of topics, including a look into the film thickness equations throughout the years in line contacts and in point contacts, a review about the numerous surface roughness parameters and a look over the specific film parameters. There is also a review on the friction coefficients in elastohydrodynamic lubrication and how to predict this coefficient of friction values in a mixed film lubrication regime.

Chapter 3 - Experimental Work: An explanation about the experimental work done is in this chapter. A flowchart of how the experiments are conducted for the film thickness and for the coefficients of friction is depicted. A brief summary of the different surface roughness parameters measured for the steel discs and steel balls used in the experiments is shown. The lubricant properties of a PAO ISO VG 150 and a TOTM lubricants are shown as well as the experimental procedure.

Chapter 4 - Film Thickness Results: In this chapter the results for the film thickness is shown. The film thickness measurements are compared with the theoretical equations and a brief discussion is then followed about the behaviour of the film thickness when different experimental parameters are changed in the experiments.

Chapter 5 - Coefficients of Friction Results: In this chapter the results for the coefficients of friction is shown. These coefficients of friction are compared with theoretical predictions and a brief discussion is then followed.

Chapter 6 - Larsson film parameter: In this chapter the Larsson film parameter is studied and a value for the boundary film regime is proposed. An analysis of the predicted coefficients of friction while using the Larsson film parameter is made.

Chapter 7 - Conclusions and Future Work: The conclusions made with this work are presented and future works are suggest in order to improve and to validate the work done in this dissertation.

Chapter 2

State of the art

2.1 Elastohydrodynamic lubrication

In the 1880s, the understanding of fluid film lubrication was established by experimental and theoretical studies [1].

Experimental investigations made in 1883 indicated, from the evidence of pressure and measured friction torques, that a coherent film of lubricant separated the bearing surfaces. Thus the friction and the load carrying capacity was determined by the laws of hydrodynamics, instead of the behaviour between rubbing solid surfaces [2, 3].

Following these experiments, Osborne Reynolds concluded that the flow of lubricant in the clearance space would be governed by the laws of slow viscous flow. He then derived his classical Reynolds equation for tribology [4].

Following the developments made in the 1880s, advanced progress was made in the analysis and experimental study of the phenomena of fluid film lubrication. However, this newfound knowledge seemed to be inadequate, since it couldn't clarify the mechanism of lubrication that was responsible for the effective operation of gears or in other types of machine elements. It was this that led to the development of the concept of elastohydrodynamic lubrication, where the general form could be applied in any machine element although it has it's beginnings in the study on basic mechanism of gear lubrication [1, 5].

So, elastohydrodynamic lubrication can be defined as the study of lubricating films between elastic deformable solids and it has a vast range of applications. At one end it covers highly stressed machine elements and in the other is concerned with the performance of soft rubber seals and event human joints [5].

2.2 Film thickness in line contacts

2.2.1 Martin

Martin solved the Reynolds equation considering two parallel rigid circular cylinders lubricated by an isoviscous fluid. He also considered a geometrically equivalent cylinder (paraboloid) near a

plane, enabling to write the film thickness equation in (2.1) [1, 6, 7].

$$\frac{h_m}{R'} = \frac{h_c}{R'} = 4.9 \cdot U \cdot W_L^{-1} \tag{2.1}$$

However, Martin's analysis fails to explain the lubrication of gear teeth in terms of hydrodynamic lubrication because the film thicknesses obtained by equation (2.1) considering realistic working conditions was only about 0.1 μm [1, 6].

2.2.2 Ertel-Gubrin

Following the analysis made by Martin, it was recognised that the hydrodynamic analysis should be associated with the elastically deformed shape of the conjunctions between loaded gear teeth. The predicted film thickness when considering this complication increased dramatically [6].

The major breakthrough was effected by Ertel and reported by Gubrin, where he assumed that the solids would retain the shape of an Hertzian dry contact, but that they would be separated by a thin, uniform layer of lubricant. The proposed equation can be found in (2.2).

$$\frac{h_c}{R'} = 1.95 \cdot U^{8/11} \cdot G^{8/11} \cdot W_L^{-1/11} \tag{2.2}$$

2.2.3 Dowson-Higginson and Dowson-Toyoda

Attempts were made to reach full numerical solutions that satisfied both the elasticity and the Reynolds equation. Petrusevich numerical solution consisted in keeping a constant load and varying the speed. This solution was in agreement with fundamental EHL theory, including a constant film thickness and pressure distribution similar to that of the Hertzian distribution [1, 6, 8, 9].

Dowson and Higginson presented a numerical solution, equation (2.3), where they used an inverse solution method rather than a straightforward iterative problem [1, 6, 9].

$$\frac{h_m}{R'} = 1.6 \cdot U^{0.7} \cdot G^{0.6} \cdot W^{-0.13} \tag{2.3}$$

This equation was later revised by Dowson to:

$$\frac{h_m}{R'} = 2.65 \cdot U^{0.7} \cdot G^{0.54} \cdot W^{-0.13} \tag{2.4}$$

A central film thickness solution for line loads was presented by Dowson and Toyoda in the following form [10]:

$$\frac{h_c}{R'} = 3.06 \cdot U^{0.69} \cdot G^{0.56} \cdot W^{-0.1} \tag{2.5}$$

2.3 Film thickness in point contacts

Contrary to line contacts, numerical solutions for point contacts didn't appear until much later on. This could be attributed to the lack of adequate computing power [6].

Hamrock and Dowson considered other effects, such contact ellipticity and lubricant starvation in the previous work made by Dowson and Higginson. The numerical solutions that were reached are the following [9, 11]:

$$\frac{h_m}{R'} = 3.63 \cdot U^{0.68} \cdot G^{0.49} \cdot W^{-0.073} \cdot (1 - \exp^{-0.68k}) \tag{2.6}$$

$$\frac{h_c}{R'} = 2.69 \cdot U^{0.67} \cdot G^{0.53} \cdot W^{-0.067} \cdot (1 - 0.61 \exp^{-0.73k}) \tag{2.7}$$

The parameter k is the ellipticity parameter that can be expressed as $k = 1.03 \cdot (R'_y/R'_x)^{2/\pi}$.

2.4 Surface roughness

The surface of a machine element, although in some cases may appear smooth, presents texture that we call roughness. These surfaces can be anisotropic or isotropic. An anisotropic surface presents a periodic configuration of surface roughness and an isotropic surface presents a random configuration of roughness, as it can been seen in Figures 2.1 and 2.2 [12].

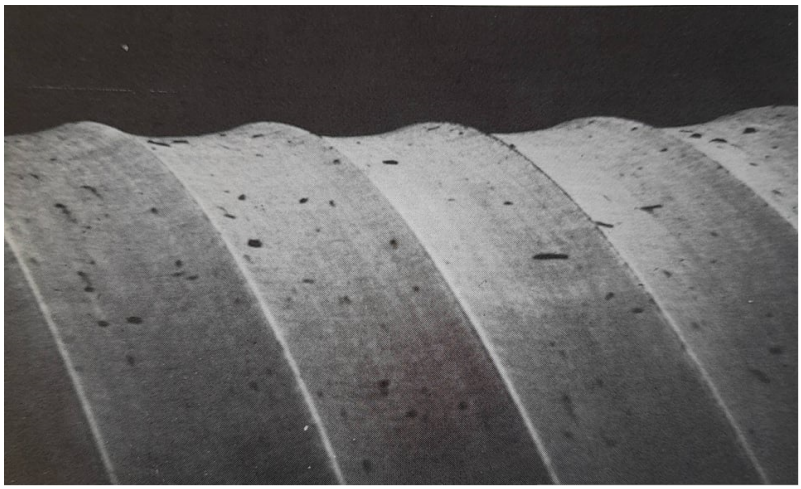

Figure 2.1: An anisotropic surface [12]

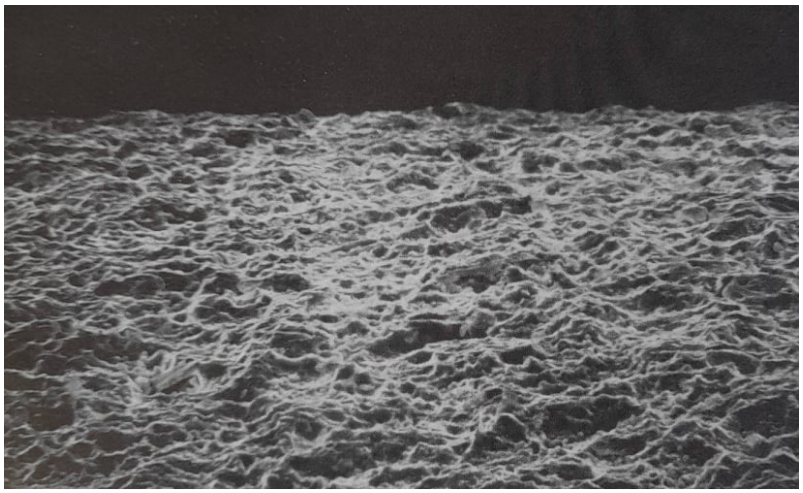

Figure 2.2: An isotropic surface [12]

First, in order to retrieve the roughness parameters used in the film parameters (section 2.5), a filter must be applied to the surface, separating the surfaces into two profiles. The first profile obtained is the waviness profile while the second is the roughness profile.

For this, a cut-off filter, λ_c, is used. This parameter is what determines what is waviness and what is roughness. This cut-off length should be at least 2.5 times the peak-to-peak spacing of the profile roughness. However, if the surface is anisotropic, the cut-off length should be selected using Table 2.1 [12].

Table 2.1: Selection of cut-off length according to DIN 4768

Cut-off λ_c **/ mm**	**Peak spacing of periodic profiles** mm	**Measured roughness** Ra **/** μ**m**	$R_{z(DIN)}$ **/** μ**m**
0.08	< 0.032	-	-
0.25	0.032-0.1	< 0.1	< 0.5
0.8	0.1-0.32	0.1-2	0.5-10
2.5	0.32-1	2-10	10-30
8	> 1	> 10	> 30

2.4.1 Roughness parameters

In order to obtain the roughness parameters the surface must be analysed. The profile is assessed over a length equal to five times the cut-off length, although the total traverse length is six times the cut-off length, as it can be seen in Table 2.2 [12].

2.4.1.1 Average roughness R_a

R_a is the average deviation from the mean line of the profile over the assessment length. This parameter is determined by the following formula [12, 13]:

Table 2.2: Relationship between cut-off and traverse length

Cut-off (λ_c) (mm)	**Traverse length L_t (mm)**
0.08	0.48
0.25	1.5
0.8	4.8
2.5	15.0
8.0	48.0

$$R_a = \frac{1}{l_m} \int_0^{l_m} |y(x)| dx \tag{2.8}$$

The average roughness parameter does not differentiate between peaks and valleys. This means that profiles in which there exists a significant difference between the peaks and valleys and other profiles where such difference is not as pronounced can have the same value of R_a, as seen in Figure 2.4.

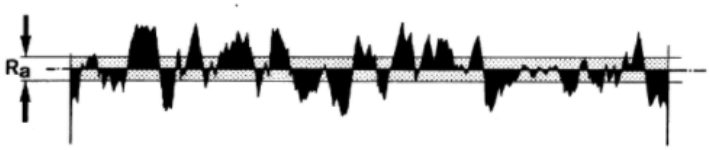

Figure 2.3: Derivation of the parameter R_a [12]

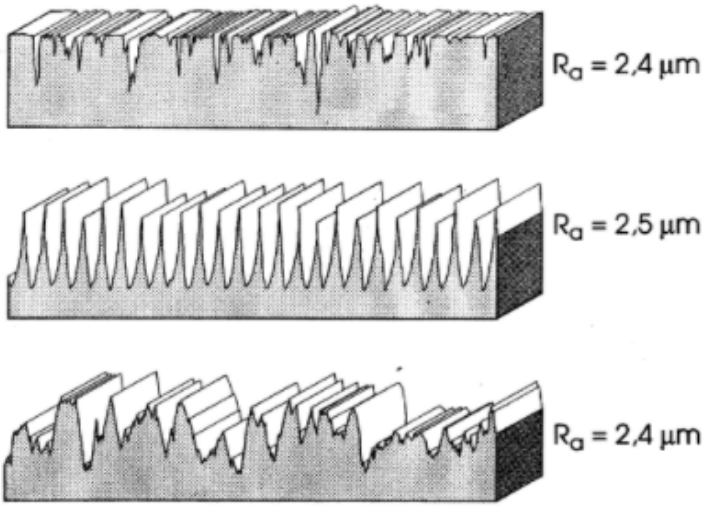

Figure 2.4: Different profiles with the same value of R_a [12]

2.4.1.2 Root-mean-square (RMS) profile height R_q

The RMS parameter is the square root of the deviation of the profile from the mean line. It can be determined by using the following formula [12, 13]:

$$R_q = \sqrt{\frac{1}{l_m}\int_0^{l_m} y^2(x)dx} \tag{2.9}$$

Unlike the average roughness, R_a, this parameter is more sensitive to peaks and valleys.

2.4.1.3 Mean peak-to-valley height $R_{z(DIN)}$

This parameter is determined by dividing the filtered profile into 5 equal lengths, each one nominally equal to the cut-off length, as seen in figure 2.5. Within each cut-off length, the maximum peak-to-valley height is determined, z_i. The parameter $R_{z(DIN)}$ is determined by equation (2.10) [12]:

$$R_{z(DIN)} = \frac{1}{5}\sum_{i=1}^{5} z_i \tag{2.10}$$

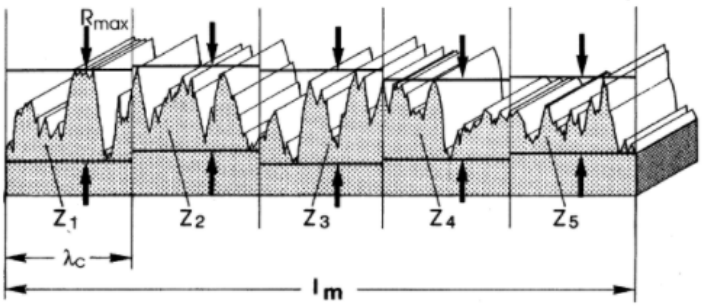

Figure 2.5: Derivation of the parameter $R_{z(DIN)}$ [12]

Because maximum profile heights are being examined and not averages, $R_{z(DIN)}$ is generally more sensitive to changes in surface finish than R_a.

2.4.1.4 Ten point height $R_{z(ISO)}$

This parameter is analogue to the roughness parameter $R_{z(DIN)}$. $R_{z(ISO)}$ is the average distance between the 5 highest peaks and 5 deepest valleys, as it can be seen in Figure 2.6. This roughness parameter is determined by [12, 13]:

$$R_{z(ISO)} = \frac{1}{5}\left(\sum_{i=1}^{5} p_i + \sum_{i=1}^{5} v_i\right) \tag{2.11}$$

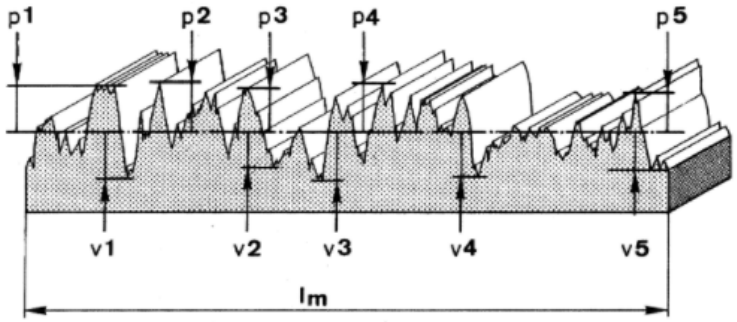

Figure 2.6: Derivation of the parameter $R_{z(ISO)}$ [12]

Unlike the mean peak-to-valley height, the five peaks and valleys used to determine $R_{z(ISO)}$ can be located anywhere along the assessment length.

2.4.2 Hybrid parameters

The material ratio is calculated at different depths through the profile and is expressed graphically as a continuous curve. This resulting curve is called the material ratio curve, or Abbott-Firestone curve, Figure 2.7 [12].

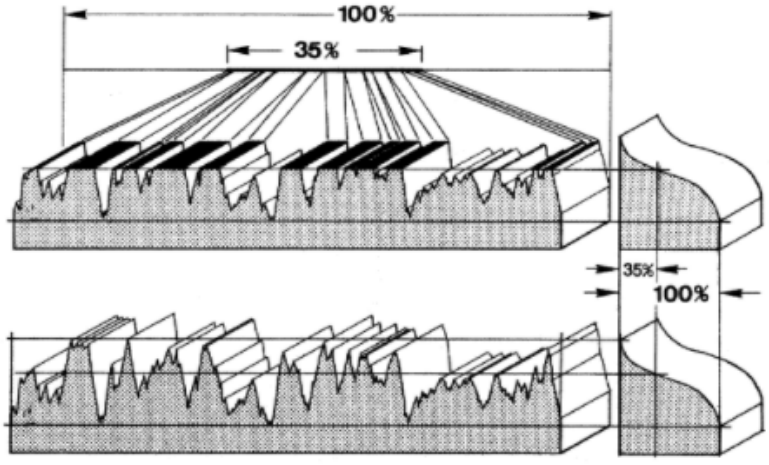

Figure 2.7: Derivation of the material ratio curve [12]

The zero percent or reference line of the Abbott-Firestone curve is located at the top of the highest peak of the evaluated profile. The result of the material ratio curve is significantly influenced by the height of the highest peak. Realistically though, a single peak has little significance

on the surface's function. To avoid the dependence of this curve on a single peak, a reference line is selected to shift the reference line below the highest profile peak. This reference line is specified as a percentage of the material ratio. Specifying a 3% reference line indicates that the top 3% of the profile are not included in the material ratio calculation [12].

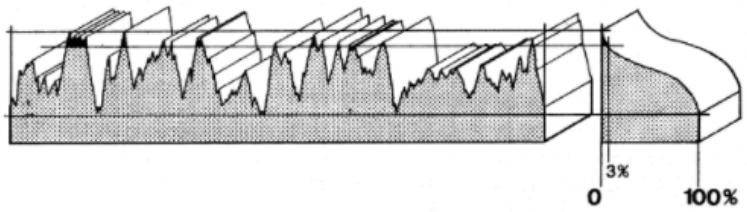

Figure 2.8: Material ratio curve showing 3% reference line [12]

2.4.2.1 Core roughness depth, Reduced peak height, Reduced valley depth, Peak material ratio, Valley material ratio $R_k, R_{pk}, R_{vk}, M_{r1}, M_{r2}$

The material ratio curve is approximated by straight lines that divides it into three parts. These three parts describe the peaks, valleys and core roughness of the surface [12].

The first step in the calculation of the parameters is to find the point of minimum slope on the "S" shaped material ratio curve. Two points are then taken on the material ratio curve, these points are labelled A and B. A and B are separated by 40% on the horizontal axis. The turning point is located by shifting points A and B until the vertical distance between them is minimum. Having a separation of 40% between them ensures that the major turning point is found in curves with more than one turning point [12].

A line is projected through the points A and B to the 0% and 100% material ratio lines. With these points being labelled C and D. The vertical distance between C and D is the core roughness depth, R_k.

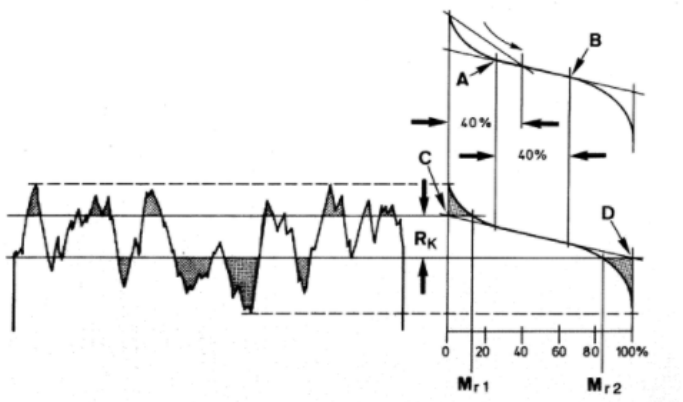

Figure 2.9: Derivation of parameter R_k [12]

The R_{pk} parameter is obtained as seen in Figure 2.10. The area that is situated under the material ratio curve and above the roughness core is determined, and is designated as A_2. R_{pk} is the height of a triangle that has an area of A_2 and a base length of M_{r1}. The parameter R_{vk} is determined in a similar way at the lower end of the material ratio curve [12].

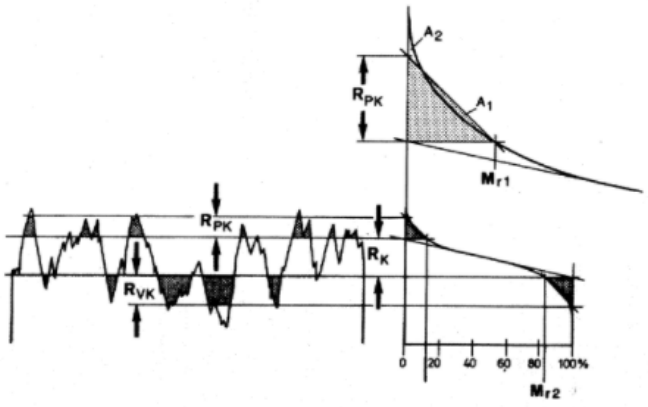

Figure 2.10: Derivation of parameter R_{pk} and R_{vk} [12]

2.4.3 Mean asperity radius

In order to know the mean asperity radius, we need to know first the radius of curvature for each peak along the assessment length [14].

The radius of curvature for each peak can be calculated by:

$$r_{pi} = \frac{2z_i - z_{i-1} - z_{i+1}}{l^2} \tag{2.12}$$

Equation (2.12) considers the 3-point peak (3PP) criterion. With this criterion, the asperity peak is defined as a point that is higher than its two adjacent peaks. However, only the asperity peaks that are above the profile mean line are considered. This is because the contact of two rough surfaces is expected to occur on the highest peaks, peaks that are certainly above the profile mean line [15].

The mean peak radius of curvature can then be calculated by using the equation (2.13).

$$r_p = \frac{1}{n-2} \sum_{i=1}^{n-2} \frac{1}{r_{pi}} \tag{2.13}$$

2.5 Specific film parameter

Lubrication is the tool that controls the friction between interacting surfaces. It has the effect of decreasing friction, making the lubricated mechanism more reliable [16]. Three lubrication regimes

are distinguished for rolling and sliding contacts: boundary lubrication regime (BL), mixed lubrication regime (ML) and the full film elastohydrodynamic lubrication regime (FF-EHL).

In order to relate the film thickness of the elastohydrodynamic lubricant contact with the surface roughness of the bodies in contact, specific film parameters were proposed in which they have the following general form:

$$\Lambda = \frac{\text{film thickness}}{\text{surface roughness}} \tag{2.14}$$

This film parameter can indicate us the EHL regime in which the machine elements operates.

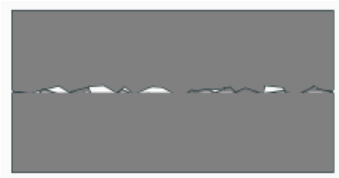

Figure 2.11: Boundary regime [16]

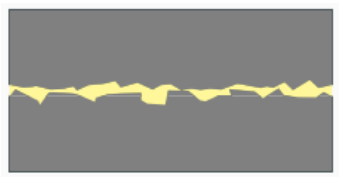

Figure 2.12: Mixed film regime [16]

Figure 2.13: Full film regime [16]

2.5.1 Tallian

Tallian proposed his film parameter to analyse the failure in rolling contact mechanics. Tallian proposed the following film parameter:

$$\Lambda = \frac{h_c}{\sigma} \tag{2.15}$$

Where σ is given by $\sigma = \sqrt{Rq_1^2 + Rq_2^2}$ and the h_c is the central film thickness of the EHL contact.

Tallian observed that a contact operating under a high Hertzian pressure can't run along a thin elastohydrodynamic film corresponding to $\Lambda = 1$. However, for values of $\Lambda \approx 3$, the wear rate is about 100 times less and it's negligible as a failure mode [18].

2.5.2 Tallian with correction (Diab)

Velex, Ville and Diab proposal for the film parameter came from the study of power loss in gears due to tooth friction in gears.

This film parameter is very similar to the one proposed by Tallian, represented in equation (2.15), however a thermal correction factor is added due to heating in the inlet. The proposed film parameter is the following [19]:

$$\Lambda = \frac{\phi_T \cdot h_c}{\sqrt{Rq_1^2 + Rq_2^2}} \tag{2.16}$$

$$\phi_T = \left\{1 + 0.1\left(1 + 14.8V_e^{0.83}\right)L^{0.64}\right\}^{-1} \tag{2.17}$$

$$L = \frac{\beta\eta_0\left(U_1 + U_2\right)^2}{k} \tag{2.18}$$

2.5.3 Michaelis, Höhn and Doleschel

Michaelis, Höhn and Doleschel came up with a new film parameter when studying the lubricant influence on gear efficiency. This new film parameter relates the film thickness proposed by Ertel-Gubrin, that is present in equation (2.2), and the surface roughness parameter R_a [20].

The parameter is as following:

$$\Lambda = \frac{h_c}{0.5 \cdot (Ra_1 + Ra_2)} \tag{2.19}$$

2.5.4 Matsumoto

Matsumoto, like Michaelis, Höhn and Doleschel, proposed a new film parameter when studying coefficient of friction in an attempt to minimise the power loss in transmission gears [21].

Matsumoto's proposed parameter comes from his formulae for estimating the coefficient of friction.

$$\Lambda = \frac{h_m}{Rz_1 + Rz_2} \tag{2.20}$$

The surface roughness parameter Rz is obtained by using the DIN method.

2.5.5 Hansen, Björling and Larsson

Hansen, Björling and Larsson developed a new film parameter for EHL elliptical contacts, with a rough surface with anisotropic and isotropic structures. For this new film parameter, it was considered the classical equations from Dowson-Hamrock for elliptical contacts, present in equations (2.6) and (2.7). This film parameter also depends from the surface roughness lay [22].

For simplicity, Larsson et al. [22] considered the idealised case where the non-Newtonian effects and oil film perturbations are neglected. So in this case, the ball tangential speed is equal to the disc speed $u_b = u_d$.

The theoretical framework for the film parameter is depicted in Figure 2.14.

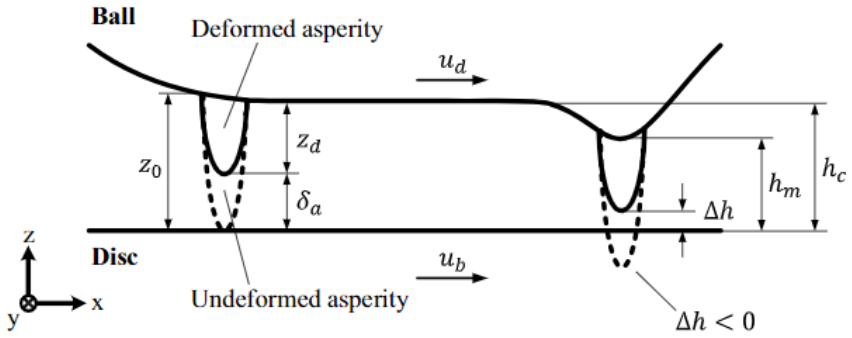

Figure 2.14: Schematic depicting the theoretical framework of the proposed film parameter

When the asperity enters in the contact inlet zone, a lubricant squeeze action allows the formation of a local micro-EHL film as the asperity deforms with a magnitude of δ_a. This phenomena originates from the increase of the local pressure that causes an elastic deformation of the asperity of z_d [22].

The criterion for a FF-EHL regime is when there isn't contact interference $\Delta h > 0$. The criterion for a mixed lubrication regime is when there is contact interference, $\Delta h < 0$ [22].

The available space at contact outlet can be expressed as:

$$h_m = \Delta h + z_d \tag{2.21}$$

The deformed asperity height is given by $z_d = z_0 - \delta_a$, so we can change it in the above equation and rearrange the terms to obtain Δh [22]:

$$\Delta h = h_m - (z_0 - \delta_a) \tag{2.22}$$

It's possible then to derive a film parameter that resembles the classical form, $\Lambda = h_m/\sigma$, considering:

$$\Delta h = (h_m + \delta_a) - z_0 = h^* - z_0 \tag{2.23}$$

FF-EHL occurs when $h^* - z_0 > 0$ and ML occurs when $h^* - z_0 < 0$, so the new lambda parameter Λ^* is defined as [22]:

$$\Lambda^* = \frac{h_m + \delta_a}{z_0} = \frac{h^*}{z_0} \tag{2.24}$$

With this film parameter, the full-film elastohydrodynamic regime occurs when Λ^* is greater than 1. The mixed film lubrication occurs when Λ^* is less than 1 [22].

The general expression for δ_a, that accounts for any asperity geometry [22]:

$$\frac{\delta_a}{h_c} = \left(\frac{u_a}{u_b}\right)^{\mathrm{X}} \cdot \left(\frac{R'_{x,a}}{R'_{x,b}}\right)^{\alpha} \cdot \left(\frac{w_a}{w_b}\right)^{\beta} \cdot \kappa \tag{2.25}$$

The variable κ is an elliptic parameter that can be expressed as:

$$\kappa = \frac{1 - \gamma_1 \times e^{-\gamma_2 \left[R'_{y,a}/R'_{x,a}\right]^{\gamma_3}}}{1 - \gamma_1 \times e^{-\gamma_2 \left[R'_{y,b}/R'_{x,b}\right]^{\gamma_3}}} \tag{2.26}$$

The coefficients needed to solve equation (2.25) and (2.26) are present in Table 2.3 [22].

Table 2.3: Input variables for equation (2.25) and (2.26)

Case	Surface roughness lay	X	α	β	γ_1	γ_2	γ_3
A	Isotropic & transversal	0.67	1.134-X	-0.068	0.61	0.75	$2/\pi$
B	Longitudinal	0.68	1.146-X	-0.073	1	1.23	2/3

Setting the speed and load terms in equation (2.25) as unitary ($u_a = u_b$ and small β), it may be realised that the curvature radii at micro and macro-scale contributes to the majority of micro-EHL film generation [22].

Introducing a dimensionless variable of micro-EHL film generation, f_q, based entirely on the radii:

$$f_q = \frac{f(r)}{f(R)} = \left(\frac{R'_{x,a}}{R'_{x,b}}\right)^{\alpha} \times \frac{1 - \gamma_1 \times e^{-\gamma_2 \left[R'_{y,a}/R'_{x,a}\right]^{\gamma_3}}}{1 - \gamma_1 \times e^{-\gamma_2 \left[R'_{y,b}/R'_{x,b}\right]^{\gamma_3}}} \tag{2.27}$$

The micro-EHL film thickness is then given by:

$$\delta_a = h_c \times f_q \tag{2.28}$$

Changing the terms, Λ^* will be given by:

$$\Lambda^* = \frac{h_m + [h_c \times f_q]}{z_0} \tag{2.29}$$

The following considerations are taken [22]:

- $R = R'_{x,b} = R'_{y,b}$ for the ball-disc configuration

- $r = R'_{x,a} = R'_{y,a}$ in the case of hemispherical roughness features.
- In the case where the surface roughness has a transversal lay to the entrainment speed, the radii of the roughness features, r, is equal to the effective radius of the asperity in the entrainment direction, $r = R'_{x,a}$. The asperity's effective radius normal to the entrainment direction is taken as the ball radius, $R'_{y,a} = R$
- In the case where the surface roughness has a longitudinal lay to the entrainment speed, the surface roughness radii is equal to the asperity's effective radius normal to the entrainment direction, $r = R'_{y,a}$. The asperity's effective radius normal to the entrainment direction is taken as the ball radius, $R'_{x,a} = R$

The asperity radii is determined by equation (2.30).

$$R_{x/y,a} = \frac{b^2_{x/y,a}}{8z_a} \tag{2.30}$$

The model extension for real surface roughness considers the parameter Rpk, changing the parameter z_0 in the equation, obtaining [22]:

$$\Lambda^* = \frac{h_m + [h_c \times f_q]}{Rpk} \tag{2.31}$$

For a composite surface peak, the value can be obtained with a simple sum: $Rpk = Rpk_1 + Rpk_2$ [22].

2.6 Friction in elastohydrodynamic lubrication

A way to decrease the energy consumption and green house emissions is to increase the efficiency of machine components. One of the ways to achieve this is to decrease the friction in the machine components [23].

In the boundary lubrication regime, the velocity between the contacting surfaces is low and the load is carried solely by the interacting asperities of the surfaces. In the mixed lubrication regime, the load is carried by the asperities of the surfaces but also from the pressure generated in the lubricant. In the full film elastohydrodynamic regime, the load is carried solely by the pressure generated in the lubricant [16].

In order to study friction in elastohydrodynamic contacts, a constitutive equation that describes the way the shear stress of a fluid film in elastohydrodynamic contact depends on parameters such as pressure, temperature, strain rate and strain history is needed. There are two main approaches to derive such equation. The first one is the analysis of friction measurements taken from elastohydrodynamic contact and extract the rheological expression that best explains these measurements.

The second one is the high-stress viscometry, where a pressurised sample of an oil is sheared at high applied strain rate in a well-defined geometry [23].

2.6.1 Rheology from elastohydrodynamic friction measurements

When the effect of the contact pressure on viscosity was taken into account, it was observed that the friction in the EHL contacts were much lower than what was predicted by Newtonian behaviour. This phenomena was studied by measurement of traction curves. Most authors in the beginning interpreted their friction measurements in terms of a "mean effective viscosity" [23].

$$\bar{\eta} = \frac{\bar{\tau}}{\dot{\gamma}} = \frac{F/A}{\Delta u/h} \tag{2.32}$$

Research was made to understand why this mean effective viscosity was lower than the mean Newtonian viscosity. With experiments, Crook found that the mean viscosity was approximately equal to the Newtonian mean viscosity at low sliding speeds, but as the rolling speed increased the mean viscosity was increasingly lower than the Newtonian value. He concluded that the effective viscosity depended on the time of passage of the fluid through the contact and then proposed that this represented a viscoelastic response of the lubricant. Crook also interpreted that because of the shear heating of the oil film, the effective mean viscosity fell of greatly below the Newtonian value at high sliding speeds [23, 24].

In experiments made by Smith, he proposed that levelling-out of friction at high sliding speeds resulted from the lubricant film yielding at a critical shear stress, coupled by shear heating [25].

Later studies made noted similar pattern variation of friction with sliding speed as the research made by Crook. The overall form of the friction versus strain rate curve could be explained if viscous shear thinning according to Eyring viscosity model was assumed. However, a direct comparison between the experimental values and prediction from this model weren't made [23, 26].

It was proposed by Johnson and Tevaarwerk that the EHL friction was controlled by a combination of behaviours that they described as "nonlinear Maxwell". Equation (2.33) shows that the strain rate originates from two components [27].

$$\dot{\gamma} = \frac{1}{G_p}\frac{d\tau}{dt} + \frac{\tau_e}{\eta_p}\sinh\left(\frac{\tau}{\tau_e}\right) \tag{2.33}$$

Equation (2.33) can be rearranged in case of stress versus strain rate form:

$$\tau = \tau_e \sinh^{-1}\left(\frac{\eta_p}{\tau_e}\left(\dot{\gamma} - \frac{1}{G_p}\frac{d\tau}{dt}\right)\right) \tag{2.34}$$

This equation shows how the elastic term reduces the shear stress in the contact by accommodating some of the applied strain. When the elastic term is negligible compared to the viscous term, equations (2.33) and (2.34) can be reduced to:

$$\dot{\gamma} = \frac{\tau_e}{\eta_p} \sinh\left(\frac{\tau}{\tau_e}\right) \tag{2.35}$$

$$\tau = \tau_e \sinh^{-1}\left(\frac{\eta_p \dot{\gamma}}{\tau_e}\right) \tag{2.36}$$

For low shear stress, i.e., $\tau << \tau_e$, equation (2.35) becomes $\dot{\gamma} = \frac{\tau_e}{\eta_p}$, the fluid becomes Newtonian. When the shear stress exceeds τ_e, equation (2.36) becomes

$$\tau = \tau_e \ln(\dot{\gamma}) + \tau_e \ln(2\eta_p/\tau_e) \tag{2.37}$$

This model suggests that at low strain rates, fluids behave in a Newtonian way if they have low viscosity or are at low pressure. However, in high-pressure contacts, the fluids show a viscoelastic response. At all contact pressures, fluid shear becomes dominated by Eyring shear thinning as the strain rate, and consequently the shear stress, is increased. This leads to a linear mean shear stress versus log(strain rate) relationship at high sliding speeds, at least until contact heating prevails [23, 27].

If the contact is assumed to operate at a constant pressure, and that the low shear rate viscosity is assumed to vary with pressure, according to the Barus equation $\eta_p = \eta_0 e^{\alpha^* p}$, we can arrive at:

$$\bar{\tau} = \tau_e(\ln(\dot{\gamma}) + \tau_e \left(\ln\left(\frac{2\eta_0}{\tau_e}\right) + \alpha^* \bar{p}\right) \tag{2.38}$$

The rise in temperature will have a significant contribution to the EHL friction measurements. Archard proposed the following equation to describe the temperature rise in a EHL contact [28]:

$$\Delta\bar{T} = \Delta\bar{T}_{flash} + \Delta\bar{T}_{oil} = \frac{1}{(2\pi K_s \rho c)^{0.5}} \left(\frac{2b}{u_e}\right)^{0.5} \bar{\tau}\Delta u + \frac{h_c}{8K_{oil}} \bar{\tau}\Delta u \tag{2.39}$$

The first term of the equation describes the mean flash temperature and the second describes the additional oil film temperature rise. The flash temperature assumes that both solids are of the same material and travel at an approximately the same speed with respect to the contact, but it can be accommodated to different materials and speeds. In the second term of the equation, the value of the denominator 8 is depends on where the heat is generated. The value 8 was derived by Archard while assuming that the heat is generated evenly through the oil film thickness while a value of 4 was obtained if all the heat is generated at the mid-plane [23].

Equation (2.39) shows that the mean oil film temperature can rise very significantly at high values of mean shear stress and sliding speed, especially when the film thickness is large. The temperature increase in the oil film has a very strong effect on EHL friction at high strain rates and is primarily responsible for the levelling out and decrease in friction seen in traction curves [23].

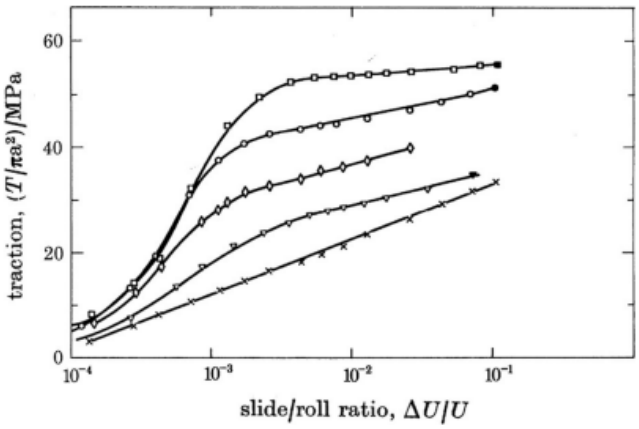

Figure 2.15: Mean shear stress versus slide–roll ratio traction curves [22]

This problem was addressed by obtaining traction curves at various temperatures. By combining the results, based on film temperatures calculated using equation (2.39), then enable isothermal traction curves to be constructed even within the "thermal" region [23, 29].

A similar approach was used by Evans and Johnson, they employed the values of $\Delta\bar{T}$ from equation (2.39) to adjust the bulk temperature and sliding speed during friction tests. The results confirmed the nonlinear Maxwell model of equation (2.33) and also identified for two of the test fluids used, a limiting shear stress, τ_c, at which the shear stress levelled out at high strain rate, suggestive of plastic yield behaviour. This limiting shear stress increases linearly with mean pressure of the lubricant film. Incorporating τ_c into Johnson and Tavaarwerk's model gives equation (2.40), where Λ_e describes the proportionality between τ_c and mean pressure [23, 30, 31].

$$\tau = \min\left[\tau_e \sinh^{-1}\left(\frac{\eta_p}{\tau_e}\left(\dot{\gamma} - \frac{1}{G_e}\frac{d\tau}{dt}\right)\right), \Lambda_e p\right] \tag{2.40}$$

The main disadvantage of using EHL friction to determine fluid rheology is that the friction measured is a composite value of shear stress integrated over a wide range of conditions within the contact [23].

An approach to analyse EHL friction data is to assume that the whole film is at the mean Hertz contact pressure, although, in practice, pressure varies greatly over an EHL contact and at high loads and low speeds can be approximated to the Hertz pressure distribution. Equations are provided by Hirst and Richmond when Hertz pressure distribution is valid. The mean shear stress can be obtained by allowing η_p to vary with pressure over a contact, and for a point contact and Eyring shear thinning this gives [23, 32]:

$$\bar{\tau} = \frac{F}{A} = \frac{2\pi\tau_e}{\pi b^2}\int_0^b r \sinh^{-1}\left(\frac{\eta_p \dot{\gamma}}{\tau_e}\right) dr \tag{2.41}$$

When $\tau > 1.5\tau_e$, this becomes

$$\bar{\tau} = \frac{F}{W} = \frac{2\pi\tau_e}{\pi b^2}\int_0^b r \ln\left(\frac{2\eta_p \dot{\gamma}}{\tau_e}\right) dr \tag{2.42}$$

According to Hertz theory, for a point contact:

$$p = p_{max}\sqrt{1 - \frac{r^2}{b^2}} \tag{2.43}$$

Assuming this pressure distribution, the Barus viscosity-pressure equation and integrating equation (2.42) we obtain

$$\bar{\tau} = \tau_e\left(\ln(\dot{\gamma}) + \ln\left(\frac{2\eta_0}{\tau_e}\right) + \frac{2\alpha^* p_{max}}{3}\right) \tag{2.44}$$

Since $p_{mean} = 2/3 \cdot p_{max}$, equation (2.44) is identical to equation (2.38).

2.6.2 Rheology from high-stress viscometers

Bair and Winer developed three high-pressure rheometers based on shear fluid between a moving piston and a stator [33]. These rheometers were used to explore the elastic and viscous behaviour of three base fluids. At high pressure and low temperature, up to about 50 °C above the glass transition temperature, all the lubricants behaved as elastic solids until the initial application of stress, with an apparent yield stress that increased with pressure, temperature and strain rate. It was also showed that at higher temperature and lower pressure, all lubricants showed shear thinning behaviour above a shear stress of approximately 10 MPa, tending towards a limiting shear stress of τ_L, that increases linearly with pressure and decreased with temperature. Equation (2.45) was proposed based on an asymptotic shear thinning expression combined with a viscoelastic term [23, 33].

$$\dot{\gamma} = \frac{1}{G_p}\frac{d\tau}{dt} - \frac{\tau_L}{\eta_p}\ln\left(1 - \frac{\tau}{\tau_L}\right) \tag{2.45}$$

This equation can be rearranged in terms of shear stress as:

$$\tau = \tau_L\left(1 - e^{-\frac{\eta_p}{\tau_L}\left(\dot{\gamma} - \frac{1}{G_p}\frac{d\tau}{dt}\right)}\right) \tag{2.46}$$

Another method to study the lubricant rheology at high shear stresses was developed by Ramesh and Clifton. The compression and shear waves transmitted from the impact of two flat

plates separated by a thin film of lubricant were measured and from this, it was possible to monitor the shear stress and strain of the film over a timescale of less than a millisecond. This approach, however, couldn't directly study the variation of shear stress with strain rate and applied only very small amounts of shear [23, 34].

Bair and Winer developed a new high-pressure viscometer in order to reach controlled high strain rates. This new viscometer addressed the problem of heating of the lubricant during shear and the consequent reduction in effective reduction. The same pattern of shear stress versus strain rate behaviour was found for the two fluids that were studied, as noted at higher pressures and lower strain rates. By combining this data with some taken at very high pressures and low strain rates, Bair and Winer suggested that the transition from Newtonian to plastic behaviour described in equation (2.46) broadened was the pressure was increased. A modification to the equation was proposed to accommodate this [23, 35, 36].

More changes were made to the viscometer to prevent significant temperature increase in the cylinder due to the flash temperature effects in the cylinder walls. Bair also suggested the use of the reduced Carreau-Yasuda equation:

$$\tau = \frac{\eta_p \dot{\gamma}}{\left(1 + \left(\frac{\eta_p \dot{\gamma}}{\tau_0}\right)^a\right)^{(1-n)/a}} \tag{2.47}$$

the coefficients a and n are constants.

Bair added a pressure-dependent, limiting shear stress to the Carreau-Yasuda model:

$$\tau = \min\left[\dot{\gamma}\eta_p \left[1 + \left(\frac{\eta_p \dot{\gamma}}{\tau_0}\right)^a\right]^{(n-1)/a}, \Lambda_c p\right] \tag{2.48}$$

2.6.3 Friction in lubrication regimes

2.6.3.1 Friction force in elastohydrodynamic lubrication

The friction in this regime is caused by shearing the lubricant in the contact. The friction force is obtained by integrating the shear stress over the contact area, by using the Eyring model, equation (2.36), the friction force generated by the elastohydrodynamic is obtained by [16]:

$$F_{f,EHL} = \int\int_{A_H} \tau_e \sinh^{-1}\left(\frac{\eta_p \dot{\gamma}}{\tau_e}\right) dA \tag{2.49}$$

This can be expressed as:

$$F_{f,EHL} = \tau_e A_H \sinh^{-1}\left(\frac{\eta_p \dot{\gamma}}{\tau_e}\right) \tag{2.50}$$

2.6.3.2 Friction force in boundary lubrication

The friction in this regime is caused by shearing the boundary layer between the contacting asperities. Integrating τ_c over the asperity contact area we obtain [16]:

$$F_{f,BL} = \sum_{i=1}^{N} \int \int_{A_{Ci}} \tau_{Ci} dA_{Ci} \tag{2.51}$$

Considering that the friction force in the asperity contact to be of Coulomb type, $\tau_{Ci} = f_C \cdot p_{Ci}$, with a constant value for the coefficient of friction f_C, the friction force can be expressed as:

$$F_{f,BL} = f_C \sum_{i=1}^{N} \int \int_{A_{Ci}} p_{Ci} dA_{Ci} = f_C F_C \tag{2.52}$$

where f_C is determined experimentally [16].

Equation (2.52) gives us the value of the friction force for simple sliding contacts. Taking the slip for the boundary lubrication, there is no theoretical model for rolling to sliding contacts. The slip will be incorporated in the shear rate, this way the coefficient of friction will be [16]:

$$\mu = f_C \frac{2}{\pi} \tan^{-1}\left(\frac{\pi}{2} \frac{SRR}{SRR_{ep}}\right) \tag{2.53}$$

where SRR_{ep} is a parameter that is determined experimentally that is a measure for the transition from elastic to plastic behaviour of the boundary layer. So combining equations (2.52) and (2.53) we have the expression for the friction force in the boundary lubrication regime [16]:

$$F_{f,BL} = f_C F_C \frac{2}{\pi} \tan^{-1}\left(\frac{\pi}{2} \frac{SRR}{SRR_{ep}}\right) \tag{2.54}$$

2.6.3.3 Friction force in mixed lubrication regime

The friction force in the mixed lubrication regime is given by the sum of the friction force generated by the asperities in contact and the friction that is generated by the shearing of the lubricant [16]:

$$F_{f,ML} = F_{f,BL} + F_{f,EHL} \tag{2.55}$$

Substituting equations (2.50) and (2.54) in (2.55), the coefficient of friction in the mixed lubrication regime will be given by [16]:

$$\mu = \frac{f_C F_C \frac{2}{\pi} \tan^{-1}\left(\frac{\pi}{2} \frac{SRR}{SRR_{ep}}\right) + \tau_e A_H \sinh^{-1}\left(\frac{\eta_p \dot{\gamma}}{\tau_e}\right)}{F_N} \tag{2.56}$$

2.7 Mixed film lubrication coefficient of friction prediction

As it was seen, the mixed lubrication regime can be given by equation (2.56), however, a simpler equation can be obtained for the mixed lubrication regime. By writing equation (2.55) in terms of traction, the following equation is obtained [37]:

$$\overline{\tau} \cdot A_0 = \tau_s \cdot A_s + \tau_f \cdot A_f \tag{2.57}$$

$$\overline{\tau} = \tau_s \cdot \frac{A_s}{A_0} + \tau_f \cdot \left(1 - \frac{A_s}{A_0}\right) \tag{2.58}$$

This results in:

$$\overline{\mu} = \frac{1}{p} \cdot \left[\tau_s \cdot \frac{A_s}{A_0} + \tau_f \cdot \left(1 - \frac{A_s}{A_0}\right)\right] \tag{2.59}$$

By rewriting $\xi = A_s/A_0$ and introducing solid and fluid coefficient of friction, μ_{bl} and μ_{EHL}, equation (2.59) can be rewritten as [37]:

$$\mu = \xi \cdot \mu_{bl} + (1 - \xi) \cdot \mu_{EHL} \tag{2.60}$$

with ξ being the load sharing.

2.7.1 Diab

The friction in the mixed film regime will be determined while using the equation (2.60). The ξ variable is determined by using equation (2.61) [37].

$$\xi = erfc(\Lambda) \tag{2.61}$$

2.7.2 Doleschel

While using the Doleschel film parameter, the friction in the mixed film regime can be determined while using the same equation (2.60). However the ξ variable is determined by the following equation:

$$\xi = \left(1 - \frac{\Lambda}{2}\right)^2 \tag{2.62}$$

2.7.3 Matsumoto

Using the Matsumoto film parameter, the friction in the mixed film regime can be determined using the same equation (2.60). The variable ξ is determined by: [37]

$$\xi = 0.5 \cdot \log_{10}\left(\frac{1}{\Lambda}\right) \tag{2.63}$$

2.7.4 Experimental ξ

By rearranging equation (2.60), an experimental equation for ξ can be obtained:

$$\xi_{exp} = \frac{\mu_{exp} - \mu_{EHL}}{\mu_{bl} - \mu_{EHL}} \tag{2.64}$$

Chapter 3

Experimental Work

Three types of experiments were made, one to measure the surface roughness, one to measure the film thickness and finally one to measure the coefficients of friction.

For the surface roughness measurements, the HOMMELWERKE equipment was used. For each steel disc three measurements were made and an average of these three measurements was performed to obtain the surface roughness parameters. These measurements were made by using a diamond tipped instrument.

The experiments for the film thickness and coefficients of friction were performed using the PCS Instruments EHD2 Ultra Thin Film Measurement System, as seen in figure 3.1.

Figure 3.1: PCS Instruments EHD2 Ultra Thin Film Measurement System

For these two experiments two lubricants were used. A PAO ISO VG 150 and an ester oil denominated as Trioctyl Trimellitate, that for now on will be denominated as TOTM.

This equipment performs two measurements for each experiment. The first measurement starts recording the results from the highest rolling speed to the lowest rolling speed, while the second measurement records the results from the lowest rolling speed to the highest rolling speed. The highest rolling speed used was of 3000 mm/s and the lowest was 10 mm/s. The measurements were made by using logarithmic intervals, with each measurement having 21 points.

The measurement of film thickness is done by a process of optical interferometry. The principle behind it is the following. A steel ball is loaded against a rotating spacer layer disc, the contact that originates between the ball and disc is illuminated by a white light source that is directed down a microscope through the disc on to the contact. The disc has a silica (SiO_2) layer and a Chromium (Cr) layer, so part of the light is reflected from the Cr layer and part travels through the SiO_2 layer and fluid film and is reflected back from the steel ball. The two light paths are recombined and an interference image is formed, which is passed into a spectrometer and a high-resolution monochrome CCD camera. The camera image is captured by a video frame grabber and analysed by the control software to determine the film thickness.

The film thickness is calculated by measuring the wavelength of the light returned from the central plateau of the contact and hence calculating the central film thickness.

3.1 Film Thickness

For the film thickness experiments, two types of discs were used, a glass disc and a sapphire disc.

The experiments with the glass disc were made as depicted in the flowchart represented in figure 3.2, a total of four experiments were made while using this type of disc.

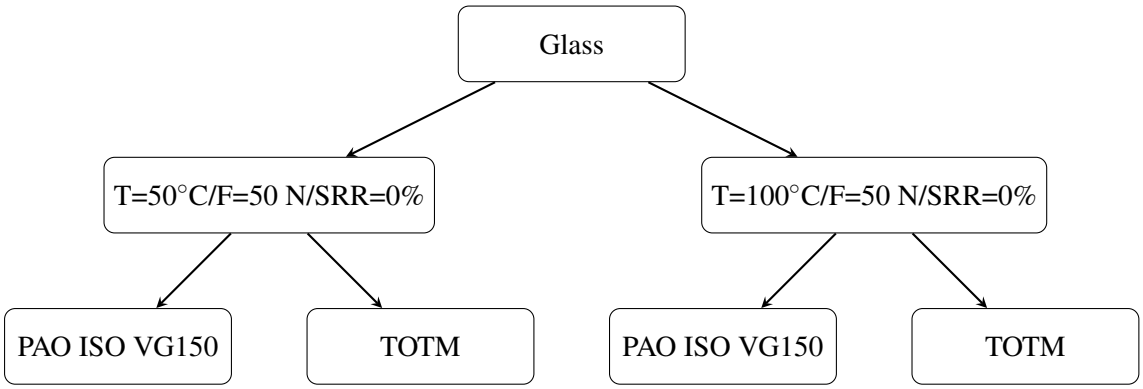

Figure 3.2: Flowchart of the experiments used to measure the film thickness in glass

More experiments were made for the sapphire disc than the glass disc. A total of ten experiments were made while using the sapphire disc. The configurations of these experiments are showed in figure 3.3. For simplification reasons, O1 is referencing the PAO ISO VG 150 lubricant while O2 is referencing the TOTM lubricant.

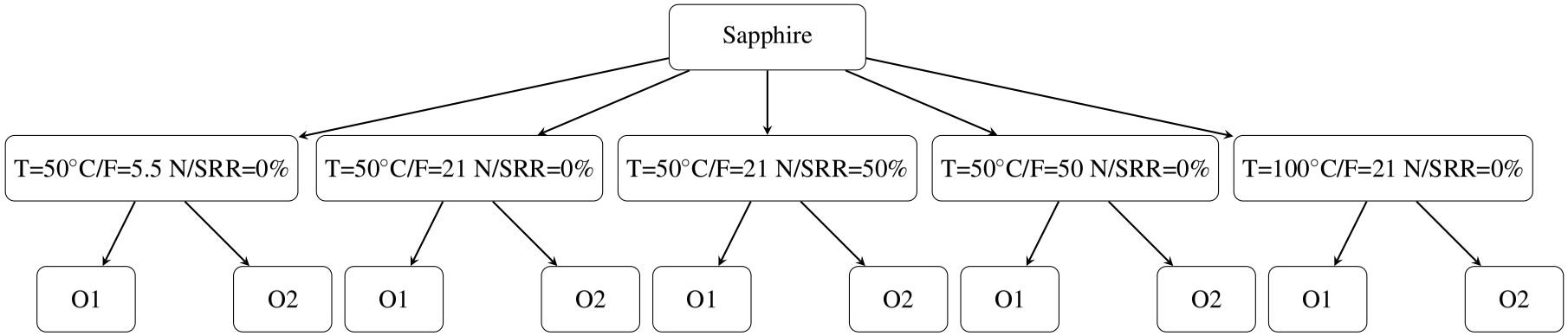

Figure 3.3: Flowchart of the experiments used to measure the film thickness in sapphire

3.2 Coefficients of Friction

As said before, the coefficients of friction experiments were made while using the same two lubricants. However, the discs used for these experiments were different from the ones used for the film thickness experiments. Instead of glass and sapphire discs, three steel discs with different surface roughness were used, denominated as Steel Disc 1, Steel Disc 2 and Steel Disc 3.

The experiments that were made while using each type of steel disc were made as depicted in the flowchart represented in figure 3.4

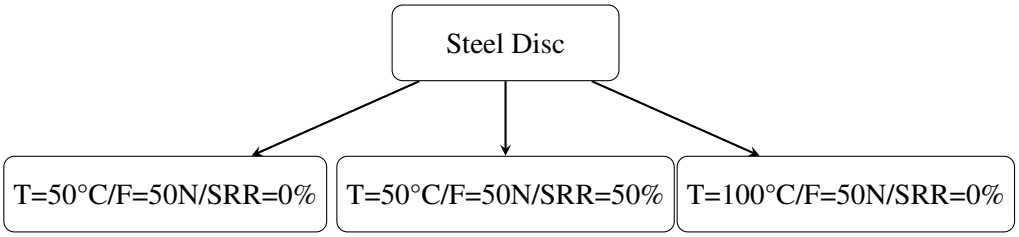

Figure 3.4: Flowchart of the experiments used to measure the coefficients of friction

All of these experiments were made while using two balls with different surface roughness.

3.3 Elements used for the measurement of film thickness and coefficients of friction

In order to calculate the film thickness, the properties of the discs and ball used must be known.

For the measurement of the film thickness, two different discs were used, a glass disc and a sapphire disc. The same steel ball was used for both experiments.

The next table shows the properties of these elements.

Table 3.1: Properties of elements used for the measurement of the film thickness

Element	E / GPa	ν	R_x / mm
Steel Ball	207	0.29	19.05
Glass Disc	75	0.22	∞
Sapphire Disc	675	0.29	∞

For the coefficients of friction experiments, three types of steel discs with different surface roughness were used, as well of two types of steel balls with different surface roughness as well.

Table 3.2 shows the different types of surface roughness for each element used in the coefficient of friction experiments. It's important to note that it wasn't possible to measure the surface roughness for the steel balls due to it's curvature. Since the tabulated value of the steel balls were the same as two of the steel discs (Steel Disc 1 and Steel Disc 3), the surface roughness values obtained for these steel discs were used on the steel balls. All of the values were obtained using a cut-off length of 0.8 mm for all discs.

Table 3.2: Surface Roughness for the Elements

Element	R_a / μm	R_q / μm	R_z / μm	R_{pk} / μm
Steel Disc 1	0.025	0.030	0.275	0.051
Steel Disc 2	0.074	0.101	0.665	0.049
Steel Disc 3	0.300	0.506	3.092	0.103
Steel Ball 1	0.025	0.030	0.275	0.051
Steel Ball 2	0.300	0.506	3.092	0.103

3.4 Lubricant Properties

In order to analyse the film thickness and the coefficients of friction, the lubricant properties must be known.

3.4.1 Properties of the PAO ISO VG 150

To measure the viscosity of the PAO ISO VG 150 lubricant, the SV10 method was employed. This method allowed to known the viscosity of the oil between the temperatures of 100°C and 40°C.

The following equation is then employed to obtain the corrected dynamic viscosity of the lubricant:

$$\eta = \frac{\eta_{experimental} \cdot \rho_{water}}{\rho_{lubricant}} \tag{3.1}$$

To kinematic viscosity of the lubricant is simply determined by dividing the dynamic viscosity by the density of the lubricant, as shown in equation (3.2).

$$\nu = \frac{\eta}{\rho} \tag{3.2}$$

The piezoviscosity coefficient was calculated according to Gold's equation:

$$\alpha^* = s \cdot \nu^t \cdot 10^{-9} \tag{3.3}$$

Where s and t are constants that are related to the type of lubricant used. This parameters are showed in Table 3.3.

Table 3.3: Values of s and t

Lubricant	s	t
Mineral	9.9040	0.1390
PAO	7.3820	0.1335
ESTER	6.6050	0.1360

Since this lubricant is a PAO, the values used in equation (3.3) will be $s = 7.3820$ and $t = 0.1335$.

To calculate the thermoviscosity coefficient the standard ASTM D341 was employed. With this standard, the thermoviscosity is calculated with the following equation:

$$\beta = \frac{m}{T}\frac{(\nu + a)}{\nu}\ln(\nu + a) \tag{3.4}$$

The constants m and a are lubricant depended constants, in which $a = 0.7$ cSt. To determine the constant m, equation (3.5) is employed.

$$m = \frac{\log_{10}\left[\frac{\log_{10}(\nu_0+a)}{\log_{10}(\nu_1+a)}\right]}{\log_{10}\left(\frac{T_1+273}{T_0+273}\right)} \tag{3.5}$$

T_0 and ν_0 are, respectively, the reference temperature of the lubricant at 40°C and the cinematic viscosity of the oil at 40°C. T_1 and ν_1 are the temperature and kinematic viscosity of the lubricant at 100°C.

Knowing that $\nu_0 = 146.96$ cSt and $\nu_1 = 18.85$ cSt and by using equation (3.5), the constant m will be 2.9586.

The thermal conductivity of the lubricant is given by equation (3.6). It's important to reference that T in this equation is given in °C instead of K.

$$k = \frac{0.12}{\rho_{lubricant}} \cdot \left(1 - 0.0005 \cdot \frac{T}{3}\right) \cdot \rho_{water} \tag{3.6}$$

Having all the necessary properties defined, a summary of the properties values is depicted in Table 3.4.

Table 3.4: Properties of PAO ISO VG 150

Density at 15°C, ρ/kg m^{-3}	853.8
Dynamic viscosity at 50°C, η/Pa s	$87.89 \cdot 10^{-3}$
Kinematic viscosity at 100°C, ν/cSt	18.85
Piezoviscosity at 50°C, α^*/Pa^{-1}	$1.3553 \cdot 10^{-8}$
Thermoviscosity at 50°C, β/K^{-1}	0.0421
Thermal conductivity at 50°C, k/ W/mK	0.1394

3.4.2 Properties of the TOTM

Unlike the PAO ISO VG 150 lubricant, the TOTM lubricant had already had its properties studies. It also had equations to predict its properties that delivered similar values to the experimental results. So experimental measurements weren't made for this lubricant.

To know the dynamic viscosity of the lubricant, equation (3.7) is employed.

$$\eta = A \exp\left(\frac{B}{T-C}\right) \tag{3.7}$$

In Table 3.5, the constants values are shown.

Table 3.5: Constant values for equation (3.7)

A	0.04612
B	1089.1988
C	168.7954

The kinematic viscosity will be also given by equation (3.2).

To calculate the piezoviscosity coefficient a linear regression was made using the experimental results. This linear regression resulted in the following equation:

$$\alpha^* = 8 \cdot 10^{-4} \cdot T - 0.1838 \cdot T + 24.246 \tag{3.8}$$

A small note, in equation (3.8), T represents the temperature in °C, instead of K.

The thermoviscosity coefficient is calculated by the same standard as used for the PAO ISO VG 150 lubricant, i.e., ASTM D341 standard.

Using equation (3.7) followed by equation (3.2), we can determine the kinematic viscosity of lubricant at 40°C and 100°C. This gives us $\nu_0 = 89.56$ cSt and $\nu_1 = 10.22$ cSt. So using equation (3.5), we can determine the constant m, which gives us that $m = 3.6092$.

Finally, the thermal conductivity is also given by equation (3.6).

A summary of the necessary properties to analyse the film thickness and coefficients of friction is given in Table 3.6.

Table 3.6: Properties of TOTM

Density at 15°C, ρ/kg m^{-3}	991.9
Dynamic viscosity at 50°C, η/Pa s	$53.51 \cdot 10^{-3}$
Kinematic viscosity at 100°C, ν/cSt	$10.22 \cdot 10^{-3}$
Piezoviscosity at 50°C, α^*/Pa^{-1}	$1.7056 \cdot 10^{-8}$
Thermoviscosity at 50°C, β/K^{-1}	0.0456
Thermal conductivity at 50°C, k/ W/mK	0.1231

Chapter 4

Film Thickness Results

The experiments to analyse the film thickness were done using a steel ball. The contact between the disc and a ball will be a point contact. This will mean that the theoretical value of the film thickness will be given by the Dowson-Hamrock equation for the centre film thickness, represented in equation (2.7).

The parameters U, G and W will be given by the following equations:

$$U = \frac{\eta \cdot u_e}{E^{'} \cdot R_x^{'}} \tag{4.1}$$

$$G = \alpha^* \cdot E^{'} \tag{4.2}$$

$$W = \frac{w_z}{E^{'} \cdot R_x^{'2}} \tag{4.3}$$

where $u_e = (u_b + u_d)/2$ and $E' = E/(1-\nu^*)$ for similar materials, for materials with different young's modulus $E^{'} = 2 \cdot ((1-\nu^{*2}_1)/E_1 + (1-\nu^{*2}_2)/E_2)^{-1}$.

4.1 Film Thickness on Glass Disc

As mentioned, a total of four experiments were made using this type of glass disc/steel ball configuration, as depicted in the flowchart present in Figure 3.2.

Following the flowchart, the first type of experiment that is going to be observed will be the one with the configuration with a temperature of 50 °C, a force of 50 N and a SRR of 0%.

From the results of the two measurements that were obtained while using the PAO ISO VG 150 lubricant, the first measurement, some points where the rolling speed was low, below 100 mm/s approximately, were deemed unnecessary because these points weren't following the trend line set by the points of the first measurement at higher rolling speeds as well as the points of the second measurement. Using the same lubricant, but increasing the temperature from 50 °C to 100 °C, while maintaining the force and SRR, another two measurements were obtained.

With the two measurements for each different configuration, an average was performed. This average will then be compared to a theoretical value that is given by the Dowson-Hamrock equation (2.7), for each of the configuration. This comparison can be seen in Figure 4.1.

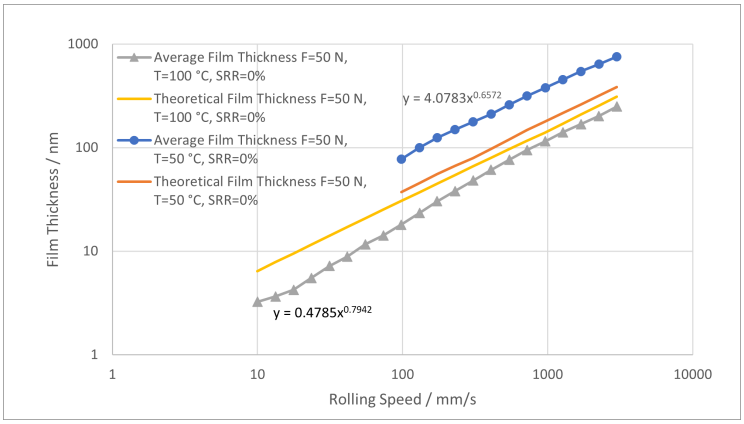

Figure 4.1: Comparison between the experimental and theoretical values using PAO ISO VG 150 using a glass disc

For a configuration of F=50 N, T=50 °C and a SRR=0%, the theoretical results and the average experimental film thickness have practically the same slope as it can be observed from the exponents from the equation of the trend line (0.6572) and the exponent from the dimensionless speed parameter from equation (2.7) (0.67). However, the experimental results have higher values than those that were predicted while using equation (2.7).

For a configuration of F=50 N, T=100 °C and a SRR=0%, the theoretical values are higher than the experimental values, and, although the theoretical results and the average experimental film thickness don't have the same slope, as it can be seen by the exponent of the trend line (0.7942), the values are much closer, specially at higher rolling speeds.

Comparing these two types of experiments, while using the same lubricant, it can be observed that with the increase of the temperature, the film thickness decreases. This is expected since with the increase in temperature, the viscosity of the lubricant decreases. The film thickness is proportional to the dynamic viscosity, as it can be seen in equations (2.7) and (4.1), so with the increase in temperature, the film thickness will decrease.

The two previous experiments will be repeated, but this time using the TOTM lubricant instead of the PAO ISO VG 150. In Figure 4.2, the operation of averaging of the two experimental results and comparison with the theoretical values can been seen.

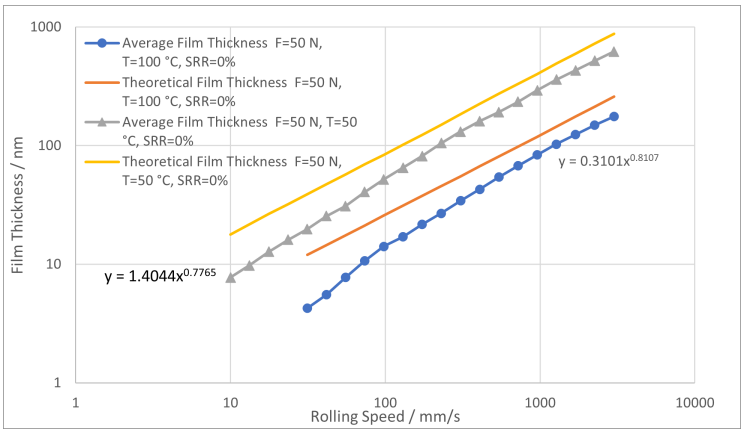

Figure 4.2: Comparison between the experimental and theoretical values using TOTM (1)

Observing Figure 4.2, the theoretical values F=50 N, T=50 °C and a SRR=0% are higher than the experimental results, with the values being closer at higher rolling speeds. Again, the slop of both results isn't the same, as it's possible to see from the exponent of the trend line and the exponent from equation (2.7).

The observations made F=50 N, T=100 °C and a SRR=0% are similar to the ones made for the previous configuration, i.e., the theoretical values are higher than the experimental results with the values getting closer with the increase in rolling speed and with the slope of both results not being the same, again by comparing the two exponents. Comparing these two glass discs experiments while using the TOTM lubricant, the same interpretations can be made. With the increase of temperature the film thickness decrease.

When comparing each type of test made with different lubricants, it can be observed that the film thickness, in a general way, is higher when using the lubricant PAO ISO VG 150. The principle is the same when comparing with temperatures, the higher the viscosity the higher is the film thickness. This is why the film thicknesses are higher when using the lubricant PAO ISO VG 150, because this lubricant is more viscous than the TOTM lubricant.

4.2 Film Thickness on Sapphire Disc

As previously mentioned, a total of ten experiments were made while using the sapphire disc/steel ball configuration. These experiments are depicted in the flowchart represented in Figure 3.3.

Calculating the average of both measurements and the theoretical values, again by using equation (2.7), a comparison between can be made. The comparison present in Figure 4.3 are for the experiments were the T=50 °C and SRR=0% but the force varies.

With F=5.5 N, the average experimental film thickness results and the theoretical values are very similar, with the theoretical values being lower than the experimental results at lower rolling speeds and higher than the experimental results at higher rolling speeds. Increasing the force from 5.5 N to 21 N, it can be observed that, once more, that the average experimental film thicknesses results and the theoretical film thickness values are very much the same for low rolling speeds.

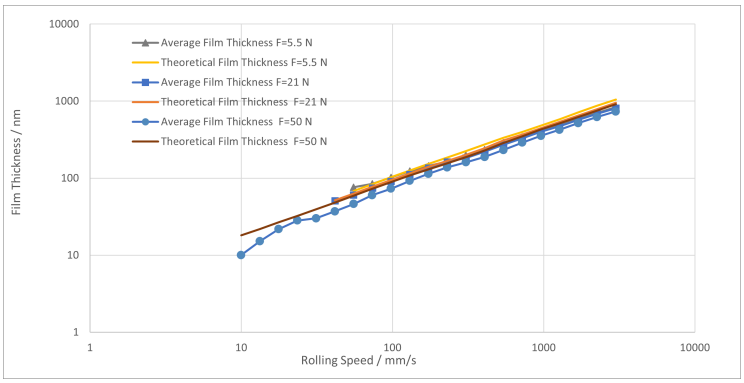

Figure 4.3: Comparison between the experimental and theoretical values using PAO ISO VG 150, T=50 °C and SRR=0%

In higher rolling speeds, the theoretical film thickness values are slightly higher. The slope of the experimental results is closer to the theoretical value than with F=5.5 N, as it can be seen by the exponent of the trend line. For F=50 N, the theoretical film thicknesses values are similar to the average of the experimental results at high rolling speeds, with a considerably deviation at lower rolling speeds. Because of this the slope is different between the theoretical and experimental results, as it can be seen the exponents.

When comparing these types of experiments, the increase in force causes a decrease in film thickness, this is expected since analysing Dowson-Hamrock centre film thickness equation, equation (2.7), it's possible to observe that the film thickness is inversely proportional to the force. So if the force increases, the film thickness decreases.

Figure 4.4 shows the comparison for the experiments were the F=21 N but the other variables vary.

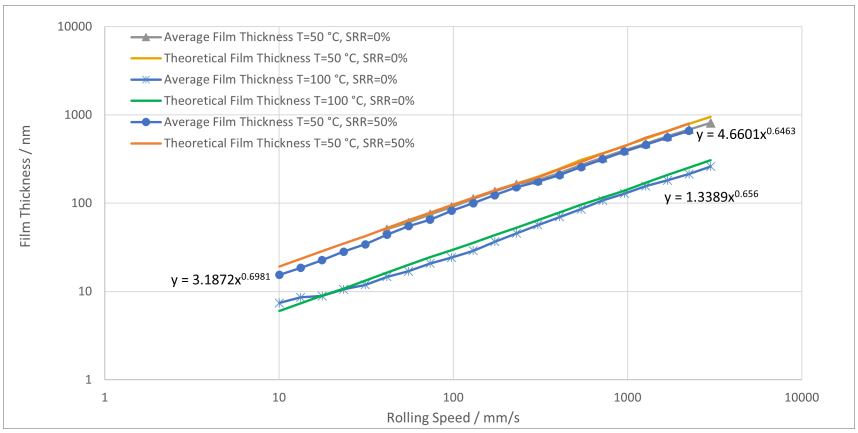

Figure 4.4: Comparison between the experimental and theoretical values using PAO ISO VG 150, F=21 N

For these experiments the theoretical film thickness results and the average film thickness are pretty much identical, the slopes are also very identical between them, as it's possible to see by the exponents.

Is possible to see that the variation of the SRR doesn't seem to cause a significant difference in the values of the film thickness. Like it happened before, the increase in temperature has a decreasing effect on the film thickness.

Changing the type of lubricant from PAO ISO VG 150 to TOTM, all of the experiments previously performed were repeated. These results can be observe in Figure 4.5.

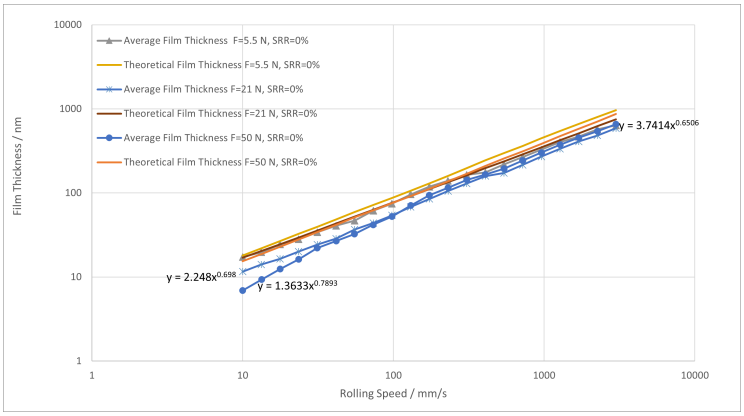

Figure 4.5: Comparison between the experimental and theoretical values using TOTM, T=50 °C and SRR=0%

The average experimental results and the theoretical values are very similar in all of the experiments. The slopes obtained are also very identical except for the configuration with a force of 50 N, where the exponent of the trend line equation is 0.7893, very different from the theoretical equation where is 0.68.

Although the results are very similar for all of the configurations, is possible to understand that, like before, with the increase in force the film thickness decreases until it reaches a rolling speed of approximately 500 mm/s. Afterwards it's possible to observe that there is a switch and with a higher force the film thickness is bigger.

Like it was done previously, Figure 4.6 shows the comparison for the experiments were the F=21 N but the other variables vary.

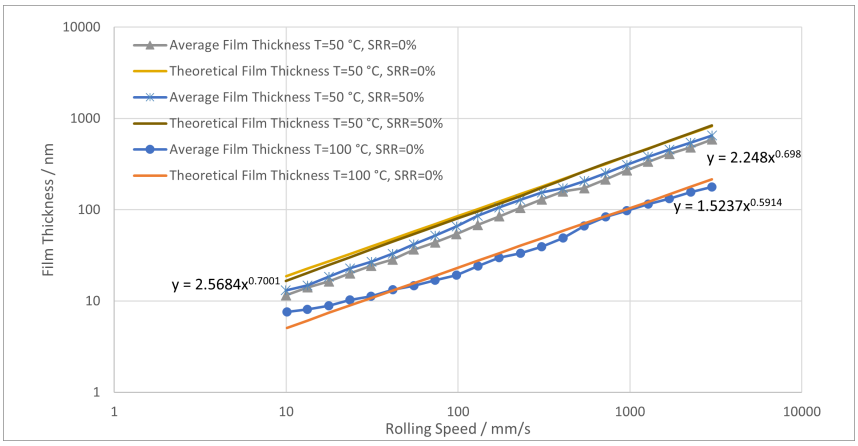

Figure 4.6: Comparison between the experimental and theoretical values using TOTM, F=21 N

In this figure it's possible to notice that, in a general way, the slope of the average experimental film thicknesses and theoretical film thickness values are very identical except for the T=100 °C, SRR=0% configuration, as it's possible to see the exponent of the trend line equation is 0.5914.

Again, the variation of SRR doesn't appear to change significantly the film thickness, although with TOTM there was slightly increase and with PAO ISO VG 150 there was slight decrease in film thickness. As seen, the increase in temperature causes a decrease in film thickness.

4.3 Summary

Analysing all of the experiments that were performed with different discs and configurations, as well as the two type of lubricants, some conclusions can be drawn out.

When the temperature increases the film thickness decreases. As it was explained before, with the increase in temperature comes a decrease in the viscosity of the lubricant. By analysing Dowson-Hamrock equation, represented in equation (2.7), the film thickness is directly proportional to the dimensionless parameter U. It's known by equation (4.1) that the parameter U is directly related to the dynamic viscosity of the lubricant. So with the increase in temperature, U decreases and so does the film thickness.

It's also seen that with the increase in force comes a decrease in film thickness. Again, by analysing the Dowson-Hamrock equation it's possible to state that the film thickness is inversely proportional to the dimensionless parameter W, which in turn is directly proportional to the applied force of the contact, meaning that with an increase in force there is an increase in the dimensionless parameter W, provoking a decrease in film thickness.

The influence of the SRR in the film thickness doesn't appear to a have a clear influence since in the experiments where the SRR changed, the film thickness changed ever so slightly and with different results in both experiments, since in one it increased and the other one it decreased.

Another conclusion that was not mentioned before but it's very obvious is that the increase in the rolling speed causes an increase in film thickness.

Finally another conclusion that can be drawn out is that the film thickness in sapphire is slightly higher than in glass. This is because the effective Young's modulus will be higher when considering the sapphire disc. All of the dimensionless parameters are related to E', however when expanding equation (2.7), it's possible to observe that the film thickness is directly proportional to the effective young's modulus, although it doesn't have a significant weight on it. Which is proven since the film thicknesses are higher in sapphire but not by much.

In the following table, a summary can be found regarding the stated observations.

Table 4.1: Film Thicknesses observations

Variable	Type of Change	Effect on Film Thickness
Temperature	Increase	Decrease
Temperature	Decrease	Increase
Force	Increase	Decrease
Force	Decrease	Increase
Rolling Speed	Increase	Increase
Rolling Speed	Decrease	Decrease
Effective Young's Modulus	Increase	Increase
Effective Young's Modulus	Decrease	Decrease

Chapter 5

Coefficients of Friction Results

As it can be seen in the flowchart presented in Figure 3.4, three experiments were made. However, after a preliminary analysis, it was noticed that for SRR=0% values the obtained coefficient of friction are pretty much zero. So experiments where the SRR=0% were discarded and only the results where SRR=50% were considered.

As it was referred in chapter 2, it's possible to predict the coefficient of friction in a mixed film lubrication regime by using equation (2.60). Each film parameter is calculated using a specific equation, as previously shown in chapter 2, and each of this parameters has a domain. In Table 5.1, a brief summary of the formulation can be seen. For the following sections it's considered that the domain of each film parameter holds true and the load sharing values (μ_{bl} and μ_{EHL}) are determined by the values of the coefficients of friction at each extreme point of the domain. The values for the load sharing function (ξ) must vary between 0 and 1.

Table 5.1: Specific film thickness formulation [37]

Author	Diab	Doleschel	Matsumoto
ξ	$\xi = erfc(\Lambda)$	$\xi = \left(1 - \frac{\Lambda}{2}\right)^2$	$\xi = 0.5 \cdot \log_{10}\left(\frac{1}{\Lambda}\right)$
Λ	$\Lambda = \frac{\phi_T \cdot h_c}{\sqrt{Rq_1^2 + Rq_2^2}}$	$\Lambda = \frac{h_c}{0.5 \cdot (Ra_1 + Ra_2)}$	$\Lambda = \frac{h_{min}}{Rz_1 + Rz_2}$
$\mathfrak{D}$	$\Lambda \in [0,3]$	$\Lambda \in [0,2]$	$\Lambda \in [0.01,1]$

5.1 Coefficients of Friction with Steel Ball 1- TOTM Lubricant

Like it was made for the film thickness, two measurements were made for each configuration, afterwards, an average was performed in all three coefficient of friction experiments and a comparison between the three steel discs was made. This comparison can be seen in Figure 5.1.

Analysing the data, it's possible to observe that the steel disc with the higher surface roughness, in other words steel disc 3, has the highest coefficient of friction out of the three discs, as expected, with the steel disc with the second highest surface roughness having the second highest coefficient of friction. Another observation that is possible to withdraw is that all of the steel discs tend to the same value of coefficient of friction with the increase of the rolling speed. This is explained by the contribution of the lubricant film thickness.

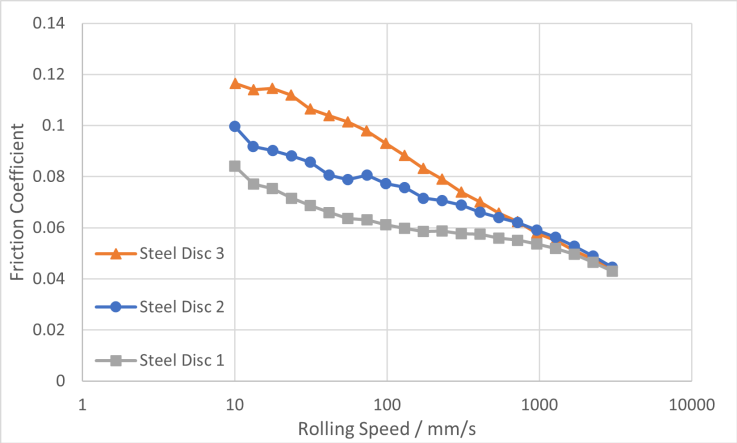

Figure 5.1: Coefficients of friction comparison between the three steel discs with Steel Ball 1 ($R_a = 0.025\ \mu$m) using TOTM

In order to determine the solid and fluid coefficient of friction, μ_{bl} and μ_{EHL}, each disc will be analysed for each specific film parameter in order to get the best values for the closest possible coefficient of friction prediction using equation (2.60). By observing Table 5.1, it's possible to see the domain for each of the coefficient friction predictions, so a value for the coefficient can be drawn out. For example, the Diab film parameter has a domain of $\Lambda \in [0,3]$, so by analysing the results of the coefficient of friction at these two values of Λ, a value can be reached. The same is true for the other film parameters in their corresponding domains. Of course this isn't a true value but an approximation, since the results don't reach $\Lambda = 0$.

For that, the stribeck curves for each specific film thickness will be analysed in order to choose the best coefficients.

Observing the stribeck curves for each specific film parameter and for each steel disc, it's possible to determine the solid and fluid lubrication coefficients that has the best approximation to the corresponding domain of the specific film parameter for each steel disc that was used.

These coefficients are shown in Table 5.2. An important aspect to notice is that the coefficients of friction in steel disc 1, for a SRR=50%, are essentially constant throughout the rolling speed, as seen in Figure 5.1, so the solid and fluid coefficients will be constant.

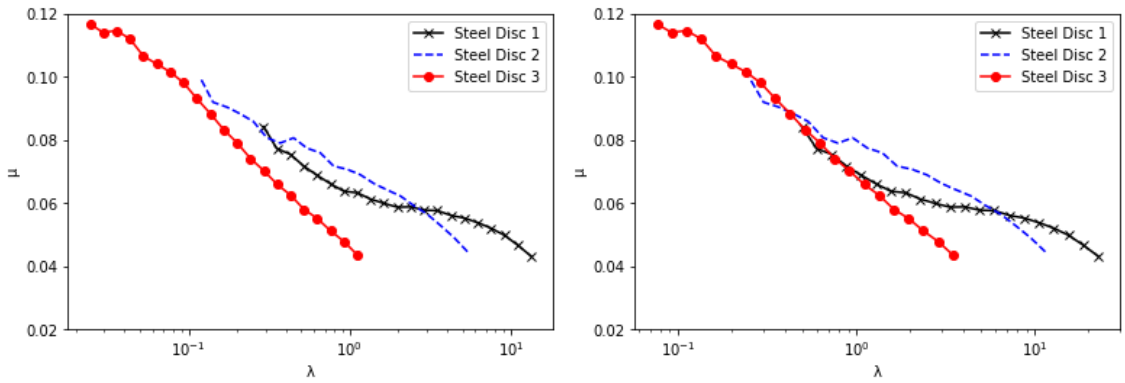

(a) Diab

(b) Doleschel

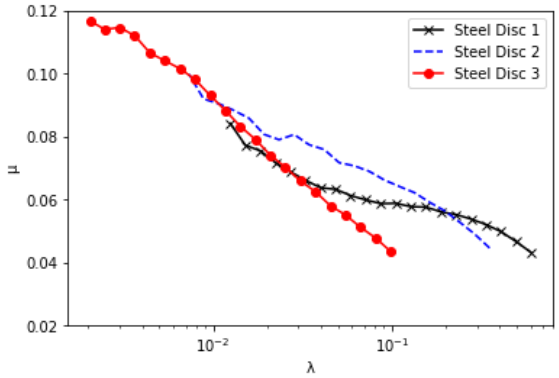

(c) Matsumoto

Figure 5.2: Stribeck Curves for Steel Ball 1 (TOTM)

Table 5.2: Solid and fluid coefficients (Steel Ball 1/TOTM)

		μ_{bl}	μ_{EHL}
Diab	Steel Disc 1	0.0950	0.0575
	Steel Disc 2	0.1000	0.0600
	Steel Disc 3	0.1200	0.0000
Doleschel	Steel Disc 1	0.1000	0.0600
	Steel Disc 2	0.1000	0.0700
	Steel Disc 3	0.1200	0.0550
Matsumoto	Steel Disc 1	0.0850	0.0350
	Steel Disc 2	0.0900	0.0350
	Steel Disc 3	0.0900	0.0000

As it can be seen in Figure 5.3, for steel disc 1, the coefficients of friction predictions made with the Diab and Doleschel film parameters are similar to the experimental results that were obtained. The Matsumoto film parameter also has good coefficient of friction prediction but it has a bigger difference in values when compared with the other two.

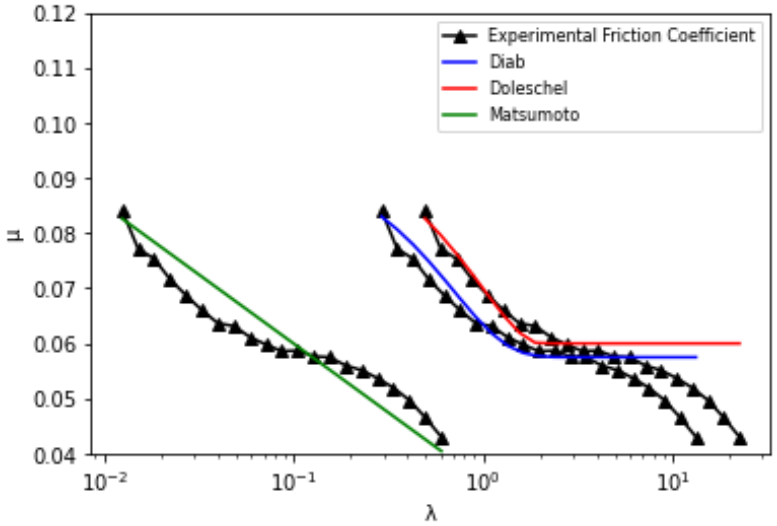

Figure 5.3: Experimental and predicted friction results with steel ball 1 ($R_a = 0.025\ \mu$m) and steel disc 1 ($R_a = 0.025\ \mu$m) (TOTM)

For steel disc 2, Figure 5.4, it's possible to see that the predicted coefficients of friction using the Matsumoto film parameter are very close to the experimental results. The Doleschel film parameter also has good approximations as well as the Diab film parameter, although a little worse than the the other two.

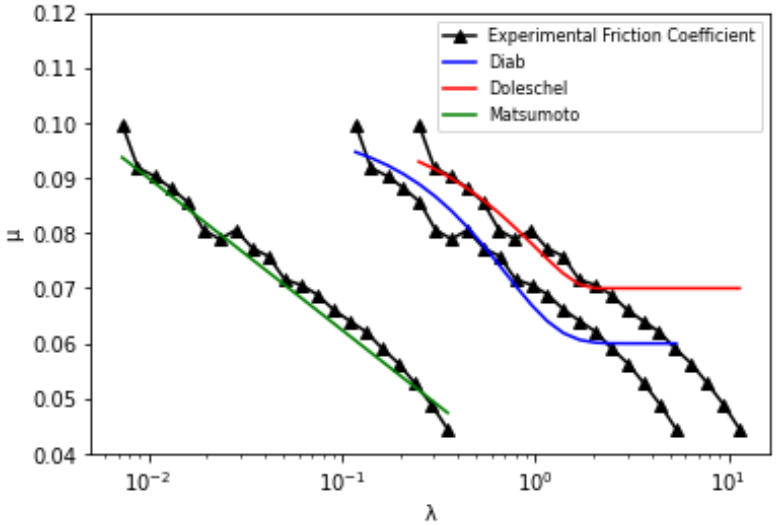

Figure 5.4: Experimental and predicted friction results with steel ball 1 ($R_a = 0.025\ \mu$m) and steel disc 2 ($R_a = 0.074\ \mu$m) (TOTM)

For steel disc 3, is possible to see by observing Figure 5.5 that the best predicted values for the coefficient of friction come from the Matsumoto film parameter. The Doleschel film parameter also has very good predictions for the coefficient of friction and the Diab film parameter has the worst predictions for the coefficient of friction.

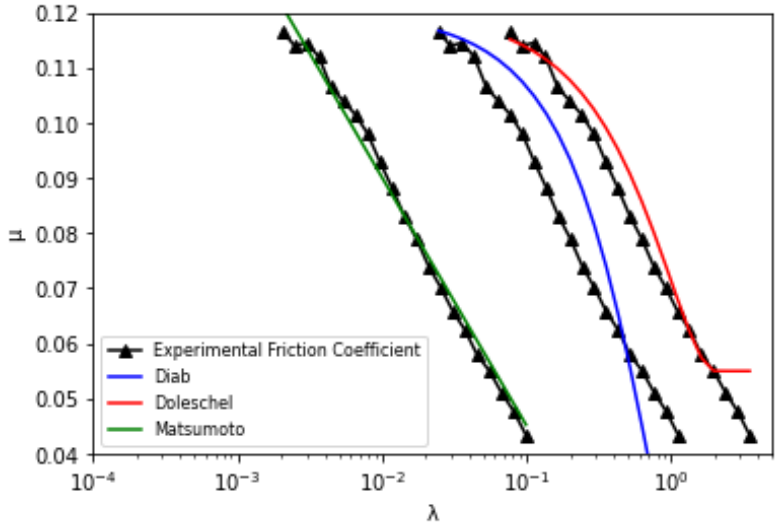

Figure 5.5: Experimental and predicted friction results with steel ball 1 ($R_a = 0.025$ μm) and steel disc 3 ($R_a = 0.300$ μm) (TOTM)

In Figure 5.6 is possible to see the experimental and theoretical ξ values. First of, is possible to see that the ξ values are between 0 and 1 for the domain of each film parameters. The Diab and Doleschel film parameters are pretty similar with the theoretical ξ values for the Doleschel film parameter following more closely the obtained experimental ξ. The ξ values for Matsumoto film parameter are also similar but it's the worst out of the three.

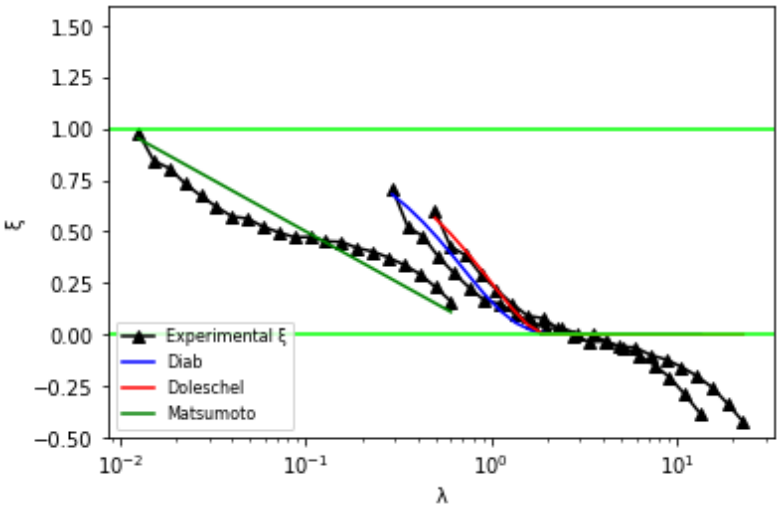

Figure 5.6: Experimental and theoretical ξ values with steel ball 1 ($R_a = 0.025$ μm) and steel disc 1 ($R_a = 0.025$ μm) (TOTM)

For steel disc 2 is possible to note by observing Figure 5.7 that the Matsumoto film parameter give the best theoretical ξ values. The Doleschel film parameters also have good theoretical values as well as the Diab film parameter, however, this last one give the worst out of the three.

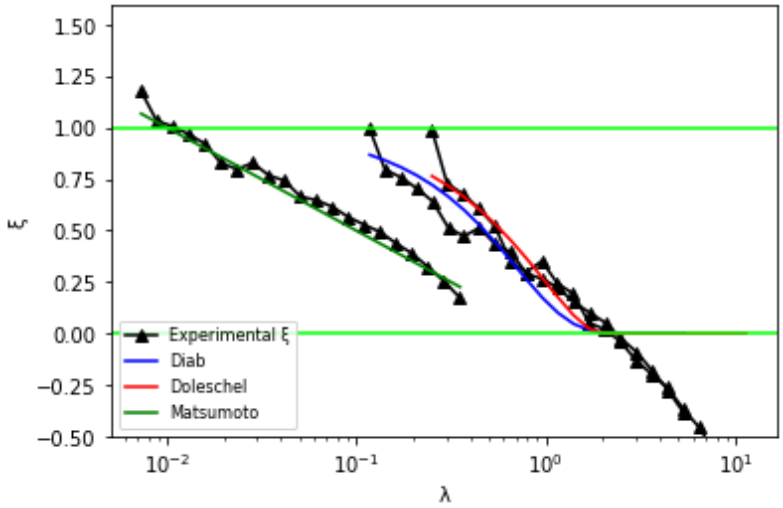

Figure 5.7: Experimental and predicted friction results with steel ball 1 ($R_a = 0.025$ μm) and steel disc 2 ($R_a = 0.074$ μm) (TOTM)

Observing Figure 5.8 is possible to note that, once more, the theoretical values for the ξ values using the Matsumoto film parameter are the ones that resembles more closely the experimental ξ values. Out of the three, the Diab film parameter has the worst theoretical ξ values.

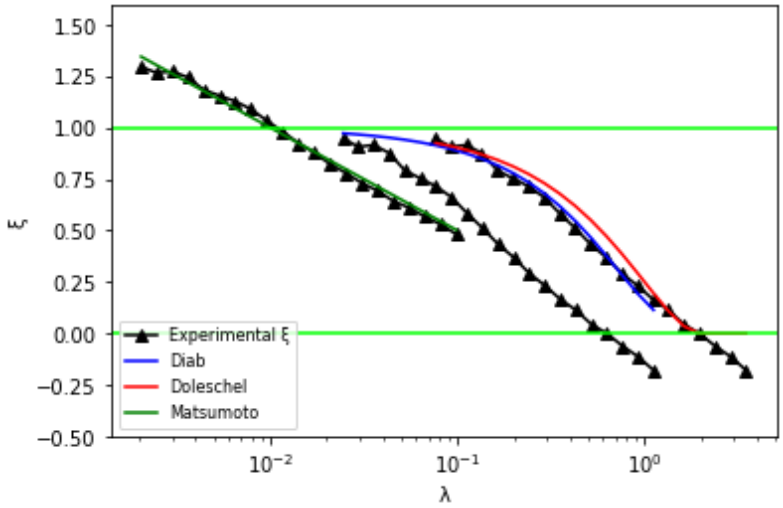

Figure 5.8: Experimental and predicted friction results with steel ball 1 ($R_a = 0.025$ μm) and steel disc 3 ($R_a = 0.300$ μm) (TOTM)

In Figures 5.9, 5.10 and 5.11, the relative errors for the coefficients of friction for the three film parameters. For all of the three film parameters is possible to observe that the errors for steel discs 1 and 2 are low (around 10% or lower). For the Doleschel and Matsumoto film parameters,

the error for steel disc 3 is also relative low, however, with the Diab film parameter this error is quite significant.

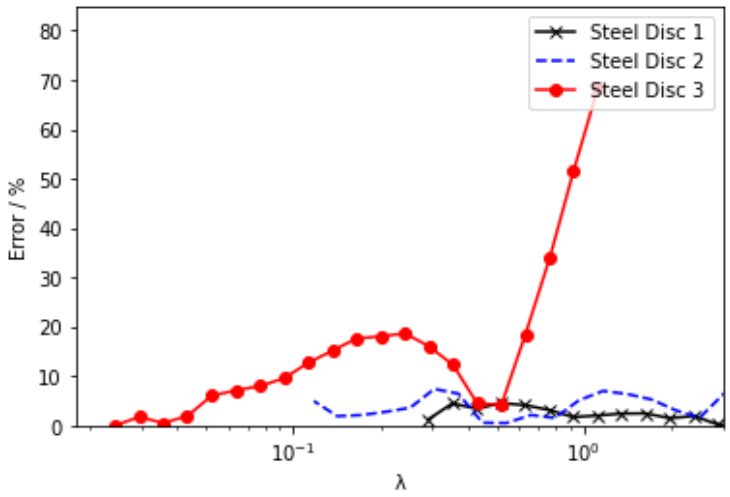

Figure 5.9: Relative error between the comparisons of friction values for Steel Ball 1 ($R_a = 0.025$ μm) and TOTM lubricant (Diab)

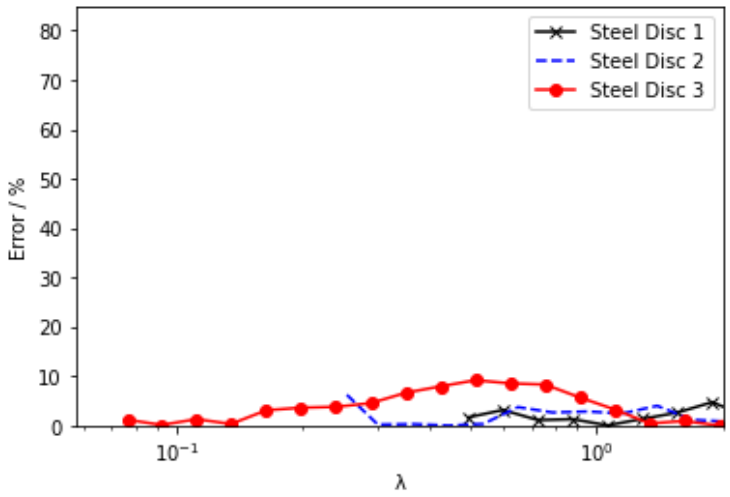

Figure 5.10: Relative error between the comparisons of friction values for Steel Ball 1 ($R_a = 0.025$ μm) and TOTM lubricant (Doleschel)

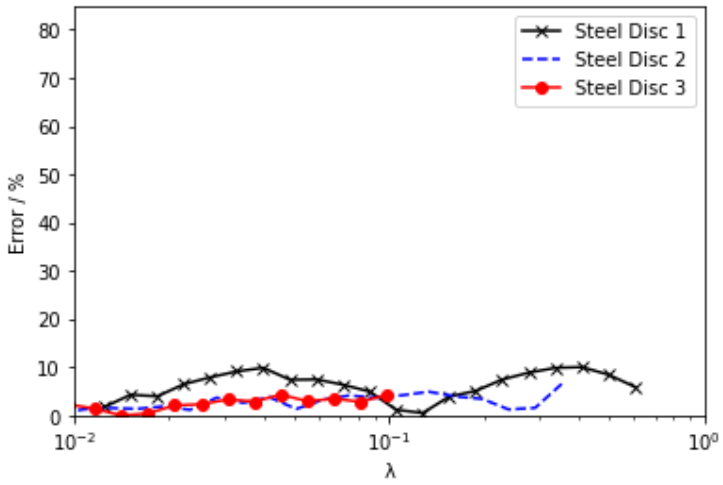

Figure 5.11: Relative error between the comparisons of friction values for Steel Ball 1 ($R_a = 0.025$ μm) and TOTM lubricant (Matsumoto)

5.2 Coefficients of Friction with Steel Ball 2- TOTM Lubricant

The comparison between the averages of all three steel discs coefficients of friction, while using the TOTM lubricant with a temperature of 50°C, a normal force of 50 N and a SRR of 50%, can be seen in Figure 5.12.

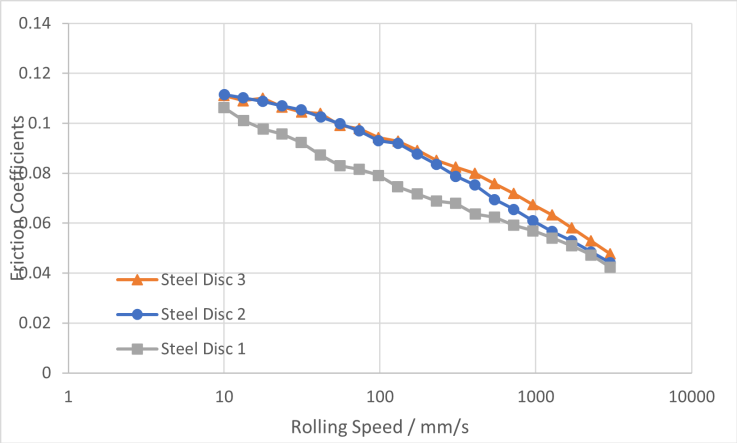

Figure 5.12: Coefficients of friction comparison between the three steel discs

Observing Figure 5.12, it's possible to see that all three steel discs have an identical value for the lowest rolling speed recorded, $u_e \approx 10$ mm/s, and they all to the same coefficient of friction with the increase in rolling speed. The values from steel disc 2 and steel disc 3 are very similar from 10 mm/s until approximately 200 mm/s. Once more, with the increase in rolling speed, the coefficient of friction decreases.

Once more, the solid and fluid coefficients of friction, μ_{bl} and μ_{EHL}, are chosen by analysing the stribeck curves for each specific film parameter in order to get the best values for the closest

possible coefficient of friction prediction using equation (2.60) that belong to the domain of the corresponding film parameter. These coefficients are present in Table 5.3.

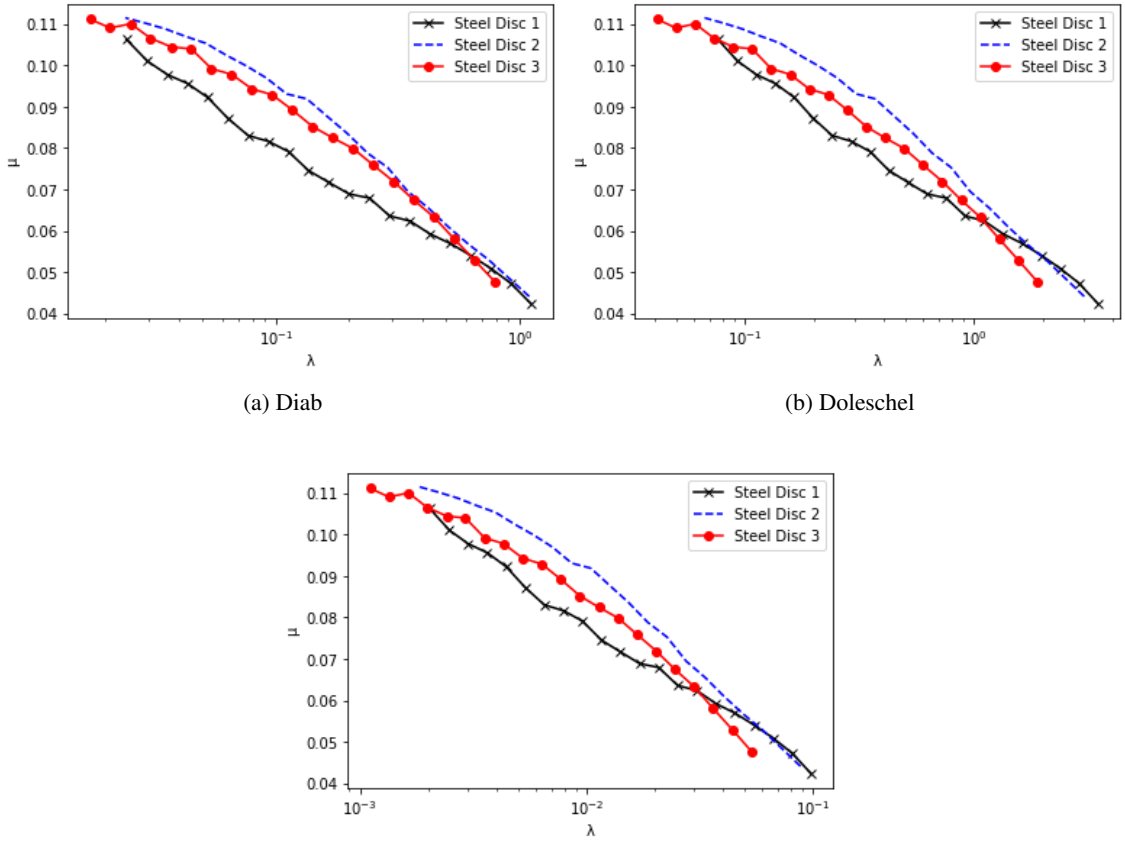

(a) Diab

(b) Doleschel

(c) Matsumoto

Figure 5.13: Stribeck Curves for Steel Ball 2 (TOTM)

Table 5.3: Solid and fluid coefficients (Steel Ball 2/TOTM)

		μ_{bl}	μ_{EHL}
Diab	Steel Disc 1	0.1000	0.0300
	Steel Disc 2	0.1100	0.0300
	Steel Disc 3	0.1100	0.0300
Doleschel	Steel Disc 1	0.1000	0.0550
	Steel Disc 2	0.1150	0.0550
	Steel Disc 3	0.1100	0.0450
Matsumoto	Steel Disc 1	0.0800	0.0200
	Steel Disc 2	0.0950	0.0000
	Steel Disc 3	0.0850	0.0000

In Figure 5.14 the comparison between the predicted and experimental values for steel disc 1 with a SRR=50% can be observed.

Observing these results, is possible to see that, for steel disc 1, the Matsumoto film parameter has predicted values that follow more closely the obtained experimental results. The predicted

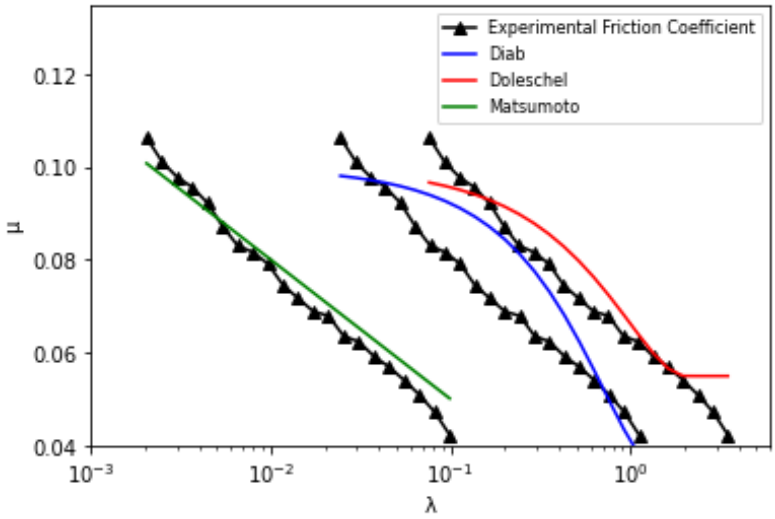

Figure 5.14: Experimental and predicted friction results with steel ball 2 ($R_a = 0.300$ μm) and steel disc 1 ($R_a = 0.025$ μm) (TOTM)

values using the Diab and Doleschel film parameters are very similar, however the values obtained using the Doleschel film parameter are closer to the experimental results.

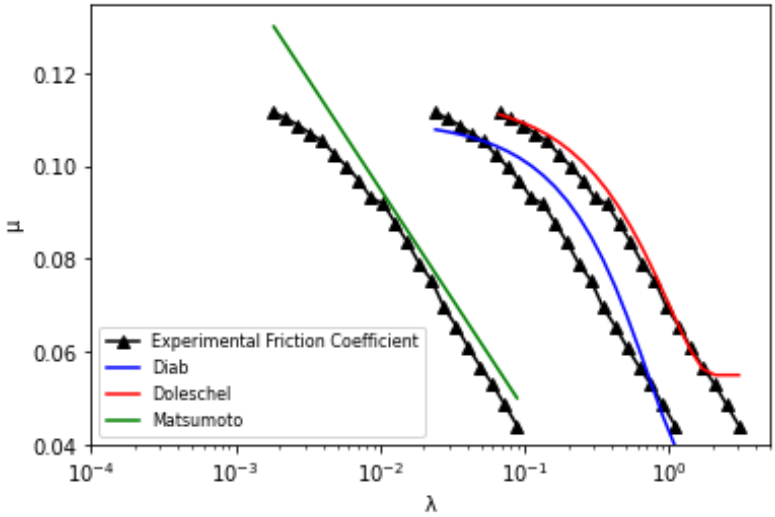

Figure 5.15: Experimental and predicted friction results with steel ball 2 ($R_a = 0.300$ μm) and steel disc 2 ($R_a = 0.074$ μm) (TOTM)

Observing the results provided by figure 5.15, is possible to see that, once more, the predicted values using the Diab and Doleschel film parameters are very similar but the Doleschel film parameter has a better prediction overall. The Matsumoto film parameter, for a higher value of Λ, has very good predictions, however, for lower values of Λ, the predictions are worse.

For steel disc 3, Figure 5.16, it's possible to see that the Doleschel film parameter is the parameter that has predicted coefficient of friction values that are more closely related in value to

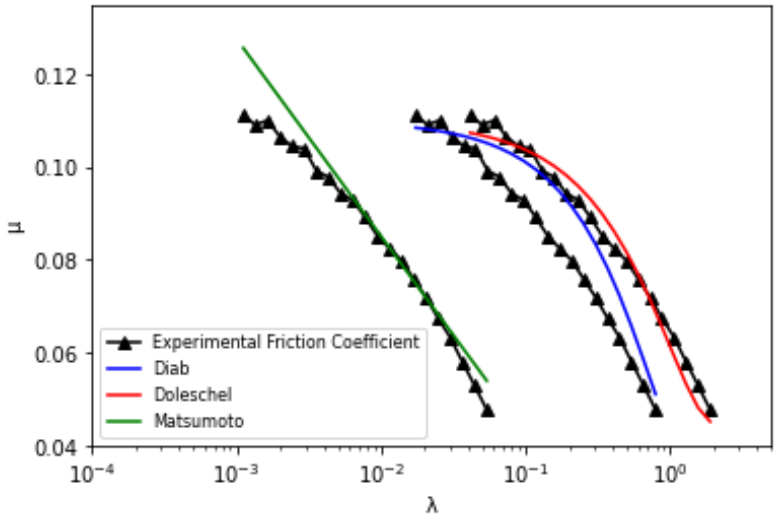

Figure 5.16: Experimental and predicted friction results with steel ball 2 ($R_a = 0.300\ \mu$m) and steel disc 3 ($R_a = 0.300\ \mu$m) (TOTM)

the experimental results. The Matsumoto film parameter also has very similar predicted coefficient of friction values, however, like previously, with lower Λ, the prediction tends to deviate from the experimental results quite significantly

In Figures 5.17. 5.18 and 5.19 the experimental and theoretical ξ values can be observed. For steel disc 1 is possible to note that the theoretical ξ values are more closely related to the experimental values for the Matsumoto film parameter.

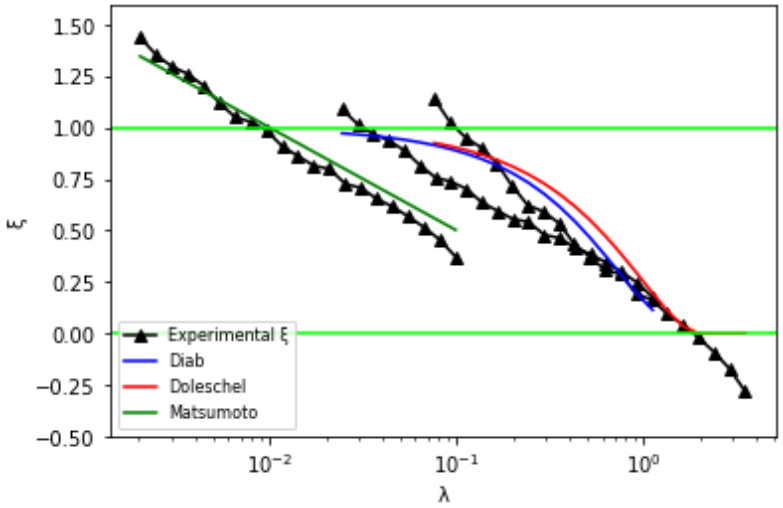

Figure 5.17: Experimental and theoretical ξ with steel ball 2 ($R_a = 0.300\ \mu$m) and steel disc 1 ($R_a = 0.025\ \mu$m) (TOTM)

For steel disc 2 is possible note that all of the three film parameters have theoretical ξ values that closely relates the experimental ξ values, with the Doleschel film parameter having the ξ values that are more similar throughout the domain.

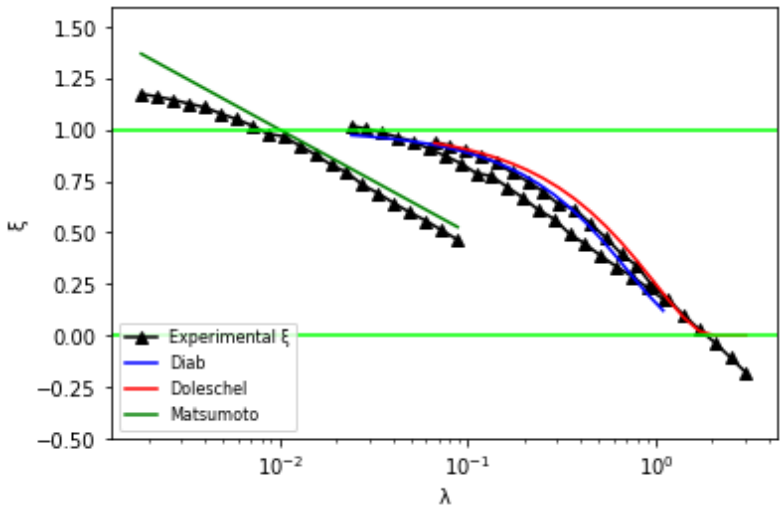

Figure 5.18: Experimental and theoretical ξ with steel ball 2 ($R_a = 0.300\ \mu$m) and steel disc 2 ($R_a = 0.074\ \mu$m) (TOTM)

Steel disc 3 has the same observations that were made for steel disc 2, i.e., the Doleschel film parameter has the ξ values that are more similar throughout the domain. Once more, is possible to see that the coefficients of friction obtained through the Doleschel film parameter has the lower relative errors.

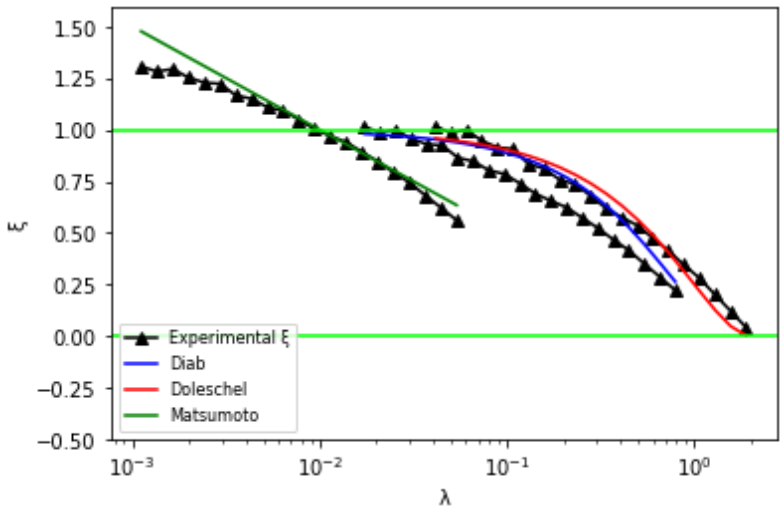

Figure 5.19: Experimental and theoretical ξ with steel ball 2 ($R_a = 0.300\ \mu$m) and steel disc 3 ($R_a = 0.300\ \mu$m) (TOTM)

In Figures 5.20, 5.21 and 5.22 it's possible to see that the Doleschel and Matsumoto film parameters have the best relative error, as it could be concluded by the previous observations.

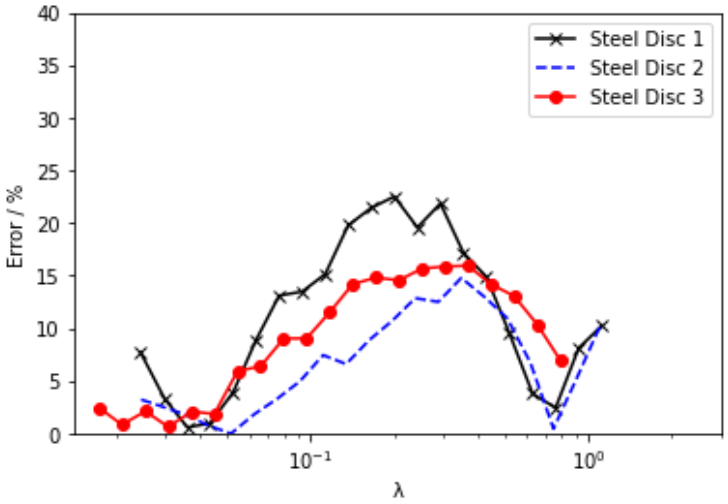

Figure 5.20: Relative error between the comparisons of friction values for Steel Ball 2 ($R_a = 0.300$ μm) and TOTM lubricant (Diab)

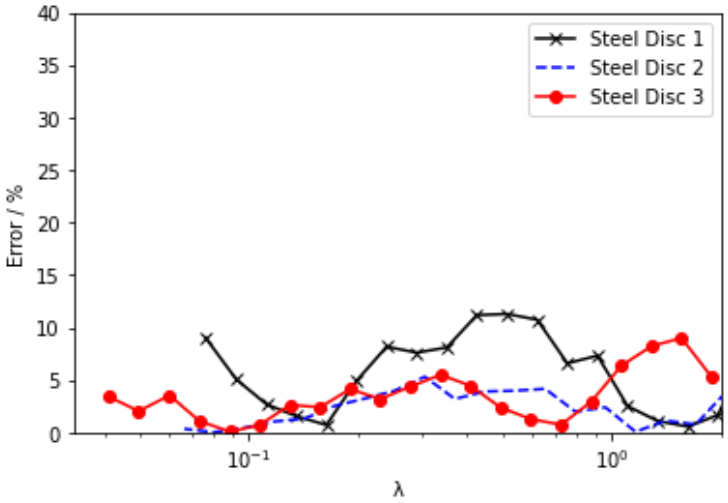

Figure 5.21: Relative error between the comparisons of friction values for Steel Ball 2 ($R_a = 0.300$ μm) and TOTM lubricant (Doleschel)

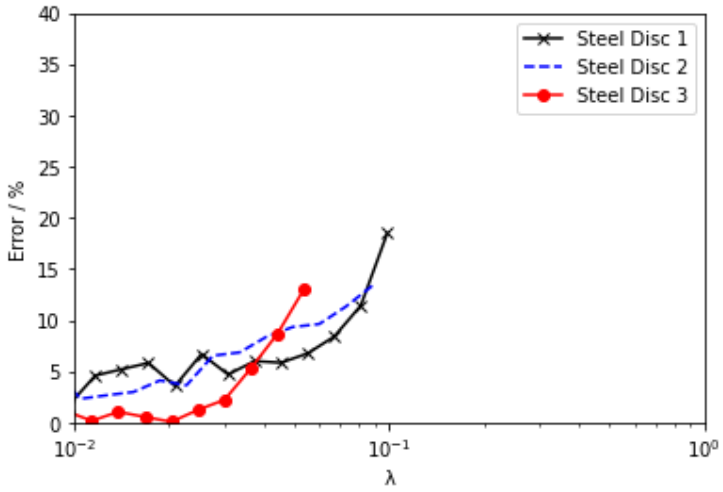

Figure 5.22: Relative error between the comparisons of friction values for Steel Ball 2 ($R_a = 0.300$ μm) and TOTM lubricant (Matsumoto)

5.3 Coefficients of Friction with Steel Ball 1-PAO ISO VG 150

In Figure 5.23, the coefficient of friction average in all three steel discs is shown. The coefficients of frictions were obtained with the PAO ISO VG 150 lubricant with a configuration of T=50 °C,F=50 N and SRR=50%. Once more, the higher the surface roughness the higher the coefficient of friction is. With the increase of rolling speed, the coefficient of friction tends to a value around 0.03.

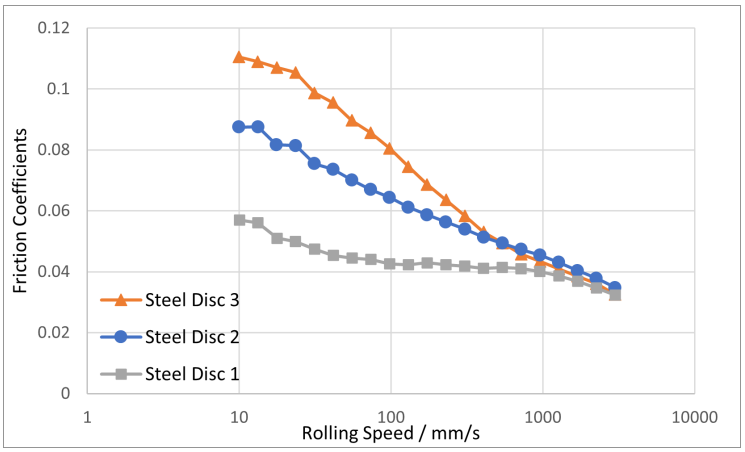

Figure 5.23: Coefficients of friction comparison between the three steel discs with Steel Ball 1 using PAO ISO VG 150 (SRR=50%)

The solid and fluid coefficient of friction, μ_{bl} and μ_{EHL}, to substitute in equation (2.60) are chosen from the Stribeck curves for each film parameter, with the same method as said before. These Stribeck curves are shown in Figure 5.24.

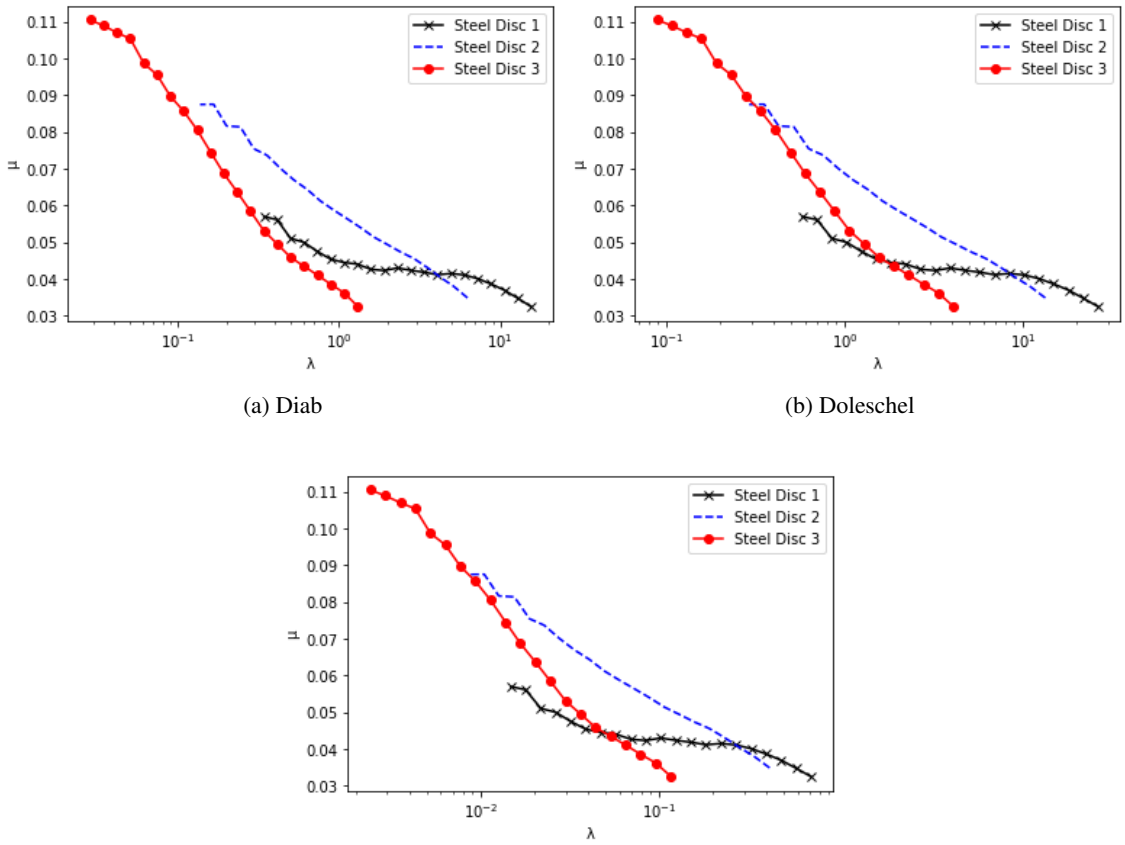

(a) Diab

(b) Doleschel

(c) Matsumoto

Figure 5.24: Stribeck Curves for Steel Ball 1 (PAO ISO VG 150)

The solid and fluid coefficients that best approximate for each steel disc, and for each film parameter, are shown in Table 5.4.

Table 5.4: Solid and fluid coefficients (Steel Ball 1/PAO ISO VG 150)

		μ_{bl}	μ_{EHL}
Diab	Steel Disc 1	0.0650	0.0450
	Steel Disc 2	0.0950	0.0500
	Steel Disc 3	0.1100	0.0300
Doleschel	Steel Disc 1	0.0700	0.0450
	Steel Disc 2	0.1000	0.0600
	Steel Disc 3	0.1150	0.0400
Matsumoto	Steel Disc 1	0.0550	0.0350
	Steel Disc 2	0.0850	0.0200
	Steel Disc 3	0.0800	0.0000

As seen in Figure 5.25, for steel disc 1, the film parameter that contributes to coefficient of friction prediction that are more close to the experimental coefficients of friction is the Doleschel film parameter. Both Diab and Matsumoto film parameters give good prediction for the coefficient of friction.

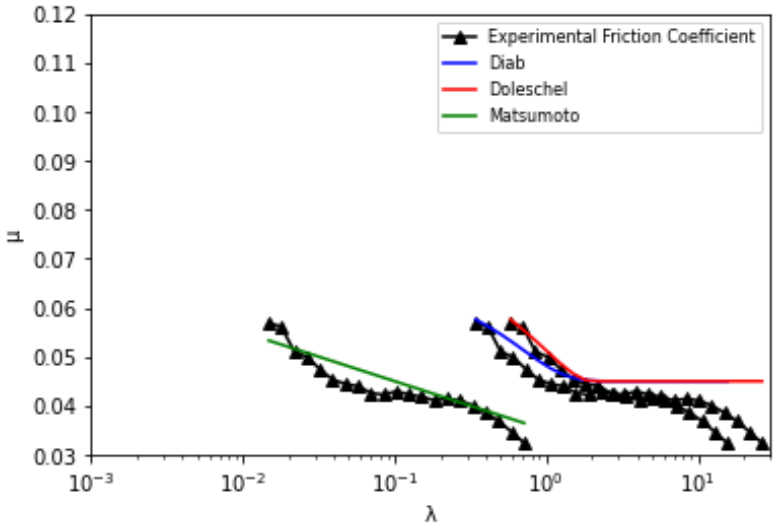

Figure 5.25: Experimental and predicted friction results with steel ball 1 ($R_a = 0.025\ \mu$m) and steel disc 1 ($R_a = 0.025\ \mu$m) (PAO ISO VG 150)

On steel disc 2, all of the film parameters give very good predictions for the coefficient of friction experimental results, as it can be seen in Figure 5.26.

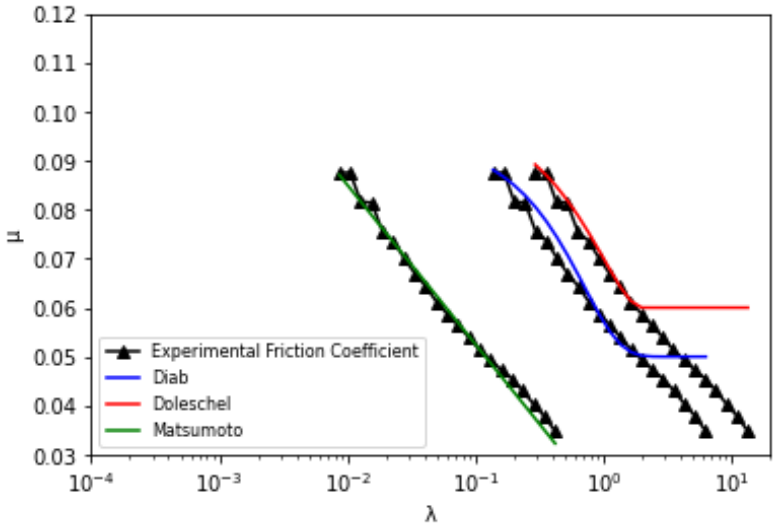

Figure 5.26: Experimental and predicted friction results with steel ball 1 ($R_a = 0.025\ \mu$m) and steel disc 2 ($R_a = 0.074\ \mu$m) (PAO ISO VG 150)

For steel disc 3, the coefficients of friction predictions using the Doleschel and Matsumoto film parameter have good approximation to the experimental coefficients of friction results. The

Diab film parameter prediction differ from the experimental results, as seen in Figure 5.27.

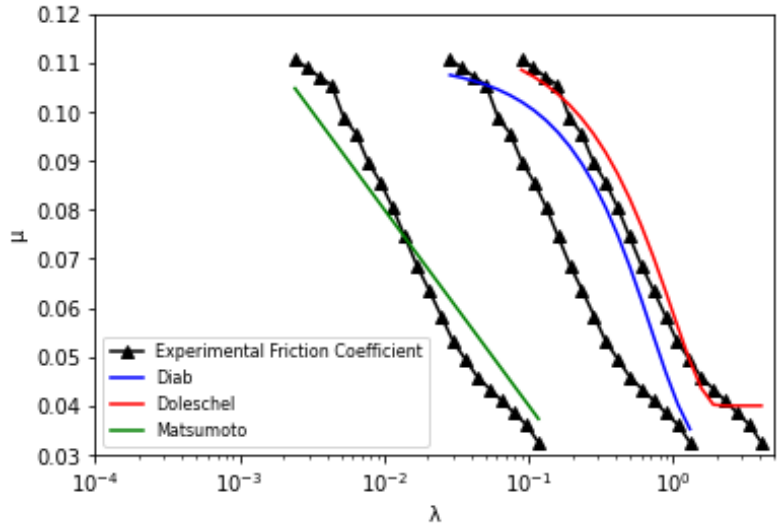

Figure 5.27: Experimental and predicted friction results with steel ball 1 ($R_a = 0.025\ \mu$m) and steel disc 3 ($R_a = 0.300\ \mu$m) (PAO ISO VG 150)

Figures 5.28, 5.29 and 5.30 show the comparison between the theoretical values of ξ with the experimental data. The conclusions that were drawn out of the comparisons between the experimental and predicted coefficients of friction also hold true in these comparisons. For steel disc 1, the Doleschel film parameter provides the best theoretical ξ values.

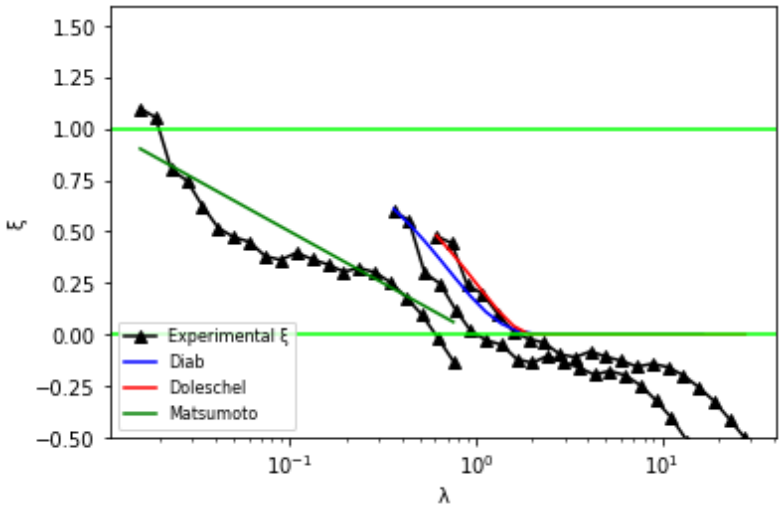

Figure 5.28: Experimental and theoretical ξ with steel ball 1 ($R_a = 0.025\ \mu$m) and steel disc 1 ($R_a = 0.025\ \mu$m) (PAO ISO VG 150)

On steel disc 2 all of the three film parameter provides good theoretical ξ values, specially the Matsumoto film parameter.

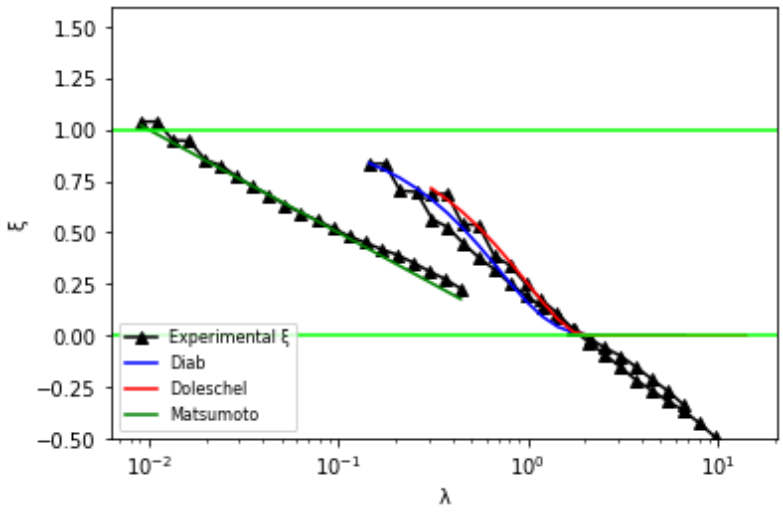

Figure 5.29: Experimental and theoretical ξ with steel ball 1 ($R_a = 0.025\ \mu$m) and steel disc 2 ($R_a = 0.074\ \mu$m) (PAO ISO VG 150)

With steel disc 3, is possible to observe that the Doleschel film parameter has the theoretical ξ values that more closely resembles the experimental ξ values.

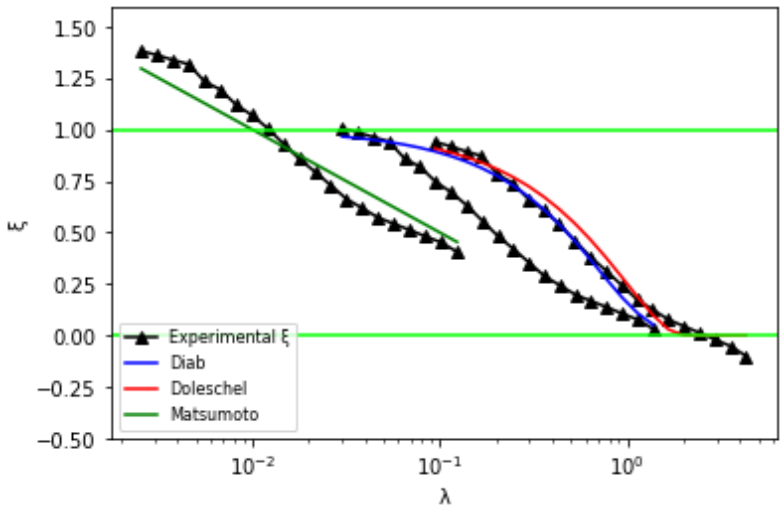

Figure 5.30: Experimental and theoretical ξ with steel ball 1 ($R_a = 0.025\ \mu$m) and steel disc 3 ($R_a = 0.300\ \mu$m) (PAO ISO VG 150)

The relative error of the predicted values when compared to the experimental results for the coefficient of friction can be seen in Figures 5.31, 5.33 and 5.33. As it can be seen, the Diab film parameter produced, on the whole, the worst prediction for the coefficients of friction. The Doleschel film parameter seems to have the lowest relative error.

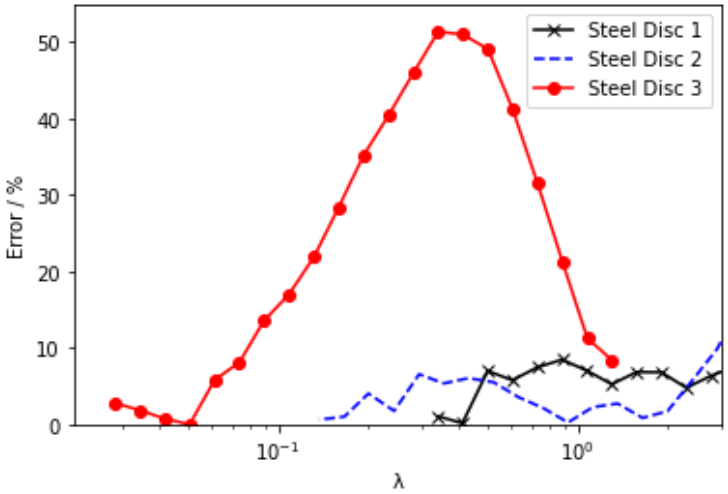

Figure 5.31: Relative error between the comparisons of friction values for Steel Ball 1 ($R_a = 0.025$ μm) and PAO ISO VG 150 lubricant (Diab)

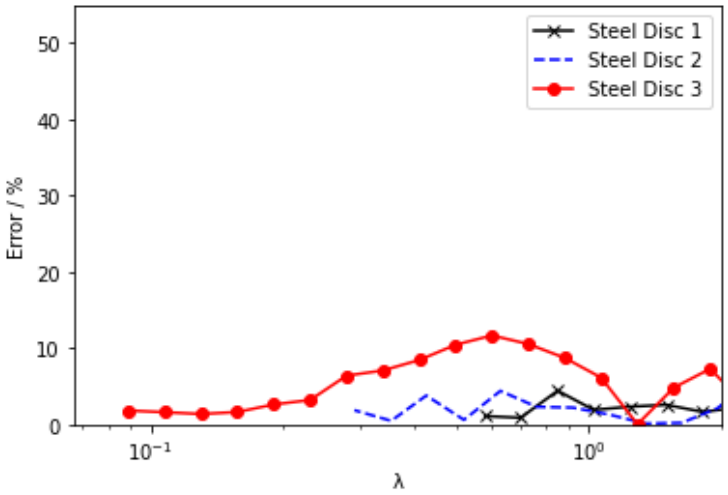

Figure 5.32: Relative error between the comparisons of friction values for Steel Ball 1 ($R_a = 0.025$ μm) and PAO ISO VG 150 lubricant (Doleschel)

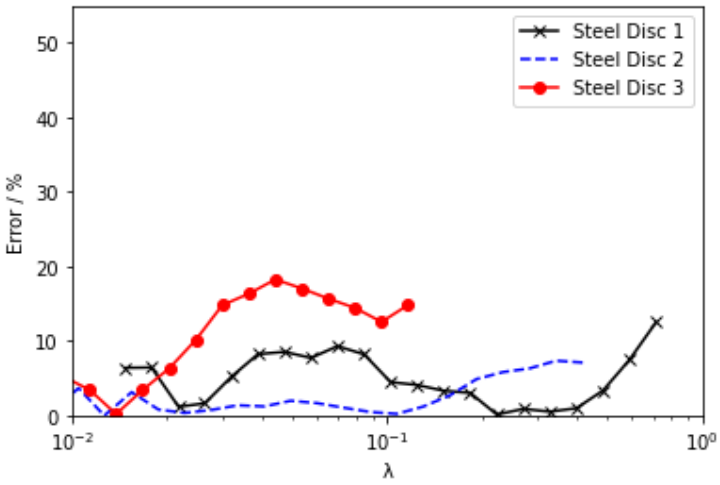

Figure 5.33: Relative error between the comparisons of friction values for Steel Ball 1 ($R_a = 0.025$ μm) and PAO ISO VG 150 lubricant (Matsumoto)

5.4 Coefficients of Friction with Steel Ball 2-PAO ISO VG 150

Figure 5.34 shows the coefficient of friction average in all three steel discs. Again the higher the surface roughness the higher the coefficient of friction is. With the increase of rolling speed, the coefficient of friction in all three discs tend 0.03.

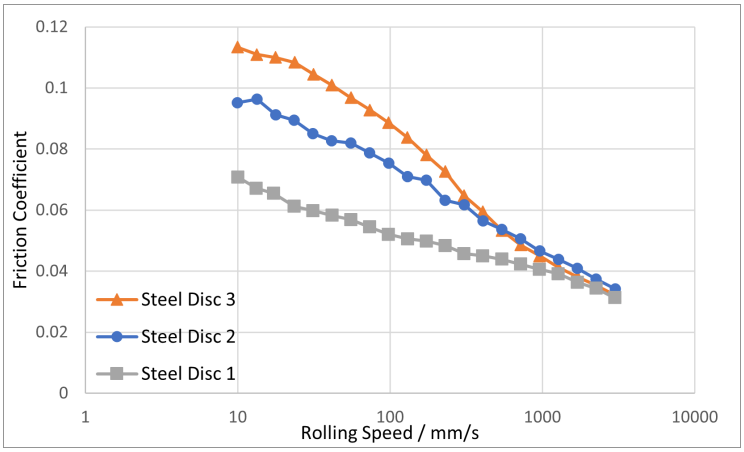

Figure 5.34: Coefficients of friction comparison between the three steel discs with Steel Ball 2 using PAO ISO VG 150 (SRR=50%)

The solid and fluid coefficient of friction, μ_{bl} and μ_{EHL}, to substitute in equation (2.60) are chosen from the Stribeck curves for each film parameter. These Stribeck curves can be seen in Figure 5.35.

The solid and fluid coefficients that best approximate for each steel disc, and for each film parameter, are shown in Table 5.5.

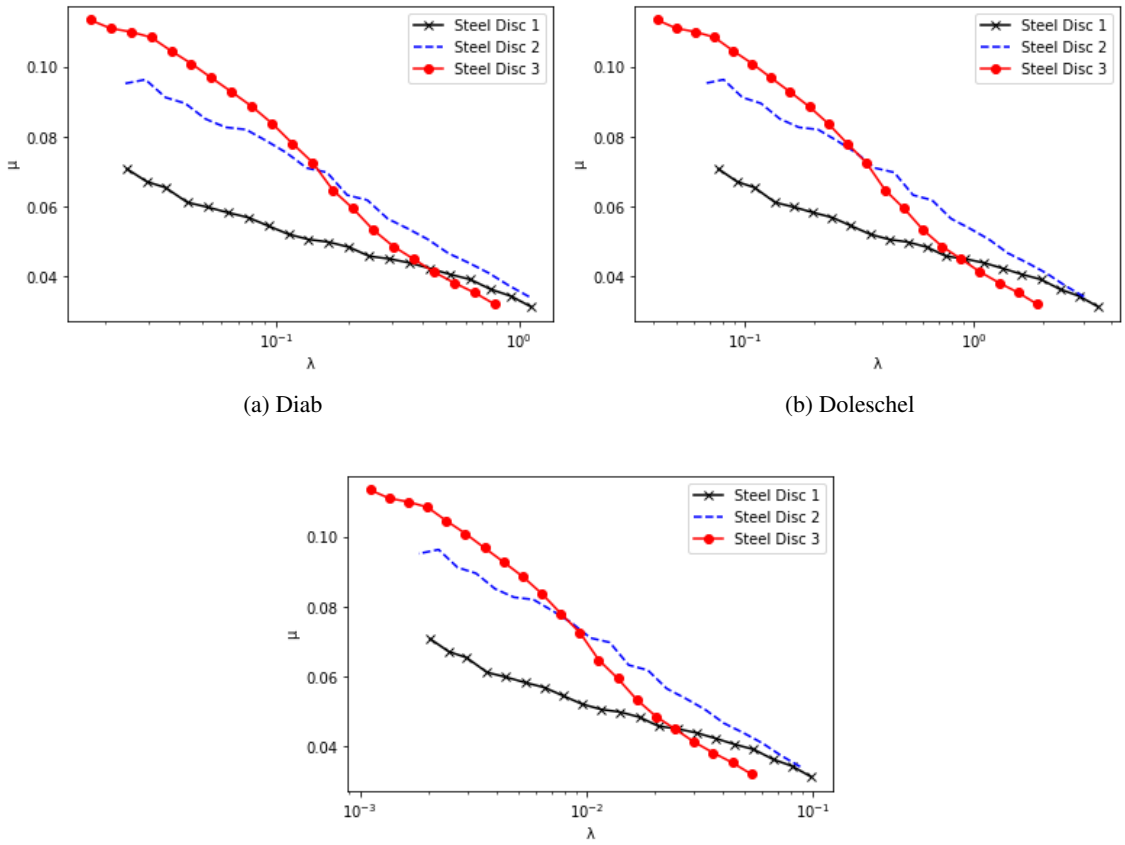

(a) Diab

(b) Doleschel

(c) Matsumoto

Figure 5.35: Stribeck Curves for Steel Ball 2 (PAO ISO VG 150)

Table 5.5: Solid and fluid coefficients (Steel Ball 2/PAO ISO VG 150)

		μ_{bl}	μ_{EHL}
Diab	Steel Disc 1	0.0700	0.0270
	Steel Disc 2	0.1000	0.0250
	Steel Disc 3	0.1150	0.0100
Doleschel	Steel Disc 1	0.0600	0.0400
	Steel Disc 2	0.1000	0.0450
	Steel Disc 3	0.1150	0.0300
Matsumoto	Steel Disc 1	0.0530	0.0100
	Steel Disc 2	0.0700	0.0000
	Steel Disc 3	0.0650	0.0000

As seen in Figure 5.36, for steel disc 1, the film parameter that contributes to coefficient of friction prediction that are more close to the experimental coefficients of friction is the Doleschel film parameter. Both Diab and Matsumoto film parameters give good prediction for the coefficient of friction.

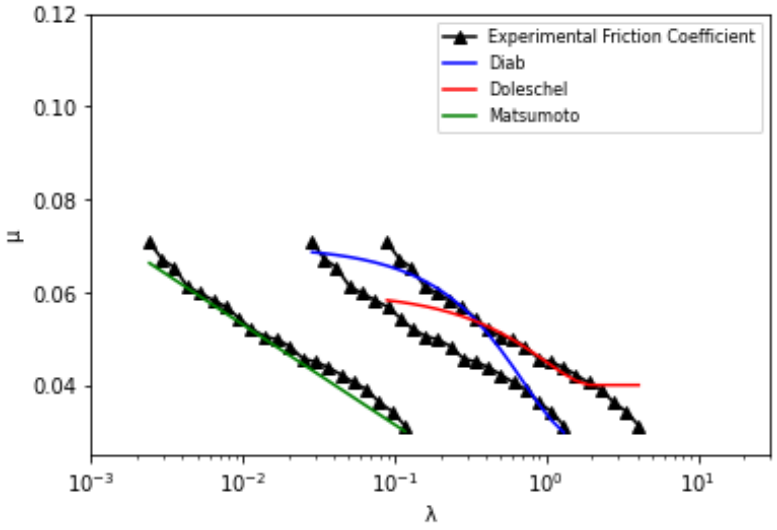

Figure 5.36: Experimental and predicted friction results with steel ball 2 ($R_a = 0.300$ μm) and steel disc 1 ($R_a = 0.025$ μm) (PAO ISO VG 150)

On steel disc 2, all of the film parameters give very good predictions for the coefficient of friction experimental results, as it can be seen in Figure 5.37.

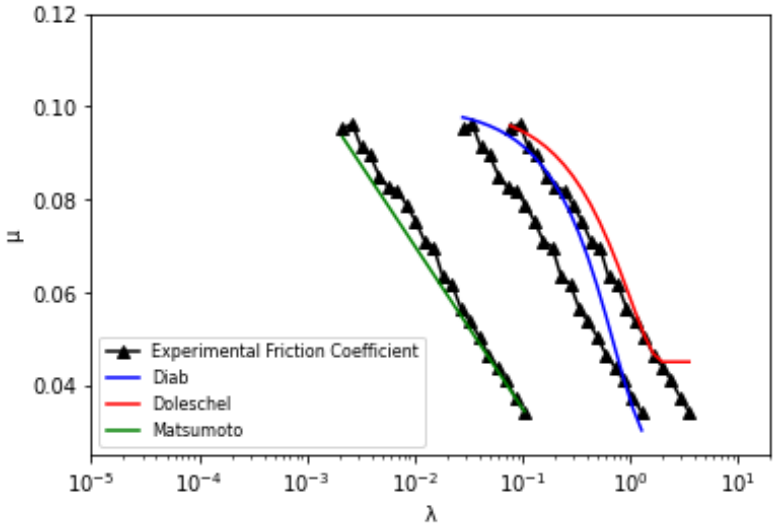

Figure 5.37: Experimental and predicted friction results with steel ball 2 ($R_a = 0.300$ μm) and steel disc 2 ($R_a = 0.074$ μm) (PAO ISO VG 150)

For steel disc 3, the coefficients of friction predictions using the Doleschel and Matsumoto film parameter have good approximation to the experimental coefficients of friction results. The

Diab film parameter prediction differ from the experimental results, as seen in Figure 5.38.

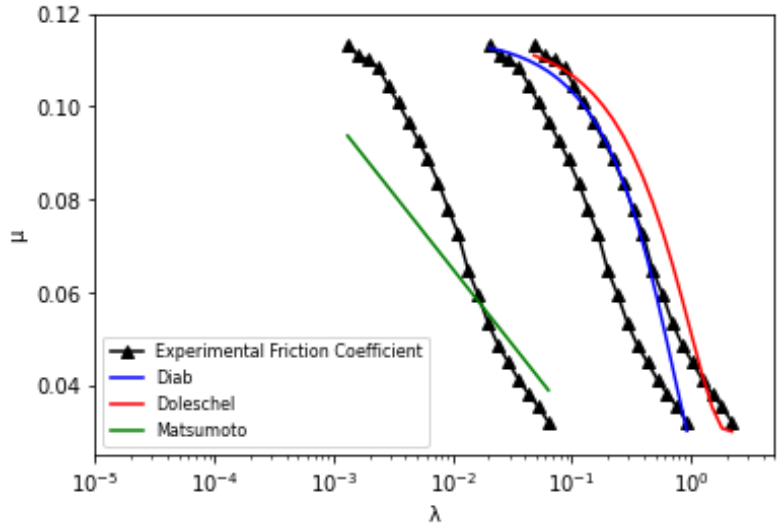

Figure 5.38: Experimental and predicted friction results with steel ball 2 ($R_a = 0.300\ \mu$m) and steel disc 3 ($R_a = 0.300\ \mu$m) (PAO ISO VG 150)

Figures 5.39, 5.40 and 5.41 show the comparison between the theoretical values of ξ with the experimental data. The conclusions that were drawn out of the comparisons between the experimental and predicted coefficients of friction also hold true in these comparisons.

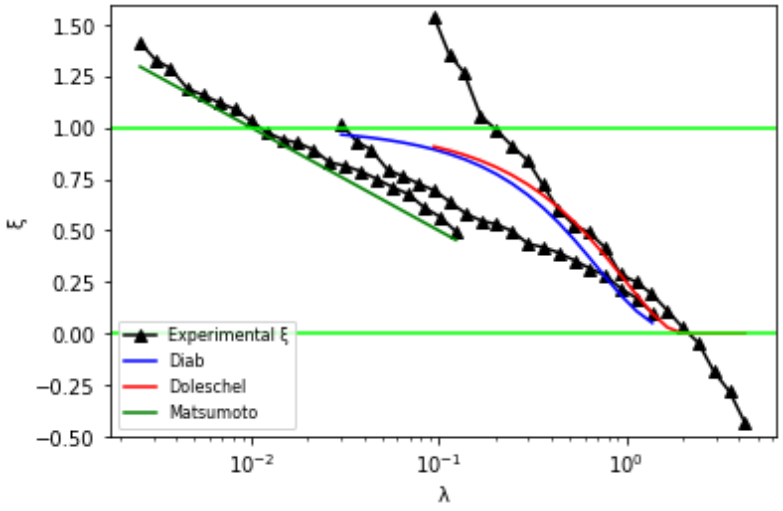

Figure 5.39: Experimental and theoretical ξ with steel ball 2 ($R_a = 0.300\ \mu$m) and steel disc 1 ($R_a = 0.300\ \mu$m) (PAO ISO VG 150)

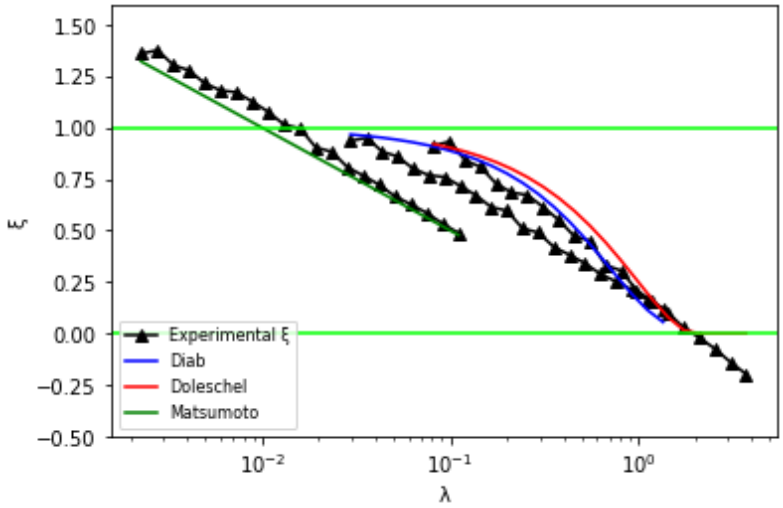

Figure 5.40: Experimental and theoretical ξ with steel ball 2 ($R_a = 0.300\ \mu$m) and steel disc 2 ($R_a = 0.074\ \mu$m) (PAO ISO VG 150)

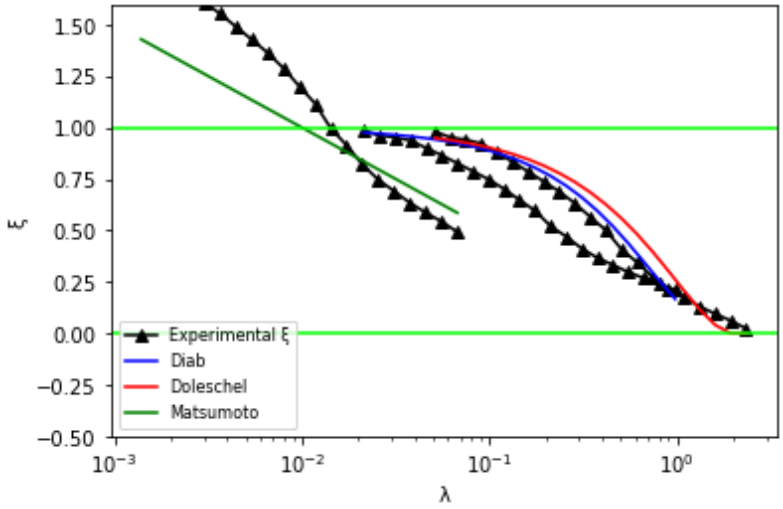

Figure 5.41: Experimental and theoretical ξ with steel ball 2 ($R_a = 0.300\ \mu$m) and steel disc 3 ($R_a = 0.300\ \mu$m) (PAO ISO VG 150)

The relative errors can be seen in Figures 5.42, 5.43 and 5.44. By observing the figures is possible to conclude that the Matsumoto film parameter provides the lowest relative errors out of all the film parameters.

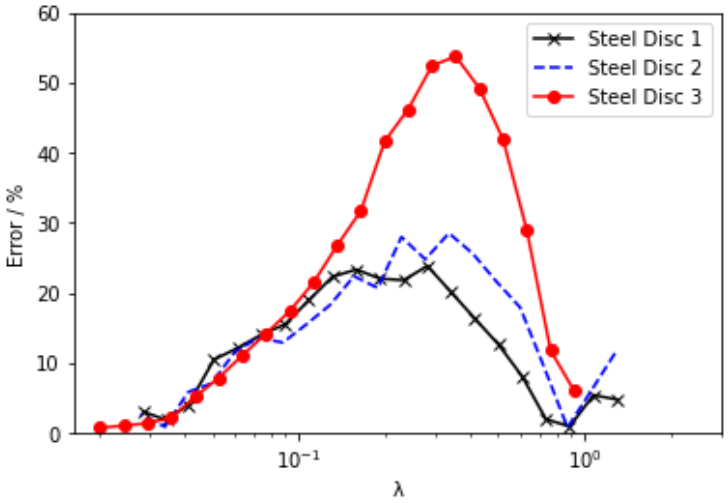

Figure 5.42: Relative error between the comparisons of friction values for Steel Ball 2 ($R_a = 0.300$ μm) and PAO ISO VG 150 lubricant (Diab)

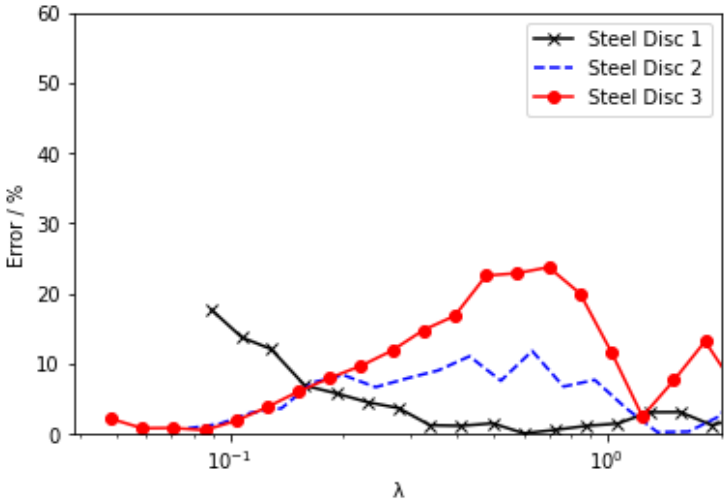

Figure 5.43: Relative error between the comparisons of friction values for Steel Ball 2 ($R_a = 0.300$ μm) and PAO ISO VG 150 lubricant (Doleschel)

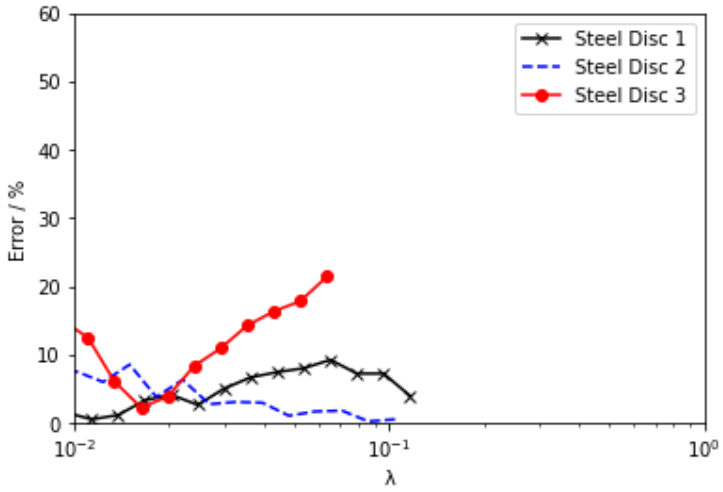

Figure 5.44: Relative error between the comparisons of friction values for Steel Ball 2 ($R_a = 0.300$ μm) and PAO ISO VG 150 lubricant (Matsumoto)

5.5 Coefficients of Friction Discussion

The error comparisons for each steel discs using the TOTM lubricant can be found in Figure 5.45. Having in mind the domain for each film parameter, present in Table 5.1, it can be seen that, broadly speaking, the predicted values using the Diab film parameter presents the worst error values of the three film parameters, with reaching relative errors up to 70% (using steel disc 3 and steel ball 1). The predictions Doleschel and Matsumoto film parameters have low relative errors, although in Figure 5.45a the error using the Matsumoto film parameter has a higher error than the other two parameters, being this case an exception.

In Figure 5.46 it's possible to see the relative error comparisons for all the combinations of steel discs and steel balls, with the different film parameters, but this time using the PAO ISO VG 150. It's possible to see that, once more, the predictions made for the coefficient of friction using the Diab film parameter have a higher error than the other two parameters, reaching relative errors around 50% (with steel disc 3). Again, both predictions for the Doleschel and Matsumoto film parameter show a low relative error.

With the two lubricants, it's possible to say that the Diab film parameter shows the worst predicted values for the coefficient of friction. The predicted coefficient of friction values using the Doleschel and the Matsumoto film parameters are the better ones but a direct comparison between the two film parameters to is difficult to do, since both of them on the whole seem to produce similar results.

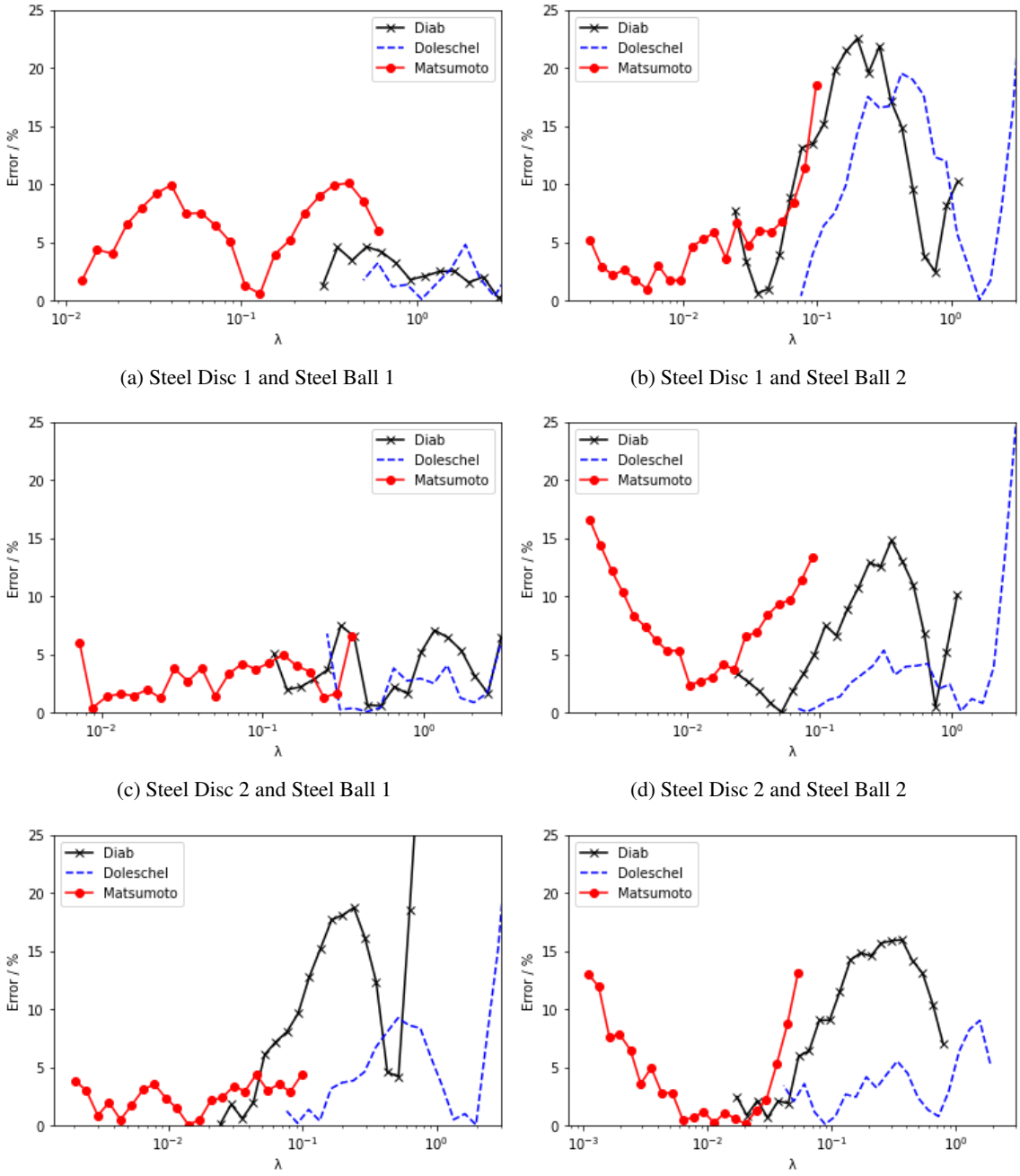

(a) Steel Disc 1 and Steel Ball 1

(b) Steel Disc 1 and Steel Ball 2

(c) Steel Disc 2 and Steel Ball 1

(d) Steel Disc 2 and Steel Ball 2

(e) Steel Disc 3 and Steel Ball 1

(f) Steel Disc 3 and Steel Ball 2

Figure 5.45: Relative errors using the TOTM lubricant and SRR=50%

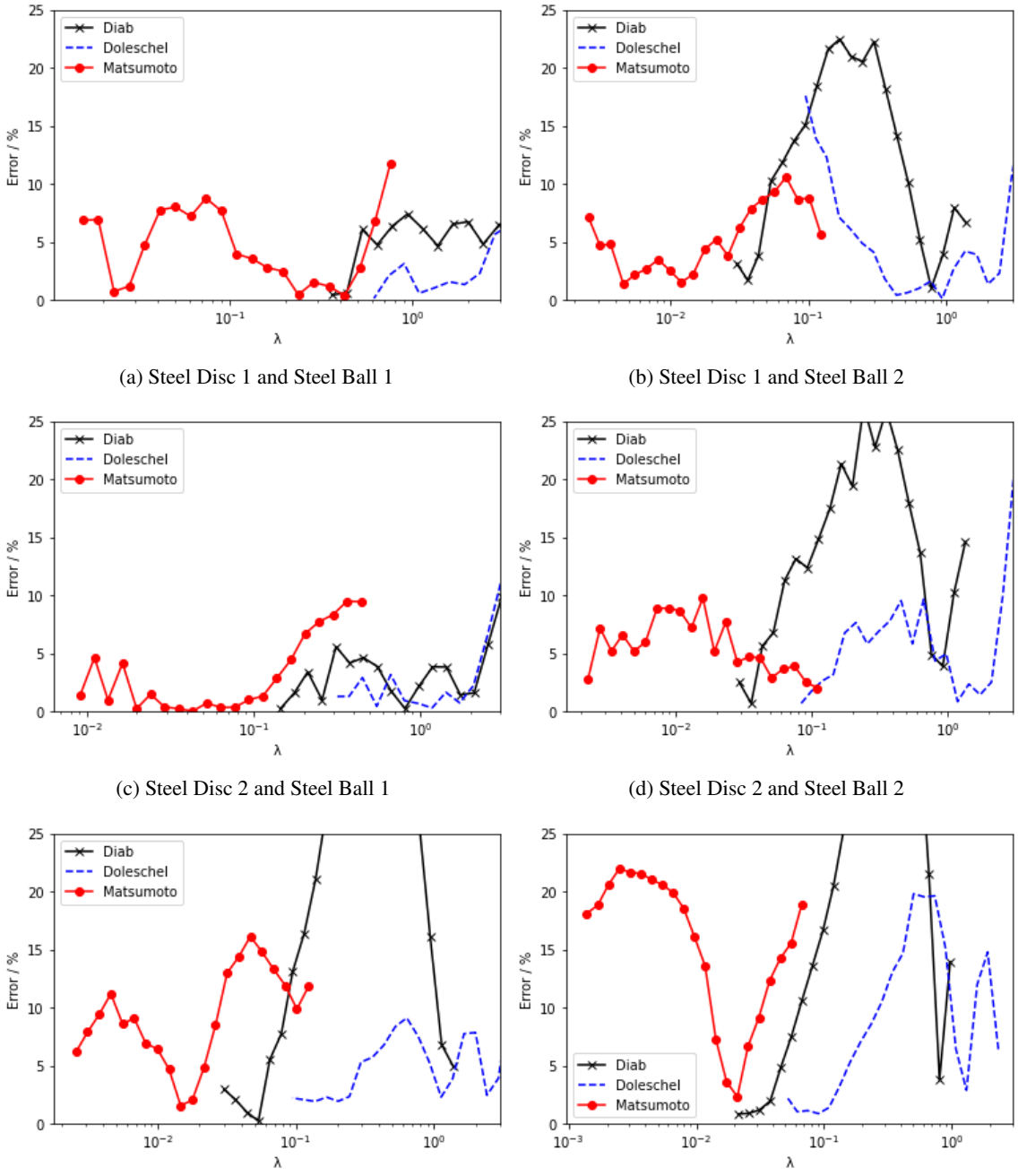

(a) Steel Disc 1 and Steel Ball 1

(b) Steel Disc 1 and Steel Ball 2

(c) Steel Disc 2 and Steel Ball 1

(d) Steel Disc 2 and Steel Ball 2

(e) Steel Disc 3 and Steel Ball 1

(f) Steel Disc 3 and Steel Ball 2

Figure 5.46: Relative errors using the PAO ISO VG 150 lubricant and SRR=50%

5.6 Comparison with fixed load sharing values

In the previous sections, the load sharing values were obtained by considering that the domain of each film parameter, present in Table 5.1, holds true. This time a fixed value, no matter what film parameter used, will be given for the load sharing values. These values are known and were obtained by using a steel disc with a surface roughness of $R_q = 0.723$ μm, a steel ball that has the same surface roughness as steel ball 1 and the PAO ISO VG 150 lubricant, so the experimental results that are going to be used for a comparison are from steel disc 3 ($R_q = 0.506$ μm). The values for the coefficient of friction at the boundary and full film regimes are $\mu_{bl} = 0.11$ and $\mu_{EHL} = 0.035$.

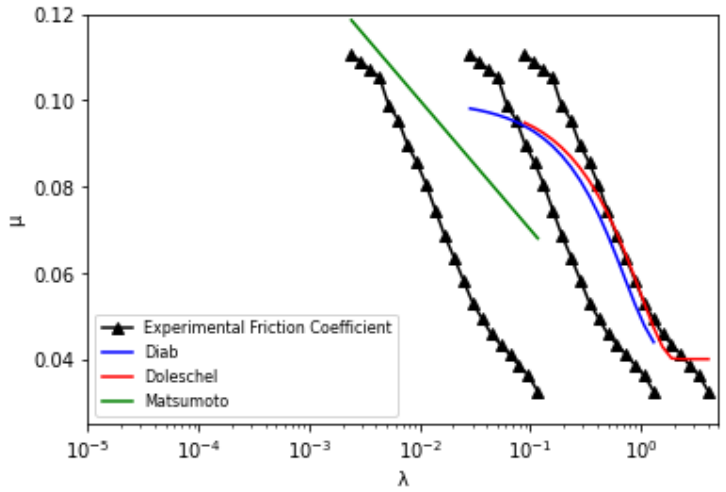

Figure 5.47: Comparison between the experimental results and predicted results with fixed load sharing values

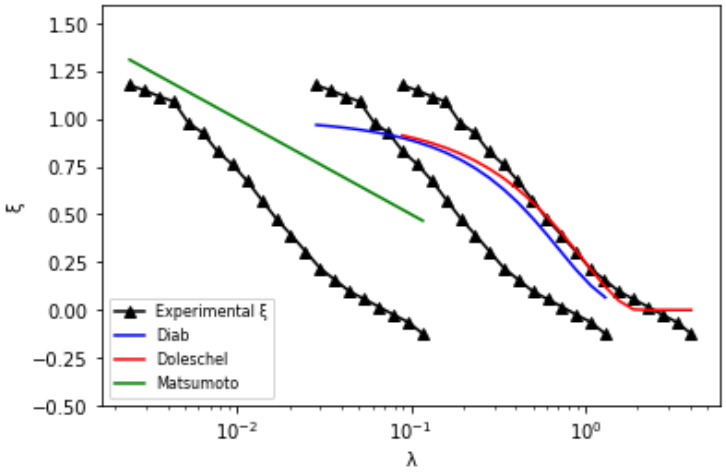

Figure 5.48: Comparison between the experimental and theoretical ξ values with fixed load sharing values

As it's possible to see, the results that were obtained with the Diab and Matsumoto film parameter differ a lot when Λ increases, this could be because the steel disc where the load sharing values were obtained with a rougher steel disc than the one where the experimental results came from. However, by observing the predicted coefficient of friction results from the Doleschel film parameter, it can be seen that this doesn't happen, on the contrary, the predicted results are very similar to the experimental results.

Comparing with the results from Figures 5.27 and 5.30, it's possible to notice as difference, specially on the results obtained from Matsumoto. This difference mainly comes from the μ_{bl} value, however this difference is quite low for the Diab and Doleschel film parameter (about 0.01) and more significantly in the Matsumoto film parameter (0.3).

It's also possible to note that, like it happened before, the Doleschel film parameter provides the better predictions for the coefficient of friction.

Chapter 6

Larsson Film Parameter

As stated in chapter 2, section 2.5, Hansen, Björling and Larsson developed a new film parameter that is calculated by equation (2.31). The Spk parameter is substituted by the Rpk parameter, which is the equivalent surface roughness parameter. Another important aspect to mention is the f_q parameter. As it's possible to see from equation (2.27), this parameter uses the asperity radii, that can be calculated by equation (2.30). However the width and height of the asperity isn't known, so this equation can't be used. For this, equation (2.12) is used to calculate the asperity radii. The values for the asperity radii can be seen in Table 6.1. Another matter is that f_q also depends on the orientation of the surface roughness lay, but again this isn't known. So, it's considered that the steel ball has a transversal surface roughness lay to the steel disc. With this in consideration, it's used the coefficients values for case A present in Table 2.3.

As it was stated, the transition between mixed film and full film lubrication occurs when $\Lambda = 1$. However, the value of Λ when the transition between the boundary film and mixed film regime occurs isn't known. To get an estimate of the Λ where this transition occurs, a coefficient of friction in function of Λ graphic will be analysed. Since the boundary film regime normally occurs when the surface roughness is higher, the graphics analysed will be the ones where steel disc 3 and steel ball 2 are used, since both of them have the higher values for the surface roughness.

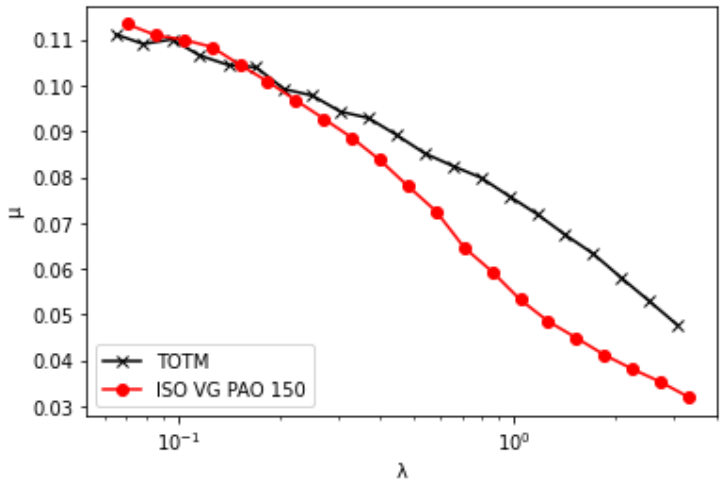

Figure 6.1: Coefficients of friction for Steel Disc 3 and Steel Ball 2 (F=50 N, T=50 °C and SRR=50%)

The boundary film regime in this type of graphic is characterised by a plateau on the lower values of Λ. By observing Figure 6.1, is possible to see that both results using the two different lubricants have similar values until $\Lambda = 0.2$, however, observing the results for the TOTM lubricant, it's possible to see a small plateau until $\Lambda = 0.1$. On the results for the PAO ISO VG 150, although not a straight plateau as the one from the TOTM results, it's possible to see that the inclination until $\Lambda = 0.1$ is smaller than the inclination that comes after $\Lambda = 0.1$. So it estimated that the transition between boundary and mixed film regime occurs around $\Lambda = 0.1$.

Table 6.1: Asperity radii values

	Asperity radii / mm
Steel Disc 1	0.7491
Steel Disc 2	0.5241
Steel Disc 3	0.8081

Since this is a new film parameter, a theoretical equation for the determination of the ξ value doesn't exist. So, the theoretical ξ will be based on the existent equations for the Diab, Doleschel and Matsumoto film parameter. The changes for those theoretical equations are the following:

$$\xi_1 = erfc(A \cdot \Lambda) \tag{6.1}$$

$$\xi_2 = (1 - A \cdot \Lambda)^2 \tag{6.2}$$

$$\xi_3 = A \cdot \log_{10}\left(\Lambda^{-1}\right) \tag{6.3}$$

A is a constant to be determined so the error between the experimental and theoretical ξ is as small as possible. The experimental ξ is calculated by equation (2.64), and the error between the theoretical and experimental ξ is calculated by:

$$error = \frac{|\xi_{exp} - \xi|}{\xi_{exp}} \tag{6.4}$$

To minimise the error, the least squares method is employed in order to determine A.

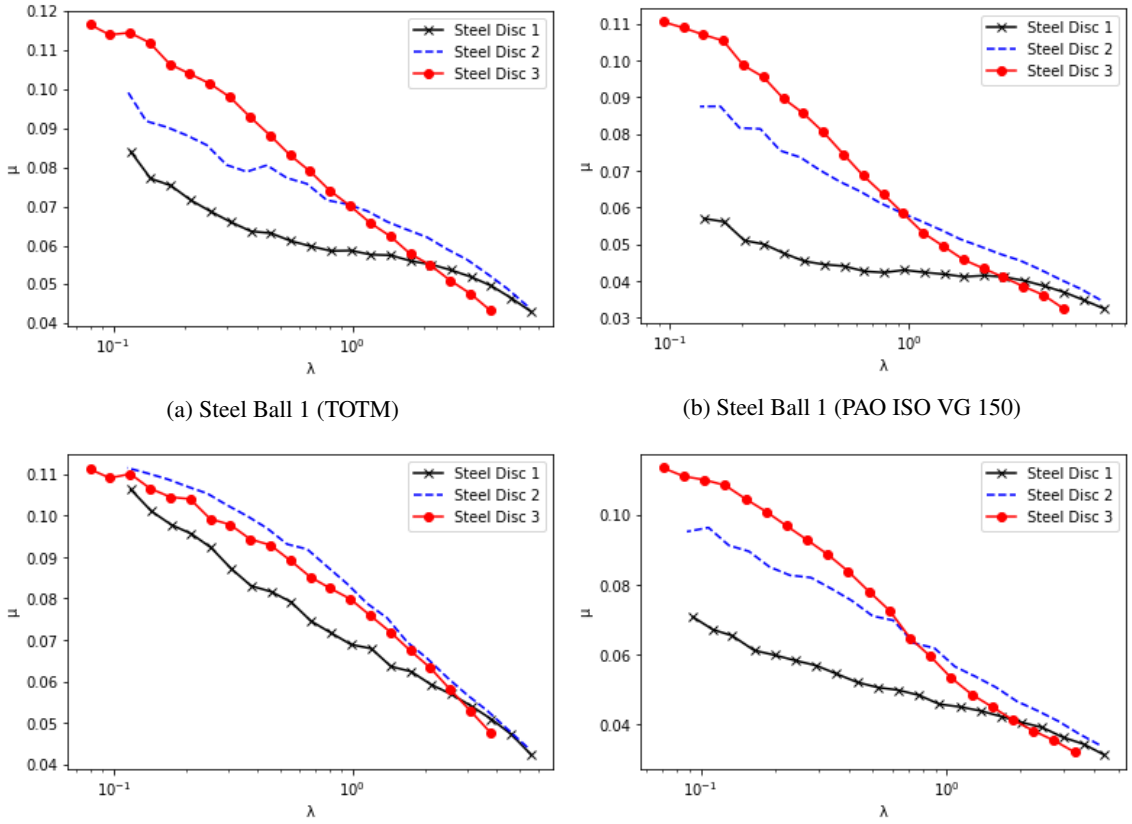

(a) Steel Ball 1 (TOTM)

(b) Steel Ball 1 (PAO ISO VG 150)

(c) Steel Ball 2 (TOTM)

(d) Steel Ball 2 (PAO ISO VG 150)

Figure 6.2: Stribeck curves (F=50 N, T=50 °C and SRR=50%)

Like it was done earlier, the Stribeck curves will be analysed in order to determine the solid and fluid coefficients of friction for equation (2.60). These coefficients are shown in Table 6.2 and have in mind the domain of $\Lambda \in [0.1, 1]$.

Table 6.2: Solid and fluid coefficients for the Larsson film parameter

		TOTM		PAO ISO VG 150	
		μ_{bl}	μ_{EHL}	μ_{bl}	μ_{EHL}
Steel Ball 1	Steel Disc 1	0.09	0.06	0.06	0.043
	Steel Disc 2	0.1	0.07	0.09	0.06
	Steel Disc 3	0.115	0.07	0.11	0.058
Steel Ball 2	Steel Disc 1	0.10	0.065	0.07	0.045
	Steel Disc 2	0.11	0.07	0.095	0.06
	Steel Disc 3	0.11	0.07	0.11	0.055

Employing the least square method, as it was mentioned, it's possible to obtain the best value for coefficient A in order to have the better approximation for the experimental value of ξ. This method is employed for the three equations that were previously shown, equations (6.1) to (6.3). The results for this coefficient for each type of configuration of lubricant, steel ball and steel disc, and for each type of equation can be seen in the following tables.

Table 6.3: Coefficients A obtained from the least square method for equation (6.1)-Diab

		TOTM	PAO ISO VG 150
Steel Ball 1	Steel Disc 1	2.428	1.004
	Steel Disc 2	1.189	1.491
	Steel Disc 3	1.531	0.772
Steel Ball 2	Steel Disc 1	1.004	2.248
	Steel Disc 2	1.491	0.744
	Steel Disc 3	0.772	1.358

Table 6.4: Coefficients A obtained from the least square method for equation (6.2)-Doleschel

		TOTM	PAO ISO VG 150
Steel Ball 1	Steel Disc 1	0.574	0.645
	Steel Disc 2	0.532	0.283
	Steel Disc 3	0.755	0.643
Steel Ball 2	Steel Disc 1	0.475	0.522
	Steel Disc 2	0.648	0.430
	Steel Disc 3	0.478	0.499

Table 6.5: Coefficients A obtained from the least square method for equation (6.3)-Matsumoto

		TOTM	PAO ISO VG 150
Steel Ball 1	Steel Disc 1	1.934	0.866
	Steel Disc 2	0.848	1.051
	Steel Disc 3	0.973	0.915
Steel Ball 2	Steel Disc 1	0.994	0.766
	Steel Disc 2	1.029	0.939
	Steel Disc 3	1.149	1.033

Having the A coefficients, it's possible to perform a simple average in order to determine a general coefficient for each equation. However, values which differ a lot from the other values are removed. These values are 2.428 and 2.248 in Table 6.3, 0.283 in Table 6.4 and value 1.934 for Table 6.5. An approximation of the average value is then used in the equations to determine ξ. These equations are then the following:

$$\xi_1 = erfc(1.5 \cdot \Lambda) \tag{6.5}$$

$$\xi_2 = (1 - 0.55 \cdot \Lambda)^2 \tag{6.6}$$

$$\xi_3 = \log_{10}\left(\Lambda^{-1}\right) \tag{6.7}$$

Having these equations in order to have a theoretical value for ξ, it's possible to compare them with the experimental values obtained for ξ. In Figure 6.3 is possible to see this comparison for all steel discs and balls using the TOTM lubricant and in Figure 6.4 the comparison when using the PAO ISO VG 150 lubricant.

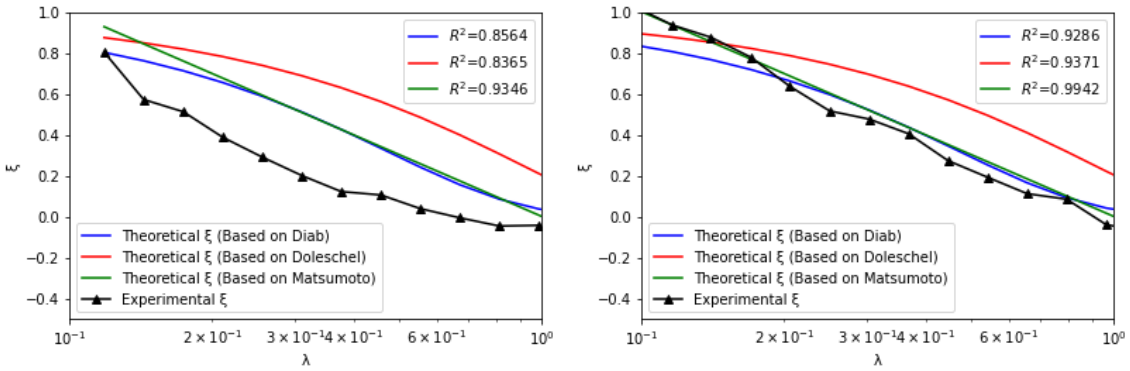

(a) Steel Disc 1 and Steel Ball 1

(b) Steel Disc 1 and Steel Ball 2

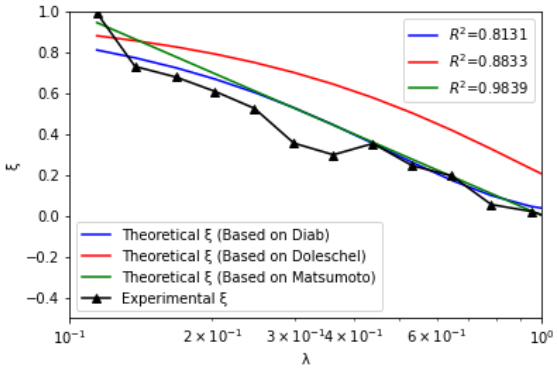

(c) Steel Disc 2 and Steel Ball 1

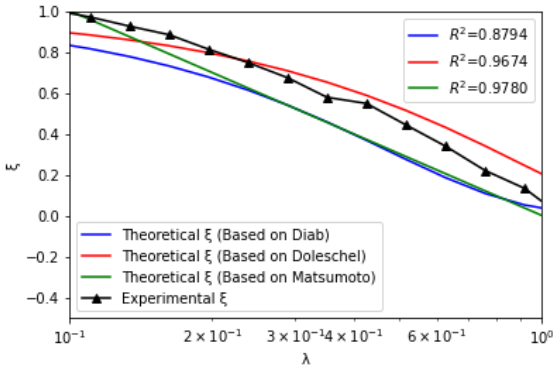

(d) Steel Disc 2 and Steel Ball 2

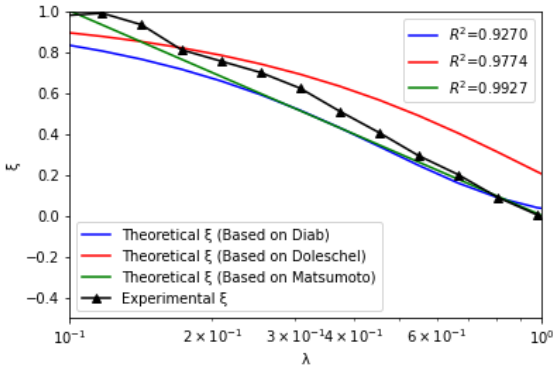

(e) Steel Disc 3 and Steel Ball 1

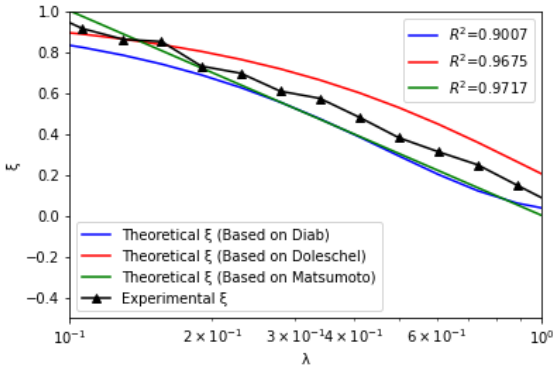

(f) Steel Disc 3 and Steel Ball 2

Figure 6.3: Comparison between the ξ values for the TOTM lubricant

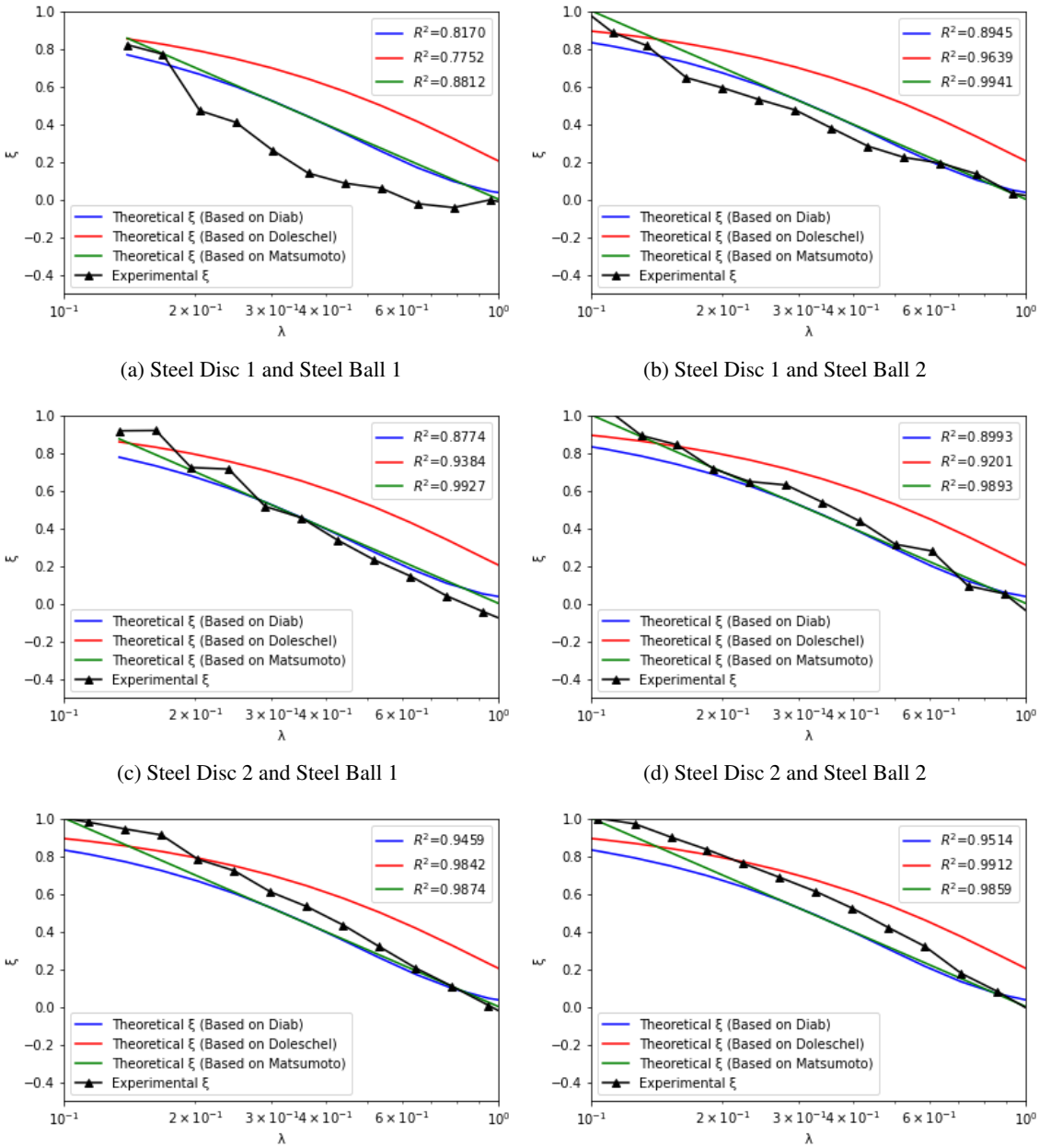

(a) Steel Disc 1 and Steel Ball 1

(b) Steel Disc 1 and Steel Ball 2

(c) Steel Disc 2 and Steel Ball 1

(d) Steel Disc 2 and Steel Ball 2

(e) Steel Disc 3 and Steel Ball 1

(f) Steel Disc 3 and Steel Ball 2

Figure 6.4: Comparison between the ξ values for the PAO ISO VG 150 lubricant

At first observation, it's possible to see that when the composite surface roughness, where steel disc 1 and steel ball 1 are combined, the theoretical ξ values are the furthest from the experimental ξ results, no matter the lubricant used. Excluding this, for all the other cases, the theoretical values using the three equations aforementioned are close in values for the experimental ξ results. Broadly speaking, the ξ values obtained from equation (6.6) have the furthest values from the experimental results, while the values obtained from equations (6.5) and (6.7) are closer to the experimental results. However, it can be observed that for the lower values of Λ, the values obtained from equation (6.5) are further away from the experimental results than the values obtained by using equation (6.7). By basing on this, it's expect that the friction predictions results using the equation (6.7) will provide better approximations.

Figures 6.5 and 6.6 shows the comparisons between the predicted values for the coefficient of friction and the experimental coefficient of friction results for the TOTM lubricant and the PAO ISO VG 150 lubricant respectively. Once more, is possible to note that the predictions for the coefficients of friction using equation (6.6) for the theoretical ξ value have, on the whole, the worst approximations. As expected, the coefficients of friction predictions using equation (6.7) have the best approximations overall.

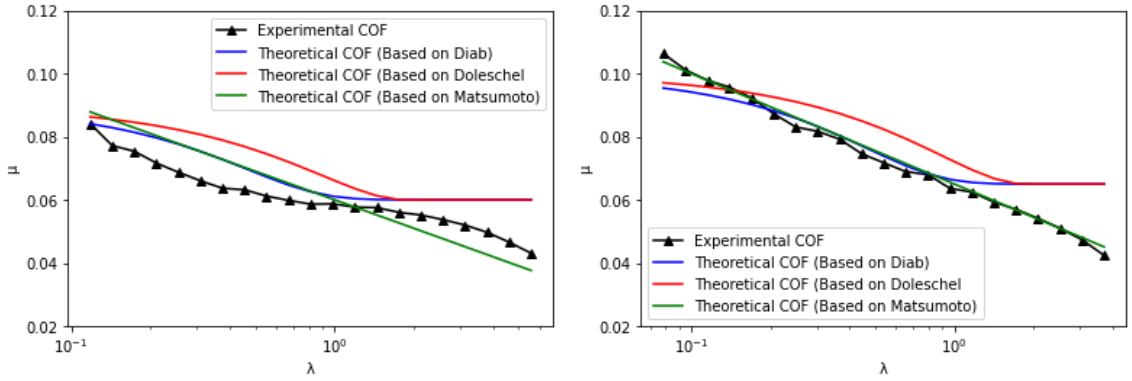

(a) Steel Disc 1 and Steel Ball 1

(b) Steel Disc 1 and Steel Ball 2

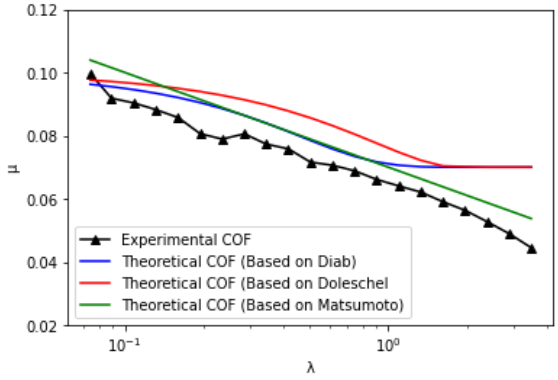

(c) Steel Disc 2 and Steel Ball 1

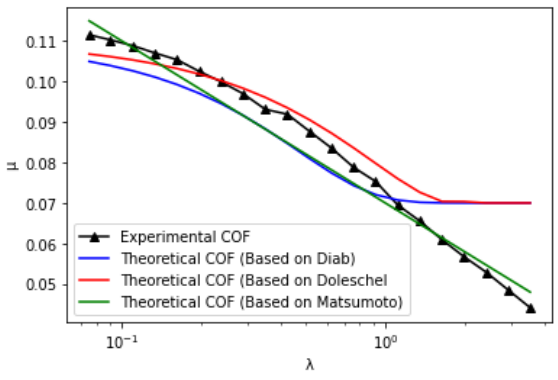

(d) Steel Disc 2 and Steel Ball 2

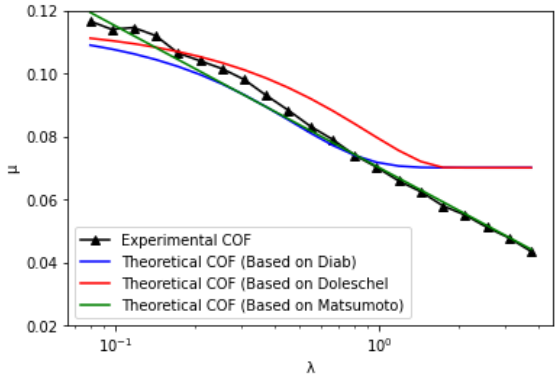

(e) Steel Disc 3 and Steel Ball 1

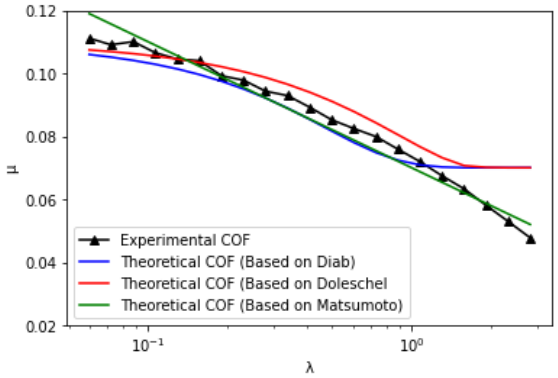

(f) Steel Disc 3 and Steel Ball 2

Figure 6.5: Comparison between the coefficients of friction results and predictions for the TOTM lubricant

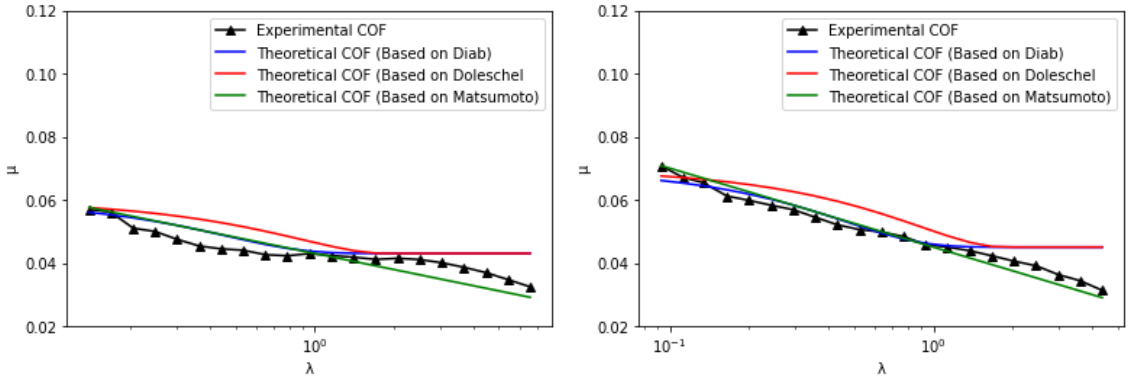

(a) Steel Disc 1 and Steel Ball 1

(b) Steel Disc 1 and Steel Ball 2

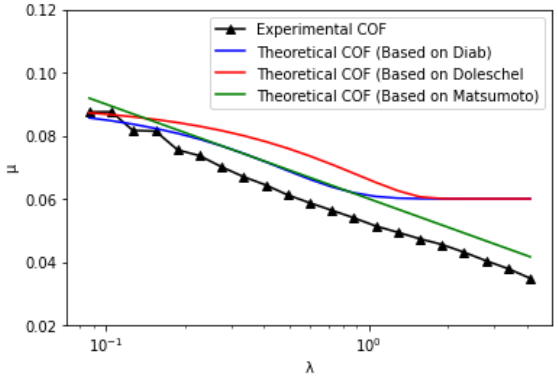

(c) Steel Disc 2 and Steel Ball 1

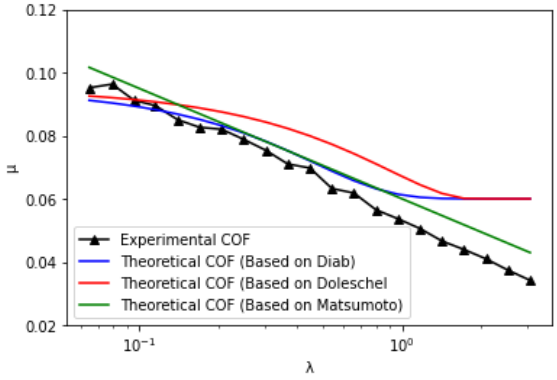

(d) Steel Disc 2 and Steel Ball 2

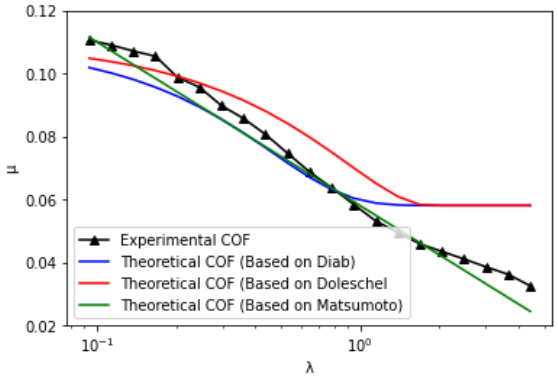

(e) Steel Disc 3 and Steel Ball 1

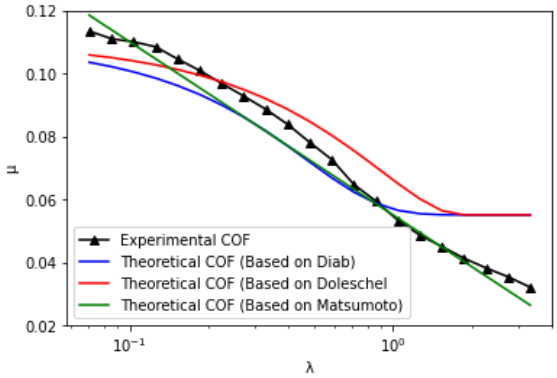

(f) Steel Disc 3 and Steel Ball 2

Figure 6.6: Comparison between the coefficients of friction results and predictions for the PAO ISO VG 150 lubricant

Chapter 7

Conclusions and Future Works

7.1 Conclusions

Starting with the film thickness experiments, it was possible to determine that the Dowson-Hamrock equations used for the calculation of the film thickness in point contacts is a good approximation for the obtained experimental results. It's also possible to observe that by changing a variable in the experiment, like the temperature, force or rolling speed, the experimental results of the film thickness will change according to the Dowson-Hamrock equation. For example, if the rolling speed increases then the film thickness also increases, if the temperature increases than the film thickness will decrease, with the same happening with the increase in force. The only change in variables that didn't provide a clear effect on the film thickness was the change in SRR. A final observation in the film thickness is that the results obtained by using the TOTM lubricant are lower than the ones where the PAO ISO VG 150 lubricant, this is because the dynamic viscosity of the TOTM lubricant is lower than the PAO ISO VG 150.

Going into the results obtained for the coefficients of friction, it's possible to note that the friction results using the TOTM lubricant are higher than the results obtained by using the PAO ISO VG 150 lubricant. This is consistent with the results obtained from the film thickness since the film thicknesses in the PAO ISO VG 150 were higher contributing then to a lower coefficients of friction.

As it was discussed in the previous section, the coefficients of friction predictions made by using the Diab film parameter present the worst predictions overall with the Doleschel and the Matsumoto film parameters presents the best results for the coefficients of friction predictions. In some cases the Doleschel film parameter has the best predictions, with a lower relative errors than the predictions made with the Matsumoto film parameter. In other cases the exact opposite happening, so a clear better option by observing the relative errors isn't possible to choose. However, by observing the direct comparison between the predictions and the experimental results it's possible to see that when using the Matsumoto film parameter, the rate in which the coefficient of friction decreases is roughly the same. With this it can be said that the Matsumoto film parameter is the better film parameter of the two.

Finally, with the Larsson film parameter it was possible a value for the boundary film regime, $\lambda = 0.1$, by turning to the Stribeck curves. However, it's important to notice that the values for the surface roughness parameters, Rpk, is taken from the values obtained for the steel discs that had the same tabled value, i.e., steel disc 1 and steel ball 1 had a tabled Ra value of 0.2 μm, so the values for the other surface roughness parameters where taken from the values obtained for steel disc 1. The same is applied to steel disc 3 and steel ball 2. So, the values for Rpk of the steel balls aren't exact but just an assumption, so this λ value can be altered significantly if it was possible to obtain the exact value for the steel balls. As for the equations for the predicted coefficient of friction values is possible to note that using the theoretical ξ equations based on Matsumoto ξ equation provide the best approximations for the experimental ξ that was obtained.

7.2 Future Works

Recommendations to improve on the topics encountered on this work and to develop it even further include:

- Use a different equipment to obtain the surface roughness parameters, a equipment where is possible to obtain these values for steel balls as well to get better values for the steel discs. The equipment used obtained the values in a one dimensional plane, a better equipment would allow to obtain the value in three dimensions, like the one used by Larsson et al [22].
- Use rougher discs and balls in order to more easily obtain a boundary film regime and to verify the λ value for the transition of the boundary to the mixed film regime.
- As said before, the orientation of the surface roughness lay was considered to be transversal. For a better analysis, different surface roughness lays should be considered in order to perceive if the λ value for the transition of boundary to mixed film changes with this factor. It would also be interesting to perceive what difference this factor would make on the other existing film parameters.
- Use steel rolls to study the validation of the Larsson film parameter in line contacts.
- Tweak the film thickness equations to obtain a theoretical value that better represents the experimental results.
- Use new load sharing values based on the steel discs used.

References

[1] D. Dowson. Elastohydrodynamic and micro-elastohydrodynamic lubrication. *Wear*, 190:125–138, 1995.

[2] Mr. Beauchamp Tower. First report on friction experiments. *Proceedings of the Institution of Mechanical Engineers*, 34(1):632–659, 1883.

[3] N.P. Petrov. First report on friction experiments. *Inzh. Zh. St-Peterb.*, pages 535–564, 1883.

[4] Osborne Reynolds. Iv. on the theory of lubrication and its application to mr. beauchamp tower's experiments, including an experimental determination of the viscosity of olive oil. *Philosophical transactions of the Royal Society of London*, pages 157–234, 1886.

[5] D. Dowson. Paper 10: Elastohydrodynamics. *Proceedings of the Institution of Mechanical Engineers, Conference Proceedings*, 182(1):151–167, 1967.

[6] D. Dowson and P. Ehret. Past, present and future studies in elastohydrodynamics. *Proceedings of the Institution of Mechanical Engineers, Part J: Journal of Engineering Tribology*, 213:317–333, 1999.

[7] MARTIN and H. M. Lubrication of gear teeth. *Engineering*, 102:119, 1916.

[8] Alfred Ivanovich Petrusevich et al. Fundamental conclusions from the contact-hydrodynamic theory of lubrication. *Izv. Akad. Nauk. SSSR (OTN)*, 2:209, 1951.

[9] Rahul Kumar, Mohammad Sikandar Azam, Subrata Kumar Ghosh, and Sanjay Yadav. 70 years of elastohydrodynamic lubrication (ehl): A review on experimental techniques for film thickness and pressure measurement. *Mapan - Journal of Metrology Society of India*, 33:481–491, 12 2018.

[10] D. Dowson and S. Toyoda. *A central film thickness formula for elastohydrodynamic line contacts.* Mechanical Engineering Publications, 1979.

[11] B.J. Hamrock and D. Dowson. Isothermal elastohydrodynamic lubrication of point contacts: Part iii-fully flooded result. *Journal of Tribology*, 99:264–275, 1977.

[12] Leigh Mummery. *Surface Texture Analysis: The Handbook*. Hommelwerke GmbH, 1992.

[13] ISO. *ISO 4287:1997: Geometrical Product Specifications (GPS) — Surface texture: Profile method — Terms, definitions and surface texture parameters*. ISO.

[14] E. S. Gadelmawla, M. M. Koura, T. M.A. Maksoud, I. M. Elewa, and H. H. Soliman. Roughness parameters. *Journal of Materials Processing Technology*, 123:133–145, 4 2002.

[15] A. Pogačnik and M. Kalin. How to determine the number of asperity peaks, their radii and their heights for engineering surfaces: A critical appraisal. *Wear*, 300:143–154, 3 2013.

[16] Radu Popovici and D.J. Schipper. Stribeck and traction curves for elliptical contacts: Isothermal friction model. *International Journal Sustainable Construction & Design*, 4, 02 2014.

[17] Luís Andrade Ferreira. *Tribologia*. PUBLINDUSTRIA, 2000.

[18] T.E. Tallian. On competing failure modes in rolling contact. *ASLE Transactions*, 10:418–439, 1967.

[19] Y. Diab, F. Ville, and P. Velex. Prediction of power losses due to tooth friction in gears. *Tribology Transactions*, 49:260–270, 2006.

[20] K. Michaelis, B.-R. Hohn, and A. Doleschel. Lubricant influence on gear efficiency. *Proceedings of the ASME International Design Engineering Technical Conferences and Computers and Information in Engineering Conference 2009, DETC2009*, 6:71–80, 2010.

[21] S Matsumoto and K Morikawa. The new estimation formula of coefficient of friction in rolling-sliding contact surface under mixed lubrication condition for the power loss reduction of power transmission gears. In *International gear conference*, pages 1078–1088, 2014.

[22] Jonny Hansen, Marcus Björling, and Roland Larsson. A new film parameter for rough surface ehl contacts with anisotropic and isotropic structures. *Tribology Letters*, 69:24–26, 06 2021.

[23] Hugh A. Spikes and Zhang Jie. History, origins and prediction of elastohydrodynamic friction. *Tribology Letters*, 56:1–25, 2014.

[24] A. W. Crook. The lubrication of rollers iv. measurements of friction and effective viscosity. *Philosophical Transactions of the Royal Society of London. Series A, Mathematical and Physical Sciences*, 255(1056):281–312, 1963.

[25] F. W. Smith. The effect of temperature in concentrated contact lubrication. *A S L E Transactions*, 5(1):142–148, 1962.

[26] J. C. Bell, J. W. Kannel, and C. M. Allen. The Rheological Behavior of the Lubricant in the Contact Zone of a Rolling Contact System. *Journal of Basic Engineering*, 86(3):423–432, 09 1964.

[27] Kenneth Langstreth Johnson and JL Tevaarwerk. Shear behaviour of elastohydrodynamic oil films. *Proceedings of the Royal Society of London. A. Mathematical and Physical Sciences*, 356(1685):215–236, 1977.

[28] J. F. Archard. The temperature of rubbing surfaces. *Wear*, 2:438–455, 10 1959.

[29] T.F. Conry, K.L. Johnson, and S. Owen. Viscosity in the thermal regime of ehd traction. *Journal of Tribology*, 03 2022.

[30] CR Evans and KL Johnson. The rheological properties of elastohydrodynamic lubricants. *Proceedings of the Institution of Mechanical Engineers, Part C: Journal of Mechanical Engineering Science*, 200(5):303–312, 1986.

[31] CR Evans and KL Johnson. Regimes of traction in elastohydrodynamic lubrication. *Proceedings of the Institution of Mechanical Engineers, Part C: Journal of Mechanical Engineering Science*, 200(5):313–324, 1986.

[32] W Hirst and J W Richmond. Traction in elastohydrodynamic contacts. *Proceedings of the Institution of Mechanical Engineers, Part C: Journal of Mechanical Engineering Science*, 202(2):129–144, 1988.

[33] WO Winer and Scott Bair. Shear strength measurements of lubricants at high pressure. *J. Lubr. Technol*, 101(3):251–257, 1979.

[34] K. T. Ramesh and R. J. Clifton. A Pressure-Shear Plate Impact Experiment for Studying the Rheology of Lubricants at High Pressures and High Shearing Rates. *Journal of Tribology*, 109(2):215–222, 04 1987.

[35] S. Bair and W. O. Winer. The High Shear Stress Rheology of Liquid Lubricants at Pressures of 2 to 200 MPa. *Journal of Tribology*, 112(2):246–252, 04 1990.

[36] S. Bair and W. O. Winer. Closure to "Discussions of 'The High Pressure High Shear Stress Rheology of Liquid Lubricants'" (1992, ASME J. Tribol., 114, pp. 9–11). *Journal of Tribology*, 114(1):11–13, 01 1992.

[37] Aitor Arana, Jon Larrañaga, and Ibai Ulacia. Partial ehl friction coefficient model to predict power losses in cylindrical gears. *Proceedings of the Institution of Mechanical Engineers, Part J: Journal of Engineering Tribology*, 233(2):303–316, 2019.